CHAPTER 1 INTRODUCTION

One of the more challenging problems facing geotechnical engineers is the determination of the shear strength of *in situ* soil deposits both during and after the occurrence of large strains. These strains may be the result of either monotonic or dynamic loading. Liquefaction is a good example of a condition that can result in large strains and deformations, and determining the shear strength of the soil deposit during and after liquefaction is fundamental in assessing its stability. Although several definitions of liquefaction have been proposed (Hazen 1920, Seed and Lee 1966, Castro 1969, Casagrande 1971, Seed and Idriss 1971, Castro and Poulos 1977, Ishihara 1985, Castro 1987), the definitions used by Castro and Poulos will be referred to in this study.

Steady State

The steady state of deformation is defined as a state of continuous deformation which occurs under a constant effective stress, constant shear stress, constant volume, and constant velocity, or time rate of deformation (Castro and Poulos 1977, Poulos 1981). The steady state approach is a method for assessing the undrained shear strength of *in situ* soil deposits. Its principle foundation is that for a particular soil, the undrained steady state shear strength depends only on the *in situ* void ratio and the effective stress in the soil. This procedure has been used to assess liquefaction susceptibility as well as stability under static loads. Castro et al. (1985, 1992) employed the procedure to analyze the failure of the Van Norman Dam (Lower San Fernando Dam) that occurred after an earthquake in Southern California in 1971. Sladen et al. (1985) used the concept to analyze the static instability and failure of underwater berms composed of loose sands. To accurately determine the

steady state shear strength, the *in situ* void ratio, the *in situ* effective stress, and the relationship between steady state void ratio and effective stress for the material of interest must be known.

The steady state line is the locus of points describing the steady state void ratios at various effective stress levels in e versus $log(\sigma')$ space, and has a negative slope as shown in Figure 1.1. If the state of a soil plots to the left and below the steady state line, negative pore pressure development during undrained loading (corresponding to dilative behavior during drained loading) will increase the effective stress in the soil until steady state is achieved. If the state of a soil plots to the right and above the steady state line, positive pore pressure development during undrained loading (corresponding to contractive behavior during drained loading) will decrease the effective stress in the soil until steady state is achieved.

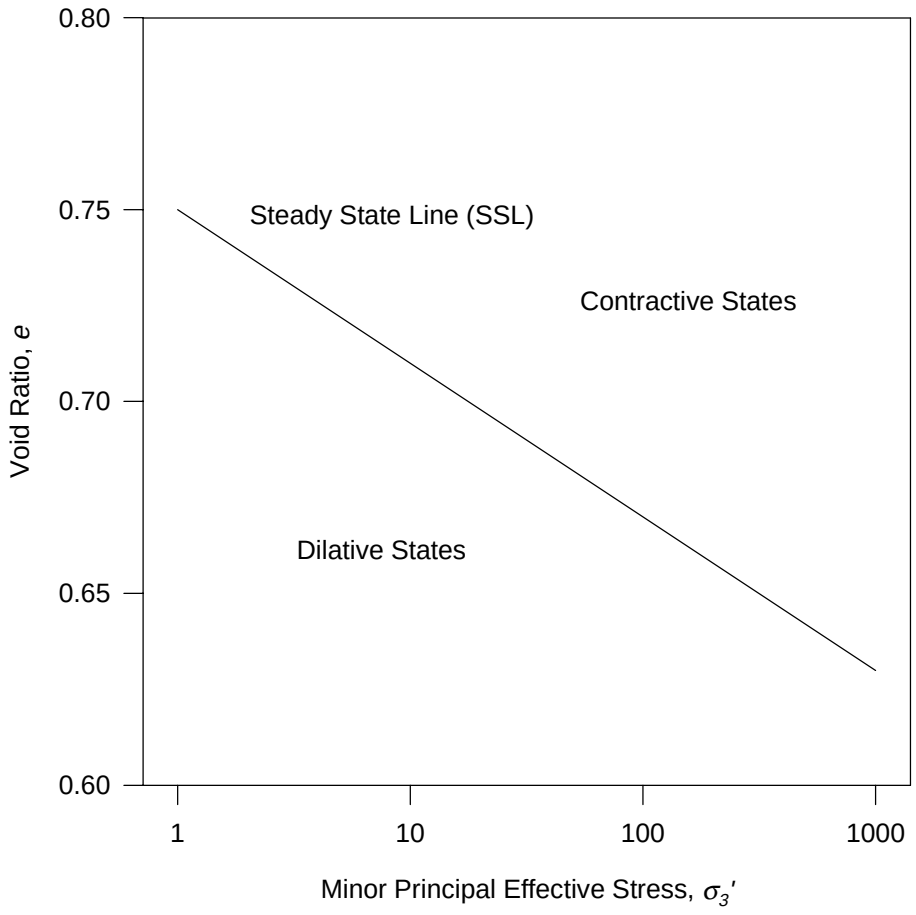

Figure 1.1 - Steady State Line Based on Minor Principal Effective Stress

Poulos et al. (1985) suggested a method for using the steady state concept for design purposes. They described the following steps:

1.) The *in situ* void ratio is measured as the void ratio of undisturbed samples retrieved using fixed-piston sampling techniques.

2.) The steady state line is determined using isotropically consolidated undrained (ICU) triaxial tests on remolded specimens.

3.) Undrained steady state shear strengths for the undisturbed specimens are determined using ICU triaxial tests. The steady state line for the *in situ* soil is assumed to be parallel to that determined for the compacted specimens.

4.) Undrained steady state shear strengths are corrected to the *in situ* void ratio.

5.) Using accepted geotechnical analysis procedures, the driving shear stresses are calculated, and the factor of safety against liquefaction is calculated.

Problems With the Steady State Approach

The steady state approach has been questioned because the steady state shear strengths determined in the laboratory may overestimate those that occur in the field, based on strengths back-calculated from observed failures (Hsing and Seed 1988, Kramer 1989, Seed et al. 1989, Finn 1990). Possible explanations for this unconservative strength prediction using the steady state approach include the inherent difficulties in measuring the *in situ* void ratio accurately and the spatial variation of both void ratio and effective stress that occurs in natural soil deposits. Another possible explanation is that the relationship between steady state shear strength and effective stress is not being determined properly. This relationship is typically determined using conventional isotropically consolidated undrained (ICU) triaxial tests (Castro 1969, Castro et al. 1982, Poulos et al. 1985), or by correlation with *in situ* tests. To determine the steady state line using ICU tests, a sample at a particular initial void ratio and stress level is sheared until the steady state condition is reached. This test results in one point on the steady state line. If a number of tests are performed at a variety of initial void ratios, the steady state line can be developed.

Triaxial Test

The procedures for conventional triaxial testing and the appropriate corrections to the data were originally developed for the primary purpose of peak strength determination, which is typically associated with small strain levels. ICU triaxial tests must be carried out to much larger strain levels in order to obtain steady state conditions, which are usually only achieved at very large strain levels. The applicability of conventional small-strain testing methodology to steady state conditions at large strain levels must be verified if the steady state approach based on triaxial test results is to be viable. It may not be possible to measure the actual material response in triaxial test specimens at large strains. Furthermore, the actual material response in the test specimen at large strains may not accurately represent *in situ* material behavior at large strains. This research effort examines the validity of using conventional ICU triaxial testing procedures for determination of the undrained steady state shear strengths of sands.

Corrections to Triaxial Test Data

The influences of the errors inherent to conventional triaxial testing on the determination of the steady state relationship are investigated. The significance of these errors is evaluated as a possible explanation for differences in laboratory and field steady state shear strengths. Conventional test data corrections, including area corrections, membrane strength corrections, and membrane penetration corrections, are examined to assess their validity at the large strain levels typically required to reach steady state conditions. Since most of the corrections are a function of strain, their influence on test results increases with increasing strain. In addition, since the steady state shear strength of loose specimens is typically less than the peak strength, the ratio of the strength correction to the overall strength is

significantly larger at steady state than at the small strain levels typically associated with peak stress behavior.

Area Corrections

Various corrections to account for the increase in specimen cross-sectional area during shear have been proposed (Bishop and Henkel 1962, Head 1986, Germaine and Ladd 1988). Several new area corrections are developed that account for nonuniform deformation during both drained and undrained shear. The assumptions associated with these area corrections and their applicability to large deformation of sand specimens are examined.

Membrane Strength Corrections

The membrane that confines the specimen has an axial strength that can contribute to the strength of the specimen (Henkel and Gilbert 1952, Duncan and Seed 1967) if the lateral support is sufficient to prevent buckling of the membrane. In addition, the membrane can add an additional confining stress to the specimen, which can increase the strength of the specimen. The membrane strength correction is a function of the type of deformation the specimen undergoes as well as the axial strain level. The influence of the membrane strength on the calculated specimen stresses, and hence test results, is evaluated.

Membrane Penetration Corrections

In addition to the influence on the measured stresses, the membrane can introduce errors due to the fact that the membrane can penetrate into the void spaces on the cylindrical surface of the specimen (Newland and Allely 1959, Kiekbush and Schuppener 1977). The membrane penetration into these void spaces is a function of the material properties of the membrane, the grain size,

void ratio, stiffness of the specimen, and the effective stress level. Once the confining stresses are applied, the specimen-membrane system reaches an equilibrium condition. During undrained shear, however, the effective stress level can change, so the amount of membrane penetration can change. If the effective stress level increases, the membrane penetration will increase and likewise if the effective stress level decreases, the amount of membrane penetration decreases. The change in membrane penetration during undrained shear can affect both the volume change characteristics and the pore pressure generation characteristics of the specimen (Lade and Hernandez 1977, Evans 1992).

Effects of Friction on the Specimen Ends

The fact that friction between the end platens and the specimen ends affects the results of the triaxial test has been recognized and accepted for quite some time (Taylor 1940). The exact nature of the effect has never been fully explained, however. Many studies have been performed in an attempt to quantify this effect (Shockley and Ahlvin 1960, Rowe and Barden 1964, Barden and McDermott 1965, Bishop and Green 1965, Duncan and Dunlop 1968, Kirkpatrick and Younger 1970, Raju et al. 1972, Lee 1978, Tatsuoka et al. 1984). The most routine practice is to use conventional end platens and use specimens with a height to diameter ratio of two or greater, which minimizes any end effects during peak strength testing (Head 1986). Whether this practice is acceptable for steady state testing, where the specimen undergoes large deformations, has not been verified. As the specimen is sheared beyond the peak stress level, the actual stress-strain characteristics of the end platen-soil interface will have more effect on the measured response of the specimen. It seems reasonable that either an end platen lubrication scheme or an increase in the height to diameter ratio would be necessary to minimize end restraint effects for steady state conditions. If the height to diameter ratio is increased,

additional problems can be introduced, including the potential for buckling of the specimen and an increased tendency for nonuniform stress or deformation conditions to develop. While the development of lubricated end platens for triaxial testing has been investigated, their use has typically been limited to testing of cohesive materials. Various lubrication schemes are investigated, with particular emphasis on their compatibility with granular materials and their friction reduction efficiency at large displacement levels.

The friction between the end platens and the specimen results in a shear stress on the top and bottom of the specimen in the radial direction as deformation progresses. The effect of this shear stress is to increase the confining stress of the material in the regions near the specimen ends, as well as to rotate the principal stresses in the specimen near the end platens. Since it is assumed that the major principal stress throughout the specimen is oriented along the axis of the specimen, error is introduced into the measured stress level whenever localized principal stress rotation occurs in the specimen. Localized failure may occur in the vicinity of the end platens since the actual deviator stress is greater than the measured or average deviator stress in this region. The significance of the imposed shear stress increases as axial (and consequently lateral) deformation increases. At large strain levels the region of influence of this phenomenon within the specimen can increase and the imposed shear stress can be much greater than at the strain levels corresponding to peak stress behavior.

Analysis of Specimen End Friction

Various attempts at closed form solutions to the restrained cylinder problem have been undertaken (Filon 1902, Pickett 1944, D'Apolonia and Newmark 1951, Balla 1960) with limited success. These analytical solutions were reviewed. In addition, finite element analyses of triaxial test specimens were

conducted to investigate the influence of variations in frictional resistance at the end platens on stress distributions in the sample, the global (measured) stress-strain response, and the shear stresses in the specimen at steady state conditions.

The analyses were based on an axisymmetric formulation and employed axisymmetric interface elements to model the friction between the specimen and the end platens. Various material models were used to simulate the test specimen, including linear elastic and nonlinear elasto-plastic constitutive models. The finite element computer program SAGE, developed at Virginia Tech to model soil structure interaction problems (Morrison 1995), was modified to satisfy the requirements for this research effort. The necessary changes included conversion of the plane strain version to an axisymmetric formulation and the addition of axisymmetric interface elements. SAGE was chosen primarily because the modular programming style adopted during the development of the SAGE code facilitated the addition of the axisymmetric formulation, various material models, and new interface elements.

The results of the analytical investigation are combined with comparison of results from the triaxial testing program employing conventional and lubricated end platens to try to quantify the influence of the friction on the specimen ends on large-strain behavior of triaxial test specimens.

Testing Program

To evaluate candidate lubrication schemes for the end platens, interface direct shear tests were performed. These tests employed a conventional square direct shear box with an aluminum insert in half of the box to simulate the end platen. Various lubrication schemes were investigated, and best scheme for ICU tests on sands was chosen based on the results of the interface direct shear tests.

Several sands that are known to be susceptible to liquefaction were used in the triaxial test program. Isotropically consolidated undrained (ICU) tests were performed on each material with both conventional end platens and with lubricated end platens. Standard test procedures were followed for the conventional ICU tests. The comparison of results from this test program was used to evaluate the influence of the friction on the specimen ends on the measured steady state properties of the materials. Particular attention was focused on the behavior of the specimens at large values of axial strain, when steady state conditions would typically occur.

Goals of the Research

The goals of the research can be summarized as follows:

1.) Examine the errors associated with triaxial testing at large strain levels.

2.) Examine the influence of various corrections to triaxial test data at large strains.

3.) Examine the influence of various degrees of end platen friction on the measured response of the specimen at large strain levels.

The errors inherent in parameters determined from large-strain triaxial tests on sands may at least partially explain differences in the steady state shear strength determined in the laboratory and the steady state shear strength determined by back-analysis of observed failures in the field. If these errors can be accounted for or minimized, the large-strain behavior at the laboratory scale can be better understood, which in turn may improve the understanding of large-strain behavior of granular materials subjected to dynamic or static loads in the field. Ultimately, the aim is to improve the ability to accurately predict material behavior and assess stability of *in situ* soil deposits using the steady state approach.

CHAPTER 2 STEADY STATE CONCEPTS

The Steady State of Deformation

The steady state of deformation for a particulate mass is defined as "that state in which the mass is continuously deforming at constant volume, constant normal effective stress, constant shear stress, and constant velocity" (Poulos 1981). The steady state is based on the concept of critical void ratio, defined by Casagrande (1936) as the void ratio at which "a cohesionless soil can undergo any amount of deformation or actual flow without volume change." While the critical void ratio concept applies to cases of drained loading, the concept of steady state encompasses both drained and undrained loading conditions, as either volume change (drained), changes in effective stress due to pore pressure development (undrained), or both can serve to bring the soil into the steady state condition. A review of important literature addressing steady state concepts is presented in Table B.1 in Appendix B.

The steady state conditions can be more easily understood by examining a state diagram, which is a plot of void ratio (or sometimes density) versus the effective minor principal stress (σ_3'). An example of a state diagram is shown in Figure 2.1. The stress is typically plotted on a logarithmic scale. The steady state condition in the state diagram is represented by the steady state line, which is defined as the locus of points at which the soil can undergo steady state deformation (Castro and Poulos 1977, Poulos et al. 1985). Note that on the state diagram, a position on the steady state line does not necessarily indicate that a soil is at steady state since the requirement of continuous deformation at a constant rate may or may not be met.

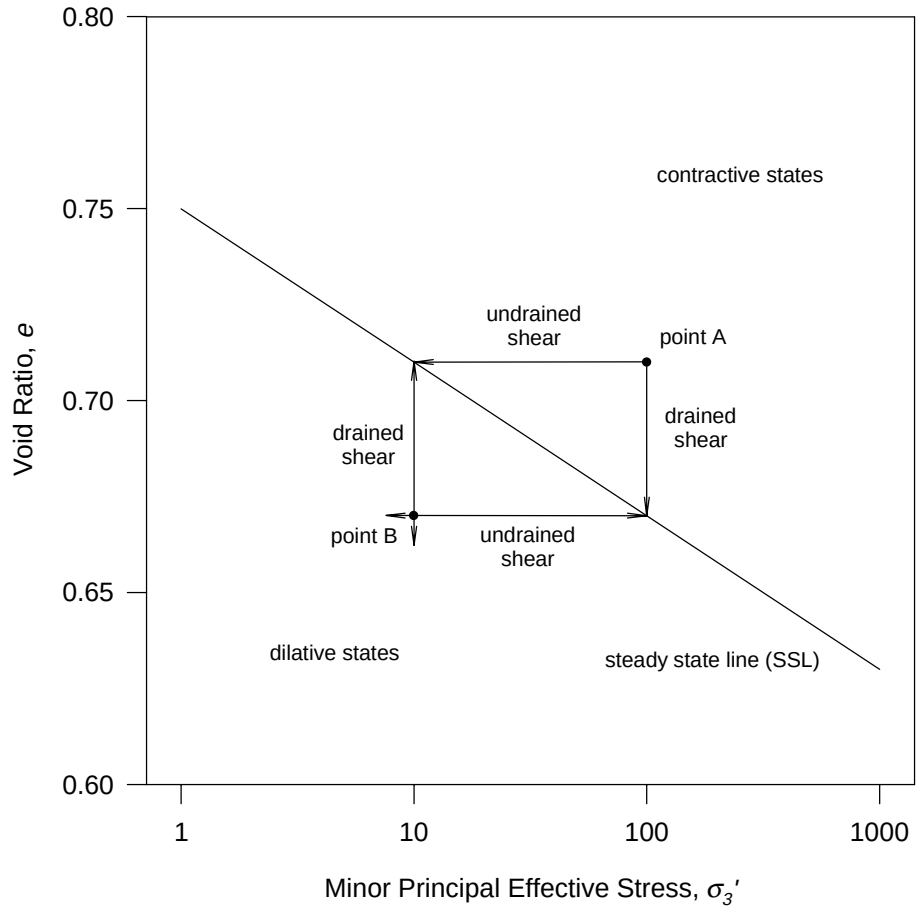

Figure 2.1 - State Diagram

Point A in Figure 2.1, represents a contractive soil, which tends to decrease in volume during shear, and will also be referred to as loose. During drained shear, this soil will decrease in volume, so the void ratio will decrease under a constant effective stress, until the soil reaches the steady state condition, at which no further volume change will occur. This corresponds to the critical void ratio as defined by Casagrande (1936). If the soil initially at point A is sheared in an undrained condition, which implies no volume change for saturated soils, the pore pressure will increase, and the effective stress will decrease while the void ratio remains constant. When the soil reaches the

steady state condition, no further pore pressure change occurs, and the effective stress and void ratio will remain constant at their steady state values as long as continuous deformation occurs at a constant rate.

Point B in Figure 2.1 represents a dilative soil, which tends to increase in volume during shear, and will also be referred to as dense. During drained shear, this soil will initially slightly decrease in volume, then increase in volume, and the void ratio will increase under a constant effective stress, until the soil reaches the steady state condition, at which no further volume change will occur. Again, this corresponds to the critical void ratio as defined by Casagrande (1936). If the soil initially at point B is sheared in an undrained condition, which implies no volume change for saturated soils, the pore pressure will initially increase slightly, then decrease, so that the effective stress will decrease slightly, then increase while the void ratio remains constant. When the soil reaches the steady state condition, no further pore pressure change occurs, and the effective stress and void ratio will remain constant at their steady state values as long as continuous deformation occurs at a constant rate. As can be seen from Figure 2.1, the steady state condition can apply to both contractive and dilative soils, and to drained shear, undrained shear, or a combination of both types of loading, as long as all of the necessary conditions for steady state deformation exist.

An essential requirement for deformation at steady state is that all initial fabric or structure has been destroyed, thus significant strains are required in order to achieve steady state deformation. In fact, Poulos (1981) notes that "the steady state of deformation is achieved only after all particle orientation has reached a statistically steady-state condition and after all particle breakage, if any, is complete, so that the shear stress needed to continue deformation and the velocity of deformation remain constant." Poulos (1981) describes the condition when all particle breakage (degradation) and re-orientation has

occurred as a *flow structure*. Restated, an essential requirement for deformation at steady state is that any initial structure or particle orientation is completely destroyed such that this flow structure is fully developed. As long as sufficient strain is generated in order to completely destroy the initial structure, steady state deformation can occur during drained or undrained loading. While the initial (low strain level) stress-strain characteristics of a soil are very dependent upon the initial fabric or structure, the stress-strain response at steady state is not; it is dependent only on the flow structure. Based on the flow structure, then, the shear strength at steady state is a function only of the effective normal stress at steady state and the velocity of deformation (Poulos 1981). As a result, a unique relationship exists between void ratio, effective normal stress, and shear stress at steady state for a particular soil and a particular rate of deformation.

Poulos (1981) stresses that the steady state of deformation implicitly requires that shear deformation is occurring at a constant rate. If no deformation is occurring, or if the rate of deformation is changing, the soil is not at steady state, even though the shear stress and void ratio may be the same as those at steady state. For example, a soil specimen may be deposited naturally or prepared in the laboratory with a void ratio and stress state that would indicate steady state conditions, but since the specimen is not undergoing any shear deformation, and the initial structure of the specimen has not been destroyed, the specimen is not at steady state. Likewise, Poulos (1981) has shown that the state of a soil can even cross the steady state line if the strain at the point when the steady state line is reached is not sufficient to completely destroy the initial structure or fabric.

Comparison of Steady State and Critical State

The concept of critical state is popular when discussing the behavior of cohesive materials, and since it is in many ways similar to the steady state concept, a comparison of the two is useful. Schofield and Wroth (1968) described critical state as "the concept that soil and other granular materials, if continuously distorted until they flow as a frictional fluid, will come into a well defined critical state." They viewed the process of deformation by *standing back* and attributed the shear resistance to friction alone, and neglected any particle orientation or degradation effects. Thus, an important distinction between steady state and critical state is that steady state requires a complete destruction of any initial fabric or particle orientation and the development of a flow structure, while critical state neglects any effects of fabric or orientation. The critical state approach, by taking a more global view of the shearing process, in effect implies randomness with regards to structure or particle orientation. The steady state approach, however, requires that the flow structure be developed by means of sufficient strain to completely remove any initial orientation or fabric.

The other important distinction between critical state and steady state is that critical state does not require that shear deformation be occurring. While shear deformation is necessary in order for the soil to reach the critical state, continuous shear is not explicitly required in order to remain at critical state. As noted previously, the steady state concept requires that constant velocity shear deformation be occurring in order to remain at steady state.

Steady State Undrained Shear Strength

The steady state undrained shear strength, S_{us}, is defined as the shear stress on the failure plane for a soil undergoing steady state shear deformation (Castro 1969). It should be noted that Poulos et al. (1985) refer to the steady state

undrained shear strength as S_{su}, but the two quantities are identical. To avoid confusion, the steady state undrained strength will hereafter be denoted by S_{us}. The concept of steady state undrained shear strength and its application to liquefaction evaluation has been advanced chiefly by Castro, Poulos, and co-workers. The steady state undrained shear strength for a particular soil is a unique function of void ratio, or density, only. It is independent of initial stress state, the type of loading encountered (cyclic or monotonic), and the initial fabric or structure of the soil deposit (Castro 1969, Castro 1975, Castro et al. 1982, Castro et al. 1992). The relationship between the steady state undrained shear strength and the principal stress difference (deviator stress) at steady state is described by:

Equation 2.1

where: S_{us} = steady state undrained shear strength
$(\sigma_1 - \sigma_3)_{ss}$ = deviator stress at steady state
ϕ'_{ss} = drained friction angle mobilized at steady state

Based on Equation 2.1, and assuming the deviator stress and drained friction angle at steady state are known, the state diagram shown in Figure 2.1 can be plotted as void ratio versus the logarithm of S_{us}, as shown in Figure 2.2. In this context, the state paths, or paths from initial state to steady state, as shown in Figure 2.1, no longer apply, since the abscissa in Figure 2.2, S_{us}, implies that steady state conditions have already been achieved.

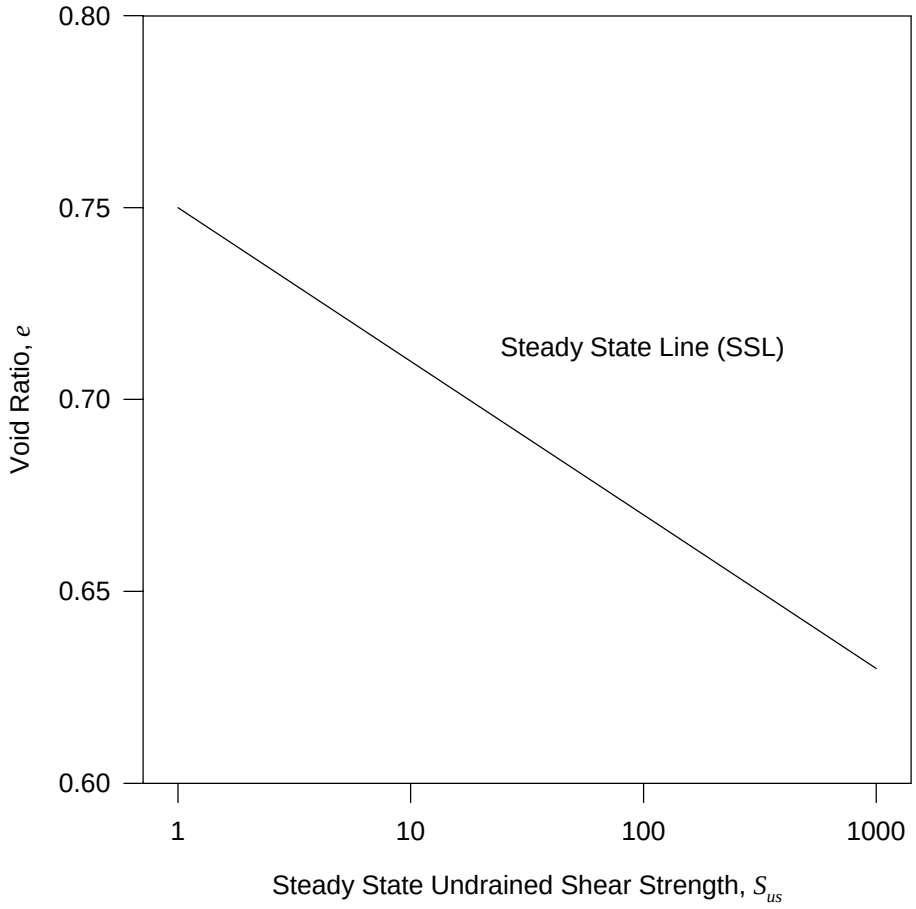

Figure 2.2 - State Diagram in Terms of Steady State Undrained Shear Strength

Other means of representing the steady state line on state diagrams have also been used. Been and Jefferies (1985) proposed using the mean effective normal stress, which is defined by:

$$\sigma'_m = \frac{1}{3}(\sigma'_1 + \sigma'_2 + \sigma'_3) = \frac{1}{3} J_1' \qquad \text{Equation 2.2}$$

where: σ'_m = mean effective normal stress
$\sigma'_1, \sigma'_2, \sigma'_3$ = effective principal stresses
J_1' = first effective principal stress invariant

Similarly, the mean effective normal stress for two dimensions, defined by:

$$p' = \frac{1}{2}(\sigma'_1 + \sigma'_3) \qquad \text{Equation 2.3}$$

where: p' = mean effective normal stress for two dimensions
σ'_1, σ'_3 = effective principal stresses

has been used by Alarcon-Guzman et al. (1988).

Been and Jefferies (1985) introduced the state parameter ψ, defined as the difference between the void ratio at the initial state and the void ratio at the steady state, at a particular effective stress level. In the e versus $log(\sigma_m')$ space, the state parameter is simply the vertical distance (Δe) from the initial state to the steady state line as shown in Figure 2.3. By convention, ψ is positive if the initial state plots above the steady state line (contractive materials), and negative if the initial state plots below the steady state line (dilative materials).

Been and Jefferies (1985) used the state parameter as a normalizing parameter for various index properties of sands. They asserted that relative density, the more common normalizing parameter for granular materials, does not acknowledge the stress dependent nature of cohesionless soils, while the state parameter does. They presented data that shows that sands with the same value of the state parameter, regardless of initial state (void ratio and effective stress), will behave similarly. They also presented correlations between the state parameter and friction angle, and state parameter and dilation rate.

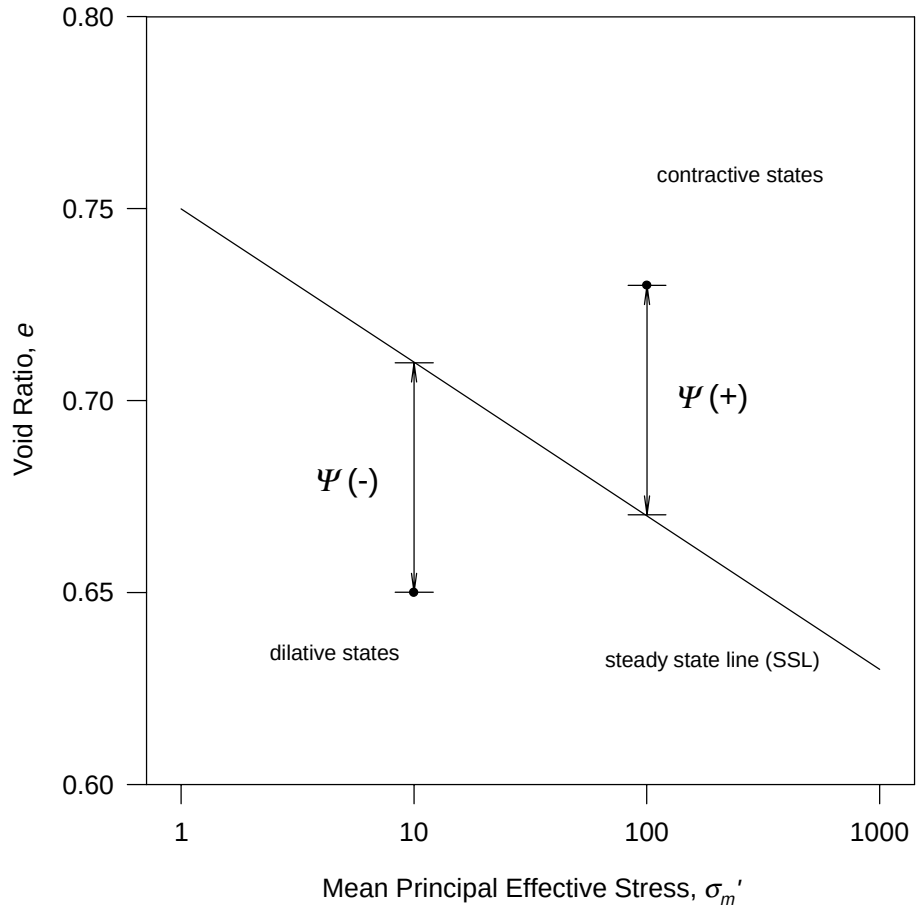

Figure 2.3 - State Diagram Used by Been and Jefferies (1985)

Been et al. (1987) used the state parameter approach to analyze the failure under a static load of an offshore, hydraulically placed sand berm. The failure was originally attributed to static liquefaction as defined by Castro and Poulos, but Been et al. contend that the sand was dilative based on its value of the state parameter. If the material is dilative, then static liquefaction as described by Castro and Poulos is unlikely. Been et al. attributed the failure largely to the failure of a clay foundation layer, and not static liquefaction of the hydraulically placed sand.

Liquefaction Evaluation Procedure Based on S_{us}

Poulos et al. (1985) suggest a rational, five-step procedure for evaluating the liquefaction potential of a soil mass based on the steady state shear strength concepts. Liquefaction is defined as a condition when the shear resistance of a soil is reduced as a result of monotonic, cyclic, or dynamic loading, to a level such that pre-existing driving shear stresses exceed the reduced shear resistance; and large, unidirectional strain or flow results (Castro 1969, Castro and Poulos 1977, Poulos et al. 1985). Based on this definition, evaluating the potential for liquefaction entails determining the *in situ* static driving shear stresses, which are the stresses required to maintain static equilibrium, and comparing them to the *in situ* reduced shear resistance, which is the undrained steady state shear strength. In this manner, the factor of safety is defined by:

$$FS_{liq} = \frac{S_{us}}{\tau_d} \qquad \text{Equation 2.4}$$

where: FS_{liq} = Factor of safety against liquefaction
S_{us} = undrained steady state shear strength
τ_d = *in situ* driving shear stress

Based on Equation 2.4, liquefaction will not occur if the undrained steady state shear strength exceeds the *in situ* static driving shear stress. If the driving shear stress exceeds the undrained steady state shear strength, liquefaction is possible, but still requires the occurrence of some triggering event that provides sufficient strain to overcome the peak strength and develop steady state conditions in the soil (Poulos et al. 1985b, Castro 1987). Also, only contractive soils (soil that tend to decrease in volume during shear) are susceptible to liquefaction since they develop positive pore pressure changes during undrained loading. This pore pressure development reduces the effective stress in the soil, and hence reduces the strength, as required by the previously stated definition of liquefaction. Since dilative soils (soils that tend

to increase in volume) develop negative pore pressure changes during undrained loading, the effective stress, and hence the strength, increase so the required reduction of shear strength is not observed, and liquefaction is not possible.

In the analysis procedure outlined by Poulos et al. (1985), the potentially liquefiable zones are identified based on correlations and *in situ* tests, such as the standard penetration test (SPT) or the cone penetration test (CPT). Once the potentially liquefiable zones have been identified, the five basic steps are:

1.) Determine the *in situ* void ratio

2.) Determine the relationship between steady state void ratio and effective stress using compacted specimens

3.) Determine the undrained steady state shear strength (S_{us}) for *undisturbed* specimens

4.) Correct *undisturbed* S_{us} to correspond to the *in situ* void ratio

5.) Calculate the *in situ* driving shear stress and the factor of safety

These steps will be discussed further in order to highlight several possible sources of error.

Step 1 - Determine in situ void ratio

Determination of the *in situ* void ratio of cohesionless soils has long been a challenge due to the sensitivity of cohesionless soils to volume change when disturbed. Poulos et al. (1985) recommend three viable methods: 1.) fixed piston sampling, 2.) freezing and coring, and 3.) sampling in test pits, and recommend fixed piston sampling as the best alternative. As will be shown later, the undrained steady state shear strength is extremely sensitive to even small changes in void ratio, so the accurate determination of the *in situ* void ratio is a key task in the analysis procedure.

Step 2 - Determine steady state void ratio as a function of effective stress

Since it is virtually impossible to sample a cohesionless soil without disturbing it, and hence changing the void ratio, the *in situ* shear strength cannot be directly determined from the results of tests on *undisturbed* specimens. In order to estimate the *in situ* S_{us}, the relationship between changes in void ratio and changes in effective stress or S_{us} must be determined. This relationship is defined by the steady state line on a state diagram as shown in Figure 2.2. Once this relationship has been determined, the steady state strength measured for the undisturbed specimens can be corrected to reflect the effects of the unavoidable changes in void ratio due to sampling, test preparation, and consolidation in the laboratory. Since the availability of undisturbed samples of identical soil at a wide range of void ratios is rarely available, the steady state line is determined based on the results of tests on reconstituted specimens. Poulos et al. (1985) recommend using five or six specimens compacted from identical soil. They suggest thoroughly mixing several undisturbed samples together and recompacting the five or six specimens to ensure that each specimen will be nearly identical in composition. Although any undrained test that allows for steady state deformation to be achieved may be used, Poulos et al. (1985) recommend the triaxial test for clean sands, and specify that strain control should be used to apply the load. Since less strain is required to achieve steady state conditions in the triaxial test for loose, or contractive, specimens than for dense, or dilative, specimens (Castro 1969), Poulos et al. (1985) recommend compacting the specimens to high void ratios and consolidating to high enough effective stresses such that all specimens will be contractive. In other words, the steady state line should be determined by approaching from the contractive, or upper side, as shown in Figure 2.1. Been and Jefferies (1985) noted that some variation in the small strain shear response of sands occurs as a result of differences in the structure or fabric of the sand specimen being tested. However, the effect of initial fabric should

only be important when examining small strain response, since the fabric should be destroyed at very large strain levels. Although any fabric or structure effects should have very little influence, samples that were prepared in the same manner should be used for the determination of the steady state line.

Step 3 - Determine S_{us} for undisturbed specimens

Once the steady state relationship for the compacted specimens has been determined, CU triaxial tests are performed on the *undisturbed* specimens from the potentially liquefiable zone. Again, it is desired that the specimen be contractive, but only limited control over the void ratio of an undisturbed specimen is afforded. The suggested procedure, then, is to consolidate the undisturbed specimens to high enough effective stresses that they will be contractive. This corresponds to achieving an initial state to the right of the steady state line as shown in Figure 2.1. Poulos et al. (1985) note that the higher the consolidation stress, the greater the difference in the *in situ* void ratio and the void ratio of the tested specimen, so that increasing the consolidation stress increases the required correction. As a result, they suggest only moderate levels of consolidation stress be used in an attempt to obtain contractive specimens. They note that dilative specimens may be used, but typically involve more error, due primarily to greater redistribution of void ratio at large strains in dilative specimens.

Step 4 - Correct measured S_{us} to the in situ void ratio

The point representing steady state for the undisturbed specimens rarely coincides with the steady state line as determined for the compacted specimens. It has been postulated that the slope of the steady state line is primarily a function of the grain shape of a given soil, while the vertical position of the steady state line depends primarily on the gradation or grain

size distribution of the soil (Castro and Poulos 1977, Castro et al. 1982). Given these assumptions, the difference in the steady state for the undisturbed specimens and the compacted specimens would be due to slight variations in the gradation of the two types of specimens. If the compacted specimens were prepared from mixing undisturbed samples together, it would be expected that the grain shape characteristics of the soil would be preserved, even if the gradation varies slightly, and hence the slope of the steady state line should be nearly equal to that for the undisturbed specimens. This is the fundamental assumption Poulos et al. (1985) use when correcting S_{us} for the undisturbed specimens to the *in situ* void ratio. The procedure is shown graphically in Figure 2.4. The point representing steady state for the undisturbed specimen is plotted as shown. Assuming that the slope of the steady state line for the undisturbed soil (*in situ* conditions) is the same as that for the compacted specimens, the *in situ* S_{us} is determined based on the *in situ* void ratio measured in step 1.

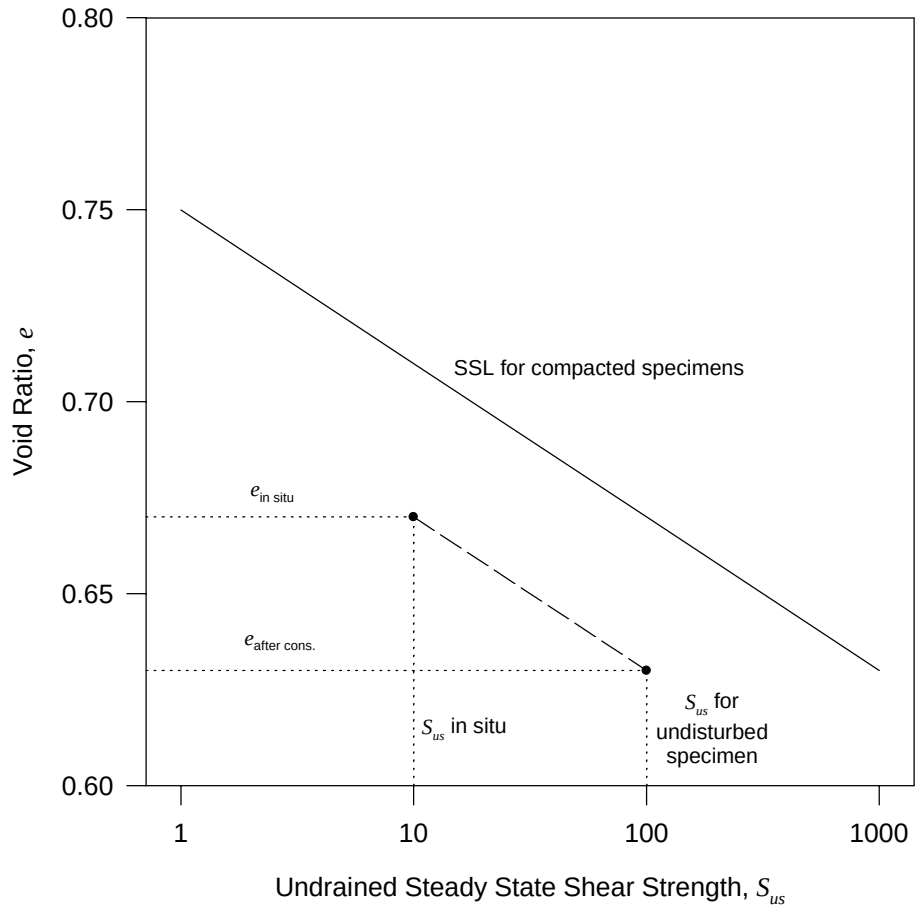

Figure 2.4 - Correction of S_{us} to the *In Situ* Void Ratio

Step 5 - Calculate in situ driving stress and factor of safety

The *in situ* driving shear stress is calculated by conventional limit equilibrium methods. Examples of sources of driving shear stress include sloping ground surfaces, as found in embankments and cut slopes, and foundation loads due to the weight of structures. It is important to note that the driving shear stresses are the shear stresses required to maintain static equilibrium of the soil mass. Thus, the presence of *in situ* shear stresses does not in and of itself mean that driving shear stresses exist (Castro 1987). For example, if the

ground surface is level and the coefficient of lateral earth pressure, K_0, is not equal to one, then shear stresses below the ground surface will exist, but there will be no driving shear stress since the existing shear stresses are not required to maintain static equilibrium.

Once the driving shear stresses have been calculated, the factor of safety against liquefaction can be calculated using Equation 2.4 and the estimated value of the *in situ* undrained steady state shear strength. For cases when the factor of safety is greater than 1, the soil mass is stable, and will not liquefy provided the estimated shear strengths and void ratios are sufficiently accurate. If the factor of safety is less than 1, the soil mass is unstable under steady state conditions, implying that liquefaction is possible. It must be remembered, however, that the steady state cannot be achieved without the occurrence of enough strain to destroy the initial structure and allow the formation of the flow structure required for steady state deformation. Until sufficient strain occurs, the undrained shear strength of the soil will be greater than S_{us}, so liquefaction may not occur. The occurrence of liquefaction, even for cases where the factor of safety against liquefaction is less than 1, requires a triggering event or loading sufficient to reduce the undrained shear strength to a level below the *in situ* driving shear stress. This triggering event can be any type of undrained loading, either monotonic, cyclic, or dynamic. Monotonic loading sufficient to trigger liquefaction might be due to a sudden increase in surface loads on a soil mass or the unloading of the toe of a slope. Dynamic loading sufficient to trigger liquefaction might be due to an earthquake, blasting, or some other dynamic load of sufficient amplitude and duration to cause a reduction in the undrained strength of the soil. The loading required to initiate liquefaction is a function of the stress-strain response of the soil and the driving shear stresses present (Castro 1969, Poulos et al. 1985). As a result, the occurrence of liquefaction may be dependent on the initial conditions of the soil such as the inherent fabric and particle orientation, but

the stability with respect to the undrained steady state shear strength, S_{us}, is not. Two conditions are required for the occurrence of liquefaction: an *in situ* driving shear stress greater than the undrained steady state shear strength, and a triggering load causing enough strain so that the undrained shear strength of the soil is reduced to the undrained steady state shear strength.

Problems With Accurate Determination of S_{us}

Comparisons of steady state strengths with strengths back-calculated from case histories of failures has suggested that significant variations in the measured and back calculated values of the steady state undrained strength occur (Castro et al. 1985, Castro et al. 1992, Kramer 1989). It is also noted that the steady state strength relationship based on laboratory data overestimates the back-calculated strengths by approximately one standard deviation (Castro et al. 1992). Kramer (1989) performed an uncertainty analysis on the procedures necessary to evaluate the liquefaction potential of a soil deposit using the steady state shear strength, and concluded that in many instances, the uncertainty in the determination of the steady state shear strength may be so severe as to make the results of liquefaction evaluation procedure useless.

If the *in situ* driving shear stresses are determined or estimated with sufficient accuracy, the validity of the liquefaction analysis lies in the determination of the *in situ* S_{us}. Steps 1 through 4 of the procedure deal with the determination of the *in situ* S_{us}. Possible sources of error in determining the *in situ* S_{us} include:

1.) the determination of the *in situ* void ratio

2.) the assumption that the steady state lines for the compacted and undisturbed specimens are parallel

3.) the determination of the steady state line for compacted specimens

4.) the determination of S_{us} for the undisturbed specimens

Since S_{us} is a function solely of void ratio, the accurate determination of the *in situ* void ratio is very important. As noted previously, this is a very difficult task. One of the criticisms of the liquefaction evaluation procedure is that it is very dependent on the accurate determination of *in situ* void ratio. The assumption that the steady state lines for the compacted specimens and the undisturbed specimens are parallel is based on the premise that the slope of the steady state line is dependent only on grain shape, and this idea has been identified as needing further verification through additional research (Castro et al. 1982). The slope of the steady state line is typically very small, so that even a small error in the void ratio measurement or in the determination of the slope can result in very significant errors in the undrained steady state shear strength.

Kramer (1989) noted that "scatter undoubtedly results from limitations of the triaxial test commonly used to obtain steady state data." The accuracy of the determination of S_{us} for both compacted and undisturbed specimens lies chiefly in the ability of the laboratory test to simulate the conditions required for steady state deformation and the ability to accurately measure the quantities that are required in order to calculate the parameters needed to characterize the steady state condition. As noted previously, Poulos et al. (1985) recommend consolidated undrained (CU) triaxial tests using strain-controlled loading for determining the steady state parameters of clean sands. It is widely recognized that the triaxial test has limitations with respect to the strain levels that can be achieved (Castro et al. 1982, Kramer 1989), and large strains are typically required to achieve the condition of steady state deformation. An examination of the limitations of the CU triaxial test with respect to the determination of steady state strength parameters, then, is of key significance

in determining the viability of the liquefaction evaluation method as proposed by Poulos et al. (1985). Castro (1991) stated:

> *"The undrained steady state strength (S_{us}) is a critical parameter for understanding the behavior of soil masses during earthquakes. Thus the profession should continue to strive for better ways of determining S_{us}, and for an objective assessment of current methods."*

This study is aimed at an objective assessment of the viability of using the ICU triaxial test to determine the steady state undrained shear strength.

CHAPTER 3 TRIAXIAL TEST - DESCRIPTION AND PROCEDURES

Historical Review of the Triaxial Test

Triaxial testing of soils was initially developed in the early 1930's. Although the strength of soils had been investigated much earlier by means of other tests, the triaxial test afforded greater control over the states of stress and drainage conditions that could be investigated than did most of the earlier tests. Saada and Townsend (1981) presented a brief overview of the early history of the triaxial test, and noted that it appears to have been developed independently, but during the same time period, in Germany, the Netherlands, and the United States.

In 1940, the War Department, Corps of Engineers initiated a Soil Mechanics Fact Finding Survey that included an extensive research program on triaxial testing that was carried out jointly by the Waterways Experiment Station, Harvard University, and Massachusetts Institute of Technology (Waterways Experiment Station 1947). This study was very significant in the development of the triaxial test, as it examined a number of variables and factors, including specimen size and shape and stress distributions within the test specimen, in order to determine which ones influenced the results of triaxial tests on both cohesive and cohesionless soils. The purpose was to study the strength characteristics and stress-deformation properties of soils in the triaxial test. The goals of the program were as follows (Waterways Experiment Station 1947):

1.) Determine the effects of specimen size and proportions (geometry and shape) on test results.
2.) Explore testing of cohesive soils using triaxial equipment.

3.) Determine the stress distributions within the specimen and their effect on test results.

4.) Determine the relationship between void ratio and stability for cohesionless soils.

5.) Examine the effects of partial saturation on the shear strength of remolded cohesive soils.

The influence of specimen size and shape was thoroughly examined, accomplishing the first goal. The recommendations were to use only circular cross sections for triaxial compression tests, and to use length to diameter ratios of 2 to 2.5, although the influence of varying the ratio between 1.5 and 3 was thought to be negligible. For tests on cohesionless soils, the recommended minimum diameter was 2.8 inches or 5 times the diameter of the largest particle in the specimen. For tests cohesive soils, the recommended minimum diameter was 1.4 inches. The determination of the shear strength of cohesive soils using the triaxial test was thoroughly explored, and found to be viable. The hypothesis that the shear strength of a saturated, normally consolidated clay is a function of water content at failure, which was formulated by Rutledge (Waterways Experiment Station 1947), was a significant result of the study on cohesive soils. Accurate stress-deformation characteristics were not readily established from the results of triaxial tests for cohesive or cohesionless materials, although the magnitude of error was believed to be much less significant for cohesive soils. The errors that obscured the stress-deformation properties were attributed to errors in the external measurement of the axial force and deformation. The distribution of stresses within the specimen was not determined, but the effects of stress distributions were believed to be negligible for practical purposes (Waterways Experiment Station 1947). Likewise, the study did not accomplish the goal of establishing a relationship between void ratio and stability of cohesionless soils. The suggested reason this relationship was indeterminate was that the

limitations of specimen size, drainage path, and boundary conditions in the triaxial test prevented the modeling of liquefaction or instability. It was suggested that large-scale tests, perhaps on the order of 5-foot diameter triaxial specimens might be required in order to reproduce the required undrained conditions needed to establish a relationship between void ratio and stability (Waterways Experiment Station 1947). The study indicated that the results of triaxial tests on cohesionless soils were not significantly affected by the following:

1.) The ratio of height to diameter in the range of 1.5 to 3
2.) The shape of the cross section of the specimen
3.) The restraint on the specimen ends caused by the friction at the end platens
4.) The rate of loading
5.) The type of loading (stress controlled or strain controlled)

The factors that did affect the results of triaxial tests on cohesionless soils were:

1.) Errors in the determination of the initial void ratio
2.) Non-uniformity of void ratio throughout the specimen
3.) Erratic piston friction

Among the ideas recommended for future research on cohesionless soils were:

1.) Investigation of stress-strain relationships and elimination of errors of measurement
2.) Investigation of liquids, plastics, or unvulcanized rubber as a substitute for elastic membranes to minimize membrane effects
3.) Tests on specimens 5 feet in diameter to investigate liquefaction and determination of critical void ratio

4.) Large-scale field tests to simulate liquefaction

Bishop and Henkel (1957, 1962) published one of the most significant references on triaxial testing, *The Measurement of Soil Properties in the Triaxial Test*, in 1957. The book presents an in-depth description of triaxial testing equipment, the standard procedures for performing tests, and discussions on various types of loading that are attainable in the triaxial test. The usefulness of this work has diminished very little since its publication. Head (1986) acknowledged that significant portions of the sections on triaxial testing in his book *Manual of Soil Laboratory Testing* could be attributed to the work of Bishop and Henkel. Head (1986) and Bishop and Henkel (1962) are likely the most widely used references on the triaxial test to date. The only significant advancements since their publication have been in the sensor, instrumentation, and measurement arena. Electronic transducers have essentially replaced mechanical means of measurement of forces, pressures, and displacements in most laboratories, and reduced the errors in measurement to some extent. However, the concerns regarding void ratio determination, void ratio uniformity, and the assumptions required to determine stress and strain based on external measurements are as equally valid today as they were when the triaxial test was first developed.

Description of the Test and Possible Sources of Error

The triaxial test is a flexible and versatile test for determining the shear strength of soils in the laboratory. In order to obtain meaningful strength or stress-strain parameters from the test, certain assumptions regarding the preparation of the specimen and the states of stress and strain in the specimen at various stages of the test are required. The accuracy of the test results obviously depends on the ability of the test procedures to validate these assumptions. If certain assumed conditions are not matched by the test conditions, then correction procedures may be employed in order to preserve

the validity of the results. An examination of these underlying assumptions and their impact on the test results follows.

The basic steps in performing triaxial tests may be grouped into three main functions: preparation and setup of the specimen, the consolidation phase, and the shear phase. Head (1986) outlined a more detailed list of procedures as follows:

1.) Perform pre-test checks on apparatus
2.) Prepare test specimen
3.) Set up specimen
4.) Saturate
5.) Consolidate
6.) Apply compression to failure
7.) Analyze data
8.) Prepare graphical and tabulated data
9.) Report results

The specimen preparation and setup phase essentially covers items 1 through 4 as described by Head. The consolidation and shear phases cover items 5 and 6, respectively. Items 7 through 9 describe the process of data reduction and analysis.

Test Preparation

The important aspects of the preparation of the test specimen are the accurate determination of the specimen dimensions, the void ratio of the specimen, and stress state of the specimen prior to the start of the test. Since almost all of the parameters obtained from the triaxial test are dependent upon density, the void ratio of the specimen during all stages of the test is a critical piece of data.

Consolidation

During the consolidation phase, a change in stress is imposed on the specimen and the volume change during consolidation is measured. At the end of the consolidation phase, the void ratio of the specimen, as well as the state of stress throughout the specimen are presumably known. After consolidation, the specimen is presumably under a uniform state of stress, which is hydrostatic if the test specimen is isotropically consolidated.

Shear

Once consolidation is completed, the soil may be sheared by applying an axial, or deviator load. In the case of a drained test, the applied deviator load, the axial deformation, and the specimen volume change are typically measured. In the case of an undrained test on a saturated specimen, it is assumed that no volume change occurs during the test, and the applied deviator load, the axial deformation, and the effective stress in the specimen are typically measured. All test results are derived from the parameters measured during specimen preparation, consolidation, and shear of the test specimen, so the reliability of the test results is directly related to the accuracy of the measured quantities as well as the assumptions used to transform the measured quantities into meaningful parameters.

Procedures for Test Preparation

The first step in performing a triaxial test is the preparation of the specimen. For cohesive soils, there are three common ways to prepare specimens: trim from an undisturbed sample, trim from a remolded consolidated sample, or compact from a disturbed sample. Trimming the specimen entails trimming excess soil from the sample until the exact desired dimensions of the specimen are achieved. Compaction entails compacting the specimen in lifts into a

specimen mold of the desired dimensions of the specimen. For cohesionless soils, specimens are typically prepared by either compaction or some type of pluviation. Pluviation can be accomplished in air or under water. The soil can be poured through a sifter arrangement, consisting of a series of plates or screens arranged vertically (one above another) with various size openings in them. The soil can also be poured from a container with a tube for an outlet, such as an apparatus similar to that used for the minimum density test based on *ASTM D4254-91* (ASTM 1995). Specimens of cohesionless soils are typically prepared in a mold, sometimes referred to as a forming jacket, with the membrane held against the inside wall of the mold by vacuum. The membrane is placed around the bottom end platen and sealed to the platen with o-rings. The forming jacket is placed around the membrane, and the top of the membrane is stretched around the top of the forming jacket so that a vacuum may be drawn between the jacket and the membrane in order to ensure that the specimen diameter is nearly uniform. With the membrane in place inside the forming jacket, the specimen may be fabricated by one of several means, as noted previously. Once the fabrication of the specimen is complete, the top end platen is placed on the specimen and the membrane is sealed against the platen with o-rings. Once the specimen and end platens are sealed, the vacuum may be transferred to the interior of the specimen via the internal drainage lines through the end platens, applying a net positive effective stress to the specimen. With the specimen under a positive effective stress, the forming jacket may be removed allowing measurement of the dimensions of the specimen. After the specimen dimensions are recorded, but prior to complete saturation in the triaxial cell, it is imperative to minimize any volume change that may occur, since a change in volume at this stage cannot be measured, and thus an unknown change in void ratio could occur. Once the specimen is saturated in the triaxial cell, volume change can be measured via changes in pore water volume, so it is crucial to minimize volume change

between the time at which the specimen dimensions are recorded and the time when the specimen is in place in the triaxial cell and is fully saturated.

With the specimen under a positive effective stress applied via internal vacuum and the forming jacket removed, the triaxial cell may be assembled and filled. Any components of the cell that must be removed for specimen preparation are reassembled and the cell is closed, locked, and filled with the cell fluid. With the cell fluid in place, the effective stress applied to the specimen may be transferred from the internal vacuum to an external cell pressure. Ideally this transfer should occur at a constant effective stress so as to minimize volume change, but practically, some change in effective stress and hence some small volume change will occur. A good practice to avoid large changes in effective stress in the specimen is to reduce the vacuum on the specimen by some small incremental amount, and immediately increase the cell pressure by the same increment of stress. Repeating this process until the effective stress is supplied entirely by the cell pressure should ensure that the effective stress change in the specimen is minimal, so the volume change associated with these changes in effective stress should be insignificant. If the test equipment allows simultaneous reduction of the vacuum and increase of the cell pressure, then the effective stress on the specimen can be maintained at a constant value during the transfer from internal vacuum to external cell pressure.

Once the specimen is under pressure in the triaxial cell, the specimen must be saturated to allow for volume change measurement or pore pressure measurement during the consolidation and shear phases of the test. This is typically accomplished by first flushing as much air as possible from the specimen and replacing it with carbon dioxide (CO_2). The reason for this step is that carbon dioxide dissolves much more easily in water than air does. While flushing the specimen with carbon dioxide, only a small pressure gradient should be used to force the carbon dioxide through the specimen, since this

pressure gradient affects the effective stress in the specimen, and effective stress changes must be kept to a minimum. The specimen should be purged with CO_2, then flushed with deaired water. The deaired water may be drawn through the specimen with a vacuum to increase the hydraulic gradient, but a very small vacuum pressure should be used so as to minimize effective stress changes. After flushing the specimen with deaired water, the drainage lines from the pore pressure board may be connected to the specimen. With the internal drainage lines connected to both the specimen and the pore pressure board, the specimen can be saturated by applying back pressure to the specimen through the drainage lines. The back pressure in the specimen is incrementally increased with the cell pressure, so that a constant effective is maintained in the specimen. The increase in back pressure, however, forces more air (or carbon dioxide) into solution in the pore fluid. The saturation level is typically determined by measuring the pore pressure parameter B, which is defined as the change in pore pressure divided by the change in hydrostatic total stress (Skempton 1954), and can be measured by increasing the cell pressure by a small increment and measuring the resulting change in pore pressure. If the specimen is fully saturated, the resulting pore pressure change should be equal to the increment of cell pressure increase. Once complete saturation is achieved, volume changes can be measured by measuring changes in the pore fluid volume. Since volume change can be measured, the specimen may be consolidated to the desired effective stress state without introducing error due to unmeasured volume change.

Consolidation Phase

With the specimen completely saturated, the void ratio throughout the specimen presumably known, and the specimen at some nominal state of effective stress, the consolidation phase of the test may be started. Given these conditions, an increase in cell pressure with no drainage allowed will

produce no change in effective stress, since the specimen is saturated and the resulting increase in pore pressure will be equal to the increase in cell pressure, or total stress. In order to consolidate the specimen to the desired effective stress state, the specimen must be allowed to compress. To initiate consolidation, the cell pressure is first increased to a value equal to the back pressure plus the desired consolidation stress. Consolidation is initiated by opening the drainage lines from the specimen and measuring the volume of pore fluid expelled with time. The rate of consolidation is observed, and can be useful in estimating appropriate rates of strain.

Shear Phase

Once the specimen has been consolidated to the desired effective stress, the shear phase of the test may be initiated. Two means of controlling the shear phase are typically used: stress-control and strain-control. Stress control involves applying an incremental deviator stress to the specimen, allowing deformation to occur until the specimen reaches a state of equilibrium, measuring the deformation, then applying the next increment of deviator stress. Strain control involves applying axial strain, usually at a constant rate, and measuring the resulting deviator stress at a number of strain levels. Strain-controlled tests are more common than stress-controlled tests, primarily due to the fact that they are more easily automated. The shear phase of the test is typically carried out until failure occurs, or until a specified level of axial strain is achieved. For determining steady state shear strength parameters from the triaxial test, however, the shear phase is carried out until the steady state condition is reached, which usually occurs at very high levels of strain. Measurement of the axial force and the axial deformation is a fairly simple task, and both are typically measured. The radial stress at the lateral boundary of the specimen is also fairly easy to determine, based on the applied cell pressure. Ultimately, however, the stress state of the specimen at various

levels of strain are desired, so the state of stress in the specimen must be derived from the cell pressure, which is known, and the force and displacement on the end boundaries of the specimen, which are measured quantities. In order to determine the stress state in the specimen based on these quantities, it is usually assumed that the horizontal and vertical planes are principal planes, so that the lateral confining pressure and the axial pressure are principal stresses. The axial stress is determined by assuming a uniform distribution across the ends of the specimen, so that the axial stress is equal to the measured axial force divided by the cross sectional area of the specimen. The axial strain is typically determined by assuming that the strain in the specimen is uniformly distributed throughout the specimen, so that the axial strain is equal to the axial displacement divided by the original specimen height. During the shear phase of the test, the specimen undergoes more significant changes in stress state than during any other portion of the test. In addition, the stress state is no longer hydrostatic once shear begins. Likewise, the specimen is strained significantly more during the shear phase than any other portion of the test. For various reasons, the assumptions about uniform distributions of stress and strain and the orientation of the principal stresses are not always valid, particularly at higher strain levels, at which the specimen has undergone significant deformation. It is useful, then to investigate the reasons that these assumptions may not be valid, and to investigate the significance of these assumptions with respect to the results of triaxial tests

Ideal Conditions During Shear

The following scenario describes what could be considered an ideal triaxial test; that is, the properties that are actually measured would be identical to the properties that are assumed to be measured. Ideally, the end platens would be perfectly frictionless, so that the specimen would deform as a right circular cylinder. In addition, the membrane-specimen interface would be perfectly

frictionless, so that no shear stresses would develop on the horizontal and vertical planes throughout the specimen. Consequently, the stresses in the horizontal (radial) and vertical (axial) direction would be principal stresses, with the axial stress being the major principal stress and the radial stress being the minor principal stress. If this were the case, then the vertical stress on the top and bottom planes of the specimen would be uniform, so that at all points in the volume of the test specimen, the stress conditions would be uniform. With uniform stresses throughout the specimen, the state of stress and strain in the soil could be accurately determined based on the applied deviator load, the applied radial stress (cell pressure), and the measured axial displacement.

Deviations from Ideal Conditions

In practice, ideal conditions can never be obtained in the laboratory. To examine the effect of deviations from the ideal conditions described above, they may be examined separately.

End Friction

For the triaxial test, one of the most significant deviations from the ideal conditions described above is the development of friction between the end platens and the ends of the specimen as shown in Figure 3.1. The consequences of the friction that develops between the ends of the specimen and the end platens are:

1.) Shear stresses are induced on the horizontal end planes of the specimen in the direction toward the axis of the specimen.

2.) The normal stresses on the horizontal end planes of the specimen are not uniform, as shown in Figure 3.2.

3.) The vertical and horizontal normal stresses are not principal stresses.

4.) The distributions of normal stresses and shear stresses within the specimen are not uniform.

5.) The distributions of normal strains and shear strains within the specimen are not uniform.

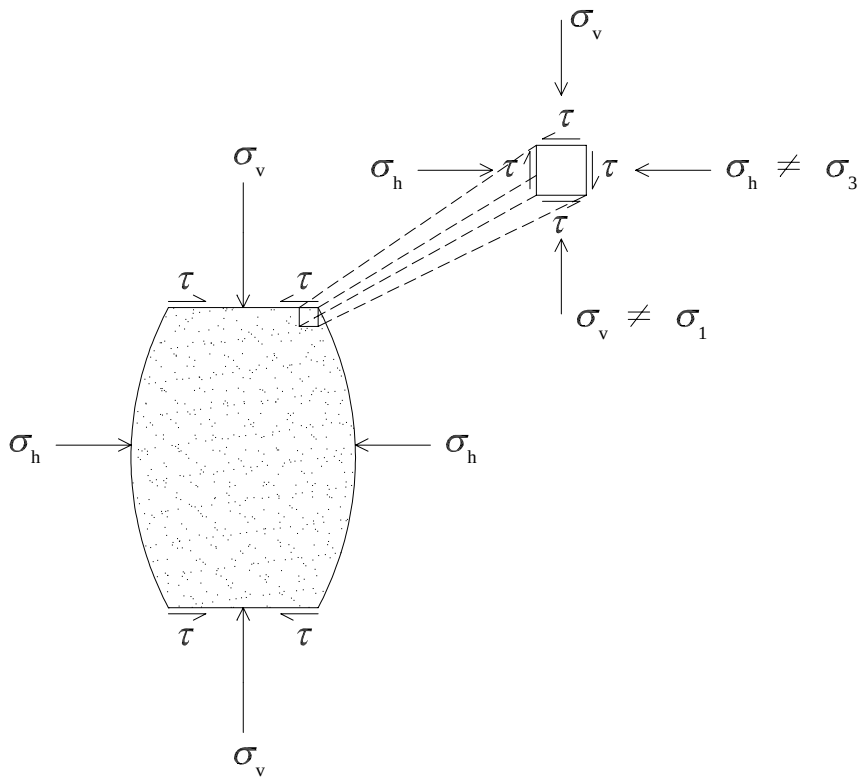

Figure 3.1 - Specimen End Friction Induced by End Platens

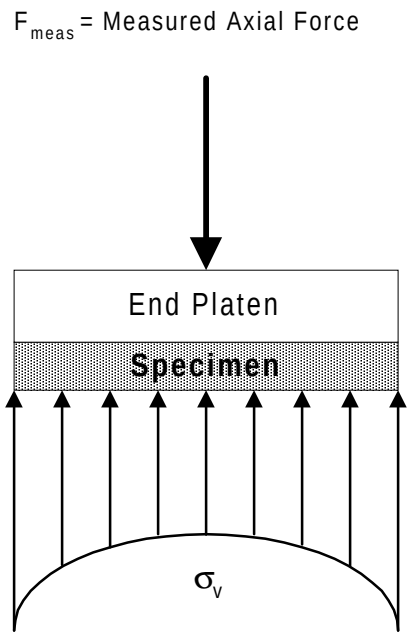

Figure 3.2 - Nonuniform Vertical Stress Due to End Friction

The shear stresses induced on the ends of the specimen by the end platens act towards the axis of the specimen. These shear stresses are a function of the normal stress on the end surface of the specimen and the radial coordinate, or distance from the axis of the specimen at which they are acting. If the normal stress on the end of the specimen was constant, the induced shear stress would increase as the distance from the axis of the specimen increased. However, the normal stress on the end of the specimen also increases as the distance from the axis of the specimen increases, as shown in Figure 3.2. The distribution of normal stress across the ends of the specimen is qualitatively similar to the distribution of normal stresses under a rigid, circular foundation on a semi-infinite elastic half-space. Since the normal stress on the specimen ends increases as the distance from the axis of the specimen increases, the variation of shear stress on the specimen end is magnified. The shear stress

induced by the end platen, then, is a maximum at the radial edge of the end of the specimen and is equal to zero at the axis of the specimen.

As a result of these induced shear stresses, the principal stresses are rotated out of their vertical and horizontal orientations, with the angle of rotation being a maximum at the radial edge of the ends of the specimen. Furthermore, the addition of the shear stresses on the horizontal and vertical planes results in an increase in the principal stress difference for given values of horizontal and vertical stress. The principal stress difference is no longer equal to the difference between the vertical and horizontal stress.

Figure 3.1 shows that due to the friction that develops against the end platen, the vertical stress in the specimen is neither uniform nor a principal stress, as is assumed when reducing triaxial test data. As a result, the horizontal and shear stresses within the specimen are not uniformly distributed either. Since the stresses are not uniformly distributed throughout the specimen, the corresponding strain distributions are also not uniform.

Membrane Stresses

The effects of having the specimen contained by a thin rubber membrane can be summarized as follows:

1.) The membrane can exhibit a resistance to axial load or deformation, so that some of the applied vertical load is carried by the membrane, as shown in Figure 3.3.

2.) As the specimen deforms against the membrane, the membrane can apply a radial compressive stress to the specimen, in addition to the applied cell pressure, as shown in Figure 3.4.

3.) The membrane can induce small shear stresses on the radial surface of the specimen if it does not deform uniformly. If the specimen bulges at its center, the direction of these shear stresses is towards the top of the specimen on the upper half of the radial surface and towards the bottom of the specimen on the lower half of the radial surface.

The capacity of the membrane to resist axial load results in a portion of the applied axial load being balanced by the resistance of the membrane. Thus, the applied axial load is not carried entirely by the soil specimen, as shown in Figure 3.3.

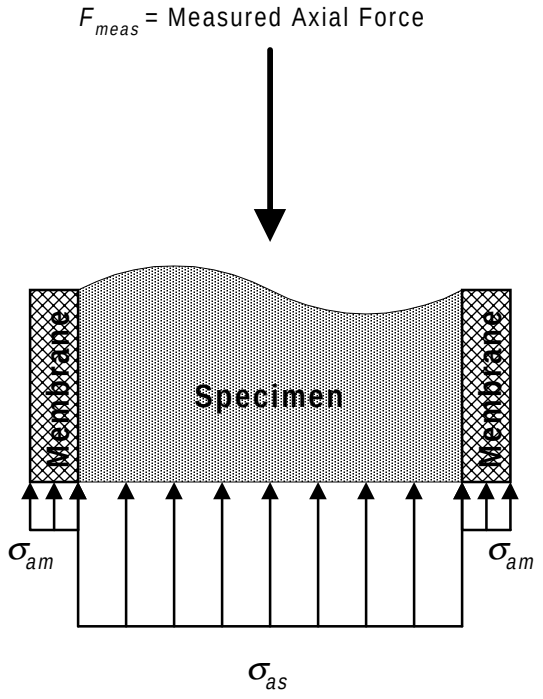

Figure 3.3 - Axial Load Resisted by Membrane

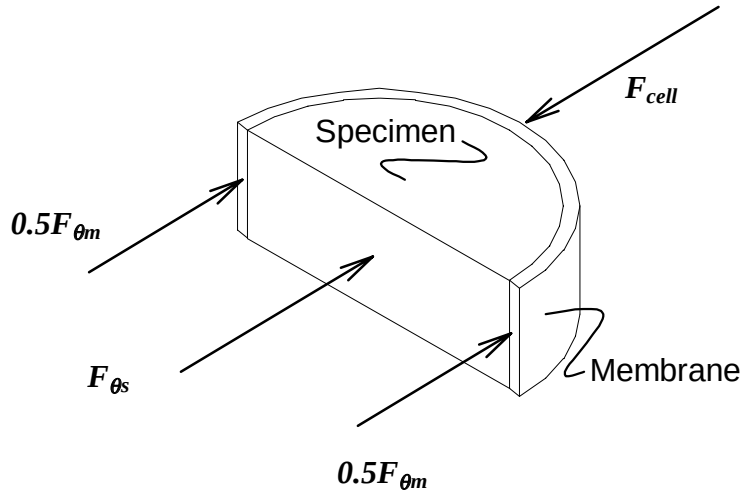

Figure 3.4 - Lateral Load on Specimen Due to Membrane and Cell Pressure

The increase in radial stress due to the membrane, if it occurs, is a result of the circumferential strains in the membrane that can develop due to excessive radial displacement of the specimen. As the membrane is displaced in the radial direction, the membrane stretches in the circumferential direction. This circumferential strain is accompanied by a decrease in circumferential stress, which must be balanced by an increase in the circumferential stress in the soil specimen in order to maintain equilibrium if the cell pressure is constant. The effect of this membrane stretching is analogous to an apparent increase in cell pressure, and increases the confining stress in the specimen.

The shear stresses on the radial surface of the specimen that are induced by the membrane are a result of the nonuniform deformation of the specimen and membrane. If the membrane deforms as a right circular cylinder, these shear stresses will be equal to zero, but in fact, the observed deformation, as a result of the changes in stress mentioned above, is not uniform along the height of the specimen. The observed pattern of deformation for cohesionless soils often exhibits a bulging toward the mid-height of the specimen. While the exact variation of radial deformation may be estimated mathematically by

various means, for the purpose of the present discussion, it is sufficient to note only that the radial deformation is a maximum at the mid-height of the specimen and that it varies along the height of the specimen. The induced shear stresses, then, act on the radial surface of the specimen towards the nearest end. On the upper half of the radial surface, the shear stresses act towards the top of the specimen and on the lower half of the radial surface they act towards the bottom of the specimen. While the shear stresses induced on the radial surface of the specimen are much less significant than the shear stresses induced on the horizontal surfaces by the end platens, their effect is similar. That is, they cause a slight rotation of principal stresses and a slight increase in the principal stress difference.

In general, the combined effects of these deviations from ideal stress and deformation conditions result in a state of stress within the specimen that is not uniform. In addition, throughout a significant portion of the specimen, the horizontal and vertical stresses are not principal stresses, which is a fundamental assumption in the reduction of triaxial test data into meaningful parameters. Qualitatively, the combined effects of the deviations from ideal stress and deformation conditions noted above could be summarized by examining the influence of the deviations at different locations within the specimen volume. While the regions of influence of these deviations have yet to be defined, the qualitative description of their effects is still valid.

Accounting for Imperfect Conditions

In order to derive acceptable data from triaxial tests, these realities associated with actual test conditions must be considered. Two approaches are possible, and both have been utilized for triaxial testing and data reduction (Saada and Townsend 1981, Head 1986, Germaine and Ladd 1988). The first approach is to try to account for the actual test conditions that deviate from the assumed

conditions when reducing the triaxial test data into meaningful parameters. This can be accomplished by developing correction factors to apply to the test data to try to account for the influences of the change in area of the specimen, the membrane, and the end platens. The second approach is to try to achieve the ideal conditions during the test itself by improving measurement capabilities or minimizing the effects that cause deviations from the ideal or assumed conditions. Most attempts at this approach have involved trying to reduce the friction at the end platens via some means of lubrication of the end platens. Another example of this approach is to increase the length of the specimen height/diameter ratio so that the region of the specimen that actually controls failure is located sufficiently far from the effect of the end platens. Since the lateral expansion of the specimen cannot be avoided and eliminating the effects of the membrane stresses during the test is difficult, accounting for these influences is usually accomplished by making corrections to the data.

CHAPTER 4 CORRECTIONS TO TRIAXIAL TEST DATA

The corrections most often applied to triaxial test data can be divided into several major groups: area corrections, membrane corrections, and side drain or filter paper corrections. Since side drains typically are not used for tests on cohesionless soils, which have permeabilities that allow for equalization of pore pressures rather quickly, the side drain corrections will not be discussed here.

The area corrections are applied to triaxial test data to account for the fact that the area of a horizontal cross section of the specimen changes during the test. The vertical normal stress in the specimen is typically calculated by dividing the measured vertical force by the area of the horizontal cross section of the specimen. Since the area changes during the test, but is not typically measured directly, the area corrections provide a means for estimating the changes in area as the specimen deforms during the test. Accounting for the change in area allows more accurate calculation of the vertical normal stress based on the vertical force (axial load) as the test progresses.

The corrections to account for the influence of the membrane can be divided into the following groups: corrections to the axial stress, corrections to the radial stress, and corrections to specimen volume due to membrane penetration effects. The correction to the axial stress is due to the fact that the membrane has an axial load capacity and thus resists a portion of the applied or measured load. The correction to the radial stress is due to the fact that the membrane can exert a stress, in addition to the cell pressure, in the radial direction on the specimen as it deforms laterally. The volume corrections are due to the fact that the membrane can partially fill voids along the surface of the specimen if the effective stress level changes. These penetration effects are usually only considered to be significant at high radial

(lateral) effective stresses and with specimens that have large pore sizes. Pore sizes in gravel specimens have been shown to be large enough to allow significant membrane penetration into the voids (Evans 1992, Evans et al. 1992), but for specimens of materials finer than coarse sands, the effects are often negligible (Newland and Allely 1959, Steinbach 1967, Kiekbusch and Schuppener 1977).

Area Corrections

Right Circular Cylinder

The most widely used and perhaps the simplest area correction is based on the assumption that the specimen deforms as a right circular cylinder (RCC) (Lambe 1951, Bishop and Henkel 1962, Head 1986). Figure 4.1 shows a cylinder undergoing RCC deformation when subjected to an axial load. If this actually occurred, the stresses and strains would be uniform throughout the specimen, and accurate determination of the stress state throughout the specimen would be possible. For this condition to actually occur, of course, the end platens would have to be frictionless and larger than the diameter of the specimen.

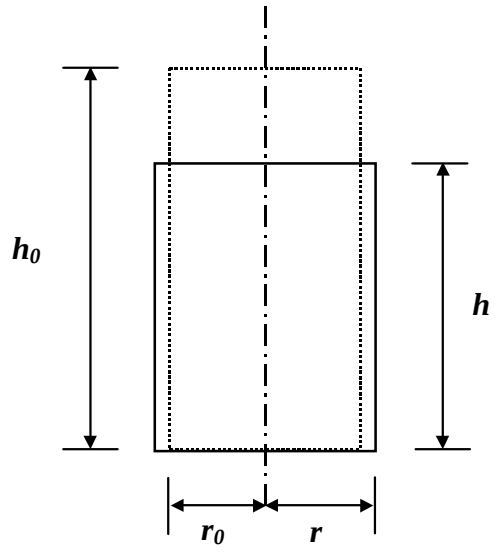

Figure 4.1 - Right Circular Cylinder (RCC) Deformation

Assuming that the strains are uniform throughout the specimen, the axial strain can be defined as the change in specimen height divided by the original height. The volumetric strain is defined as the change in volume divided by the original volume. In keeping with the sign convention most widely used in soil mechanics for stress and strain, the axial and volumetric strains are positive for compression, and are defined by the following equations:

$$\varepsilon_a = 1 - \frac{h}{h_0} \qquad \text{Equation 4.1}$$

$$\varepsilon_V = 1 - \frac{V}{V_0} \qquad \text{Equation 4.2}$$

where: ε_a = axial strain
ε_V = volumetric strain
h = specimen height at strain value of ε_a
h_0 = original specimen height

The corrected area is typically expressed in terms of the original area of the cross section of the specimen. For RCC deformation, the corrected area is expressed by Equation 4.3 as follows:

$$A_{corr} = A_0\left(\frac{1-\varepsilon_V}{1-\varepsilon_a}\right) \qquad \text{Equation 4.3}$$

where: A_{corr} = corrected cross sectional area
A_0 = original cross sectional area
ε_V = volumetric strain
ε_a = axial strain

Equation 4.3 is typically applied to drained test data that includes volume change measurements. For undrained tests, the volume typically does not change, and Equation 4.3 reduces to:

$$A_{corr} = A_0\left(\frac{1}{1-\varepsilon_a}\right) \qquad \text{Equation 4.4}$$

where: A_{corr} = corrected cross sectional area
A_0 = original cross sectional area
ε_a = axial strain

Partial Right Circular Cylinder

A first order approximation of the corrected area for a specimen that, as a result of the end platen friction, does not expand laterally at the ends may be expressed by assuming that a central section of the specimen exhibits RCC deformation while the end sections do not deform laterally. This type of correction is sometimes referred to as the bulging area correction (Germaine and Ladd 1988). The size of this central section may be expressed as a fraction of the specimen height. Figure 4.2 shows an example of partial RCC deformation, where c represents the fraction of the specimen height that expands laterally. A typical value of c might be 0.5, which implies that only the

middle half of the specimen expands laterally and approximates RCC deformation as shown in Figure 4.2.

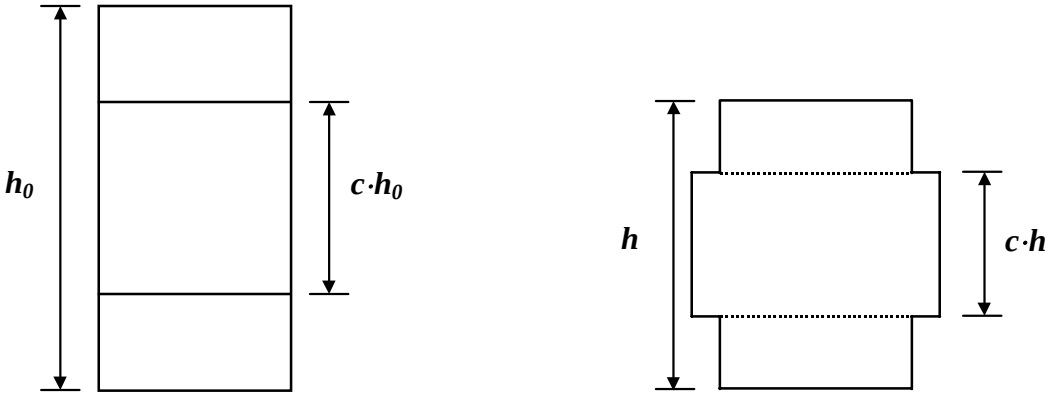

Figure 4.2 - Partial RCC Deformation

Some assumptions regarding the distribution of strain within the specimen are necessary, since the strain is not uniform throughout the entire specimen in this case. If the end sections are assumed to be rigid, then the volumetric, axial, and lateral strains are all zero in the end sections. In this case, any measured deformation corresponds to strain in the central, deformable section. The area correction is expressed by Equation 4.5, in which the average strains are the strains computed based on external measurements assuming uniform strain throughout the specimen, as follows:

$$A_{corr} = A_O \left(\frac{c - \varepsilon_V}{c - \varepsilon_a} \right) \qquad \text{Equation 4.5}$$

where: A_{corr} = corrected cross sectional area
A_O = original cross sectional area
c = fraction of height of the specimen that deforms laterally
ε_V = average volumetric strain
ε_a = average axial strain

Another possible assumption about the distribution of strain is to assume that the lateral strain is zero in the end sections, but that the axial strain is distributed uniformly with height. In this case, the volumetric strain is greater in the end sections than in the middle section, since the axial strain is uniform and lateral expansion can only occur in the central section. Based on these conditions, the area correction may be expressed by Equation 4.6 as follows:

$$A_{corr} = A_O \left[\frac{1-\varepsilon_V}{c(1-\varepsilon_a)} + 1 - \frac{1}{c} \right] \qquad \text{Equation 4.6}$$

where: A_{corr} = corrected cross sectional area
A_O = original cross sectional area
c = fraction of height of the specimen that deforms laterally
ε_V = average volumetric strain
ε_a = average axial strain

A third possible assumption about the distribution of strain is to assume that the lateral strain is zero in the end sections, but that the volume change is distributed uniformly with height. In this case, the axial strain is greater in the end sections than in the central sections since the volumetric strain is equal in all sections of the specimen. For these conditions, the area correction may be expressed by as follows:

$$A_{corr} = A_O \left[\frac{1}{\frac{1-\varepsilon_a}{c(1-\varepsilon_V)} + 1 - \frac{1}{c}} \right] \qquad \text{Equation 4.7}$$

where: A_{corr} = corrected cross sectional area
A_O = original cross sectional area
c = fraction of height of the specimen that deforms laterally
ε_V = average volumetric strain
ε_a = average axial strain

Germaine and Ladd (1988) presented the following equation for the bulging area correction:

$$A_{corr} = A_O\left(\frac{1-\varepsilon_V}{1-a\varepsilon_a}\right) \qquad \text{Equation 4.8}$$

where: A_{corr} = corrected cross sectional area
A_O = original cross sectional area
ε_V = average volumetric strain
ε_a = average axial strain
a = experimental constant between 1 and 2

If the constant a is approximated as the ratio of the total specimen length to the length of the bulging section, as suggested by Germaine and Ladd (1988), then a will be equal to the inverse of c as defined previously. Making this substitution into Equation 4.5 results in the following expression:

$$A_{corr} = A_O\left(\frac{1-a\varepsilon_V}{1-a\varepsilon_a}\right) \qquad \text{Equation 4.9}$$

which differs from the expression presented by Germaine and Ladd (1988) in the fact that a is multiplied by both the volumetric and axial strains. If the average volumetric strain is equal to zero, which corresponds to zero net volume change conditions in undrained tests, then Equation 4.5, Equation 4.7, and Equation 4.8 are all equivalent.

These corrections are used to calculate the cross sectional area of the central, deformable section, so that the vertical normal stresses determined using the correction are the stresses in the central section, or at the specimen mid-height. The calculation of stress based on the partial RCC deformation further assumes that no shear stresses are transferred from the end sections to the central, deformable section, which would certainly not be the case if this type of deformation occurred. Nonetheless, the partial RCC corrections provide a

good first approximation of the deformation and cross-sectional area change that occurs if friction restrains the ends of the specimen.

Parabolic Bulging

A better approximation of the deformed area for cases where the shear stress at the end platens restrains lateral deformation at the specimen ends is based on the assumption that the lateral surface of the deformed specimen assumes a parabolic shape. In other words, the shape of a deformed specimen could be described by rotating a parabola in the r-z plane about the axis of the undeformed cylinder, as shown in Figure 4.3. Germaine and Ladd (1988) presented an equation for corrected area based parabolic deformation for the undrained case only:

$$\frac{A_{corr}}{A_O} = \left\{ -\frac{1}{4} + \frac{\sqrt{25 - 20\varepsilon_a - 5\varepsilon_a{}^2}}{4(1-\varepsilon_a)} \right\}^2 \qquad \text{Equation 4.10}$$

The development of a more general parabolic area correction that includes volume change is detailed in Appendix **B**. If parabolic deformation occurs, the lateral strain varies along the height of the specimen, so the cross sectional area does also. The lateral deformation at the ends of the specimen is constrained, so the cross sectional area at the ends does not change, and the maximum value of the corrected cross-sectional area corresponds to the mid-height of the specimen. When using the parabolic area correction to calculate stresses, this maximum area is typically used.

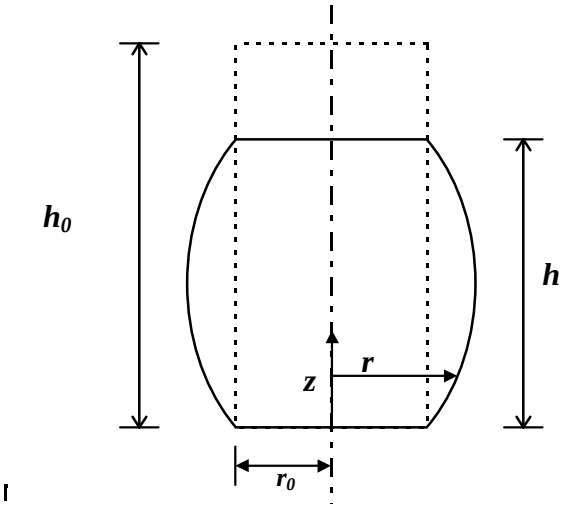

Figure 4.3 - Parabolic or Sinusoidal Deformation

The expression for corrected area at any point along the height of the specimen is:

$$A_{corr} = A_O \cdot \left\{ 1 + \left[\left(\frac{z}{h} \right)^2 - \frac{z}{h} \right] \cdot \left[5 - \sqrt{30 \cdot \left(\frac{1-\varepsilon_v}{1-\varepsilon_a} \right) - 5} \right] \right\}^2 \qquad \text{Equation 4.11}$$

where:
- A_{corr} = corrected cross sectional area
- A_O = original cross sectional area
- ε_V = average volumetric strain
- ε_a = average axial strain
- z = distance from the end of the specimen
- h = specimen height

At the mid-height of the specimen ($z = h/2$), the expression for the parabolic area correction is as follows:

$$\frac{A_{corr}}{A_O} = \left\{ -\frac{1}{4} + \frac{1}{4}\sqrt{30\left(\frac{1-\varepsilon_v}{1-\varepsilon_a}\right) - 5} \right\}^2 \qquad \text{Equation 4.12}$$

where: A_{corr} = corrected cross sectional area
A_O = original cross sectional area
ε_V = average volumetric strain
ε_a = average axial strain

For the undrained condition, when the average volumetric strain is zero, this expression is equivalent to that given by Germaine and Ladd (1988).

Sinusoidal Bulging

Another means of accounting for cross sectional area changes for the case when the specimen ends are restrained, due to end platen friction, from deforming laterally is to assume that the deformed specimen shape is sinusoidal along the specimen height. Figure 4.3 shows the general geometry, coordinate directions, and specimen dimensions for sinusoidal bulging deformation. The expression for the ratio of corrected area to original area in this case is:

$$\frac{A_{corr}}{A_O} = \left[1 + \frac{4}{\pi} \cdot \left(\sqrt{1 + \frac{\pi^2}{8} \cdot \left[\frac{(1-\varepsilon_v)}{(1-\varepsilon_a)} - 1 \right]} - 1 \right) \cdot \sin\left(\pi \cdot \frac{z}{h} \right) \right]^2 \qquad \text{Equation 4.13}$$

where: A_{corr} = corrected cross sectional area
A_O = original cross sectional area
ε_V = average volumetric strain
ε_a = average axial strain
z = height of the point of interest
h = specimen height

At the mid-height of the specimen ($z=h/2$), the expression for Equation 4.13 is:

$$\frac{A_{corr}}{A_O} = \left[1 + \frac{4}{\pi} \cdot \left(\sqrt{1 + \frac{\pi^2}{8} \cdot \left[\frac{(1-\varepsilon_v)}{(1-\varepsilon_a)} - 1 \right]} - 1 \right) \right]^2 \qquad \text{Equation 4.14}$$

where: A_{corr} = corrected cross sectional area
A_O = original cross sectional area
ε_V = average volumetric strain
ε_a = average axial strain

Slip Plane

Another area correction that has been applied to triaxial tests on clays is referred to as the slip plane correction (La Rochelle 1967, Head 1986, La Rochelle et al. 1988). This correction assumes that the specimen deforms by displacing along a inclined shear plane and that the two halves of the specimen are rigid. The equation for the slip plane correction (Head 1986, La Rochelle et al. 1988) is:

$$\frac{A_{corr}}{A_O} = \frac{2}{\pi} \cdot (\beta - \sin\beta \cdot \cos\beta) \qquad \text{Equation 4.15}$$

where: $\beta = \arccos\left(\frac{2 \cdot \varepsilon_a}{\tan\alpha} \right)$
α = inclination of the shear plane

Since the two halves of the specimen are considered rigid, the corrected area actually decreases as axial strain increases, and the effect of applying the correction is to increase the calculated deviator stress. For undrained tests conducted on loose sands, shear planes typically do not develop until relatively large strain levels, if at all. Since the specimen is significantly deformed when a shear plane appears, it is very unlikely that attempting to apply a shear plane correction in these cases would improve the stress determination accuracy. As

a result, the shear plane corrections were not considered for application to the ICU tests performed on loose sand specimens for determination of steady state parameters.

Comparison of Area Corrections

A comparison of the deformed shapes based on the various modes of deformation discussed above is shown in Figure 4.4 at an axial strain of 15% for undrained or zero volume change conditions. Figure 4.5 shows the deformed shapes at an axial strain of 30% for undrained or zero volume change conditions. For the RCC case, the radius, and hence the cross sectional area are constant along the height of the specimen. For the parabolic and sinusoidal cases, the radius, and hence the cross sectional area vary along the height of the specimen. The parabolic and sinusoidal shapes are very nearly identical, but the radius and corrected area at the mid-height of the specimen is slightly greater for the sinusoidal deformation case. The most common approach to selecting which cross sectional area to use when computing stresses is to use the largest cross sectional area. This results in using the area at the mid-height of the specimen, and is considered to be conservative for determining shear strengths since the largest area will yield the lowest stress for any particular measured axial load.

A comparison of corrected radii based on different modes of deformation for a 2.8-inch diameter specimen with no volume change is shown in Table 4.1. Table 4.2 shows the corrected areas for the same specimen. The corrected area increases as axial strain increases if no volume change occurs. Likewise, the variation of corrected area with height for nonuniform deformation modes increases as axial strain increases. The difference between the corrected area based on RCC deformation and the corrected area based on nonuniform deformation also increases as axial strain increases. The variation of radius

with increasing axial strain for the various modes of deformation is shown in Figure 4.6. The variation of corrected area with increasing axial strain for the various modes of deformation is shown in Figure 4.7.

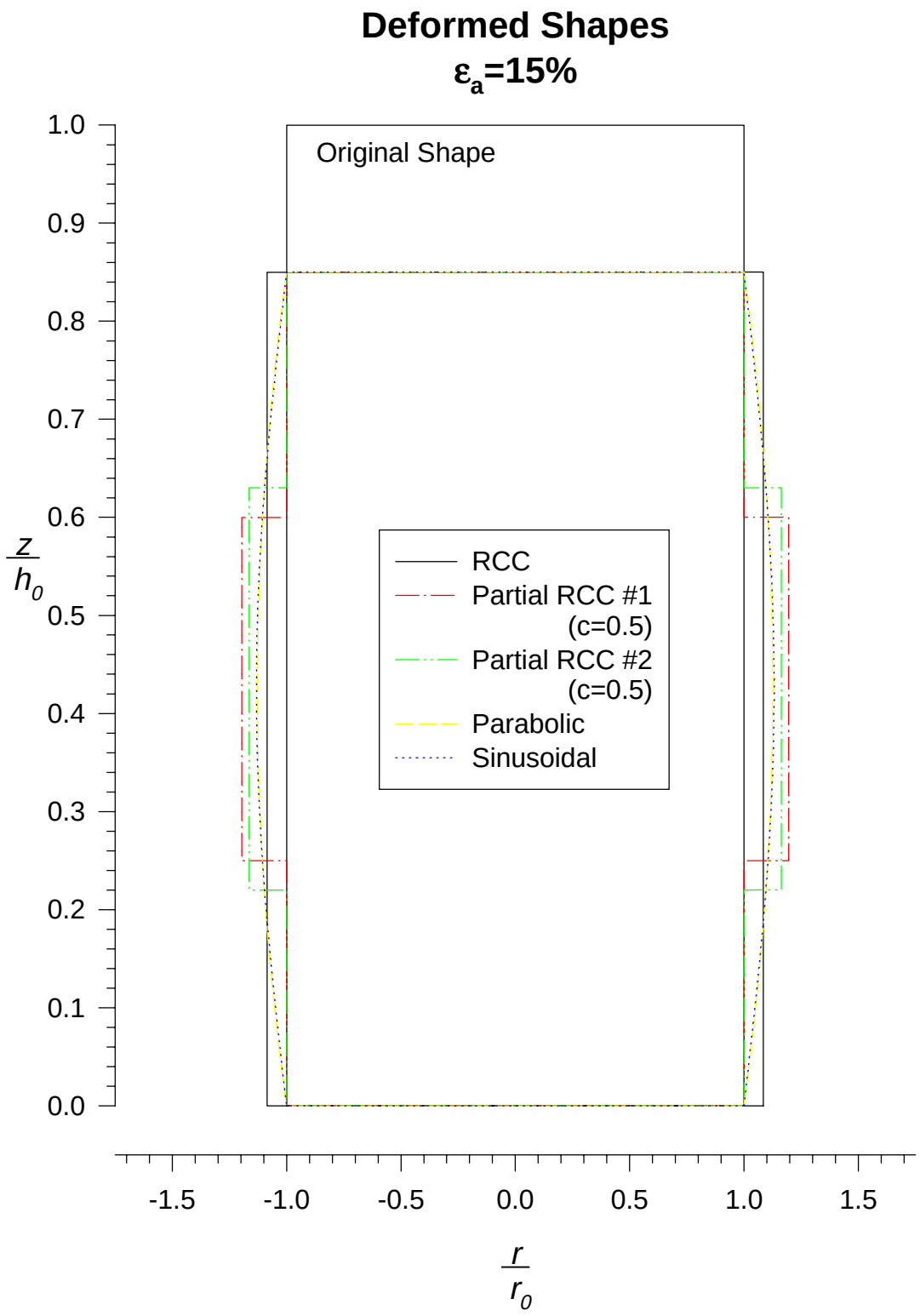

Figure 4.4 - Deformed Shapes at 15% Axial Strain

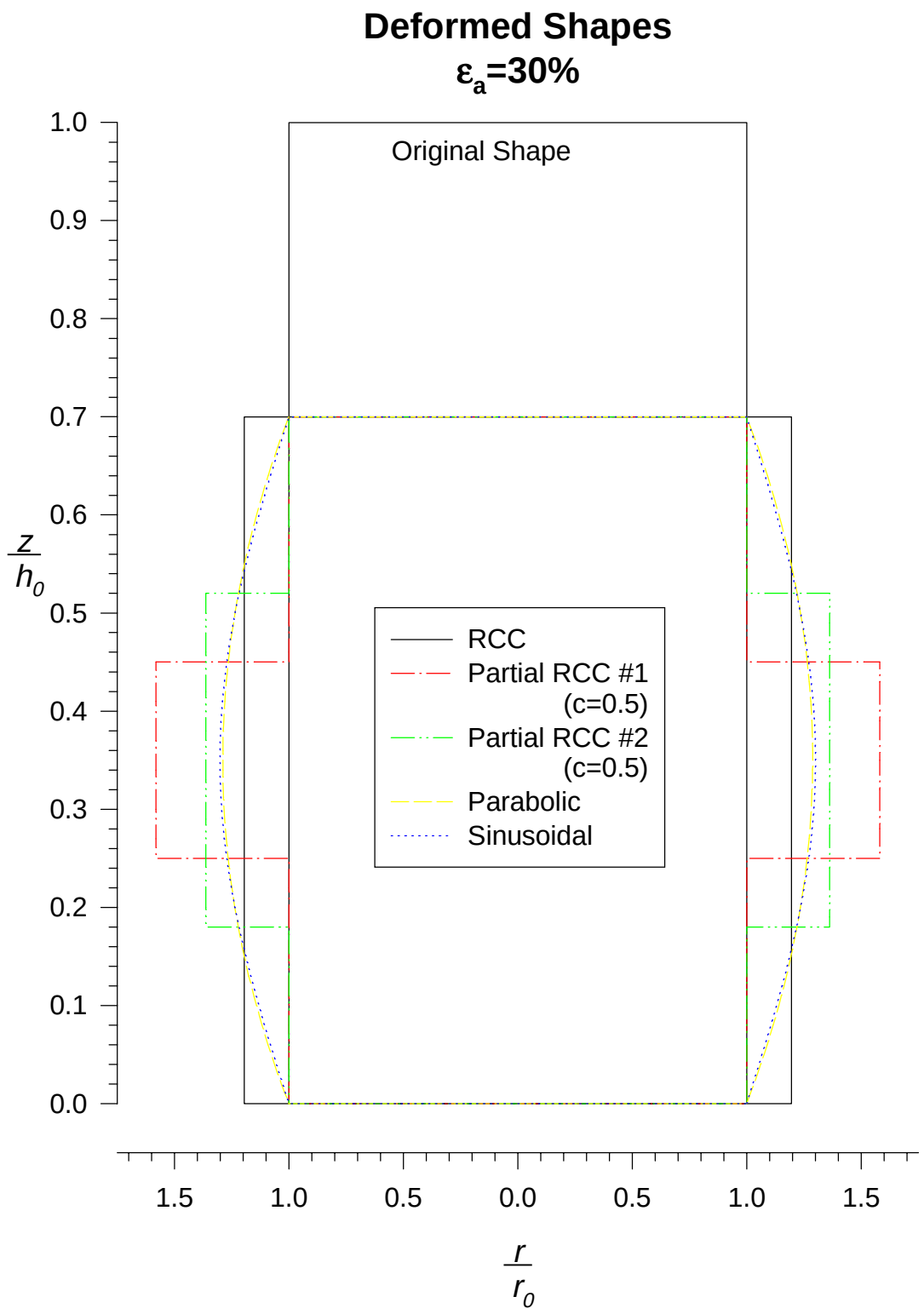

Figure 4.5 - Deformed Shapes at 30% Axial Strain

Table 4.1 - Comparison of Radii for Different Modes of Deformation

	Corrected Normalized Radii (r_{corr}/r_0)					
	ε_a = 15%			ε_a = 30%		
z/h	RCC	Parabolic	Sinusoidal	RCC	Parabolic	Sinusoidal
1.00	1.085	1.000	1.000	1.195	1.000	1.000
0.75	1.085	1.095	1.093	1.195	1.216	1.213
0.67	1.085	1.112	1.114	1.195	1.256	1.261
0.50	1.085	1.126	1.132	1.195	1.288	1.301
0.33	1.085	1.112	1.114	1.195	1.256	1.261
0.25	1.085	1.095	1.093	1.195	1.216	1.213
0.00	1.085	1.000	1.000	1.195	1.000	1.000

Table 4.2 - Comparison of Areas for Different Modes of Deformation

	Corrected Normalized Area (A_{corr}/A_0)					
	ε_a = 15%			ε_a = 30%		
z/h	RCC	Parabolic	Sinusoidal	RCC	Parabolic	Sinusoidal
1.00	1.176	1.000	1.000	1.429	1.000	1.000
0.75	1.176	1.198	1.195	1.429	1.479	1.471
0.67	1.176	1.237	1.241	1.429	1.578	1.589
0.50	1.176	1.268	1.281	1.429	1.659	1.693
0.33	1.176	1.237	1.241	1.429	1.578	1.589
0.25	1.176	1.198	1.195	1.429	1.479	1.471
0.00	1.176	1.000	1.000	1.429	1.000	1.000

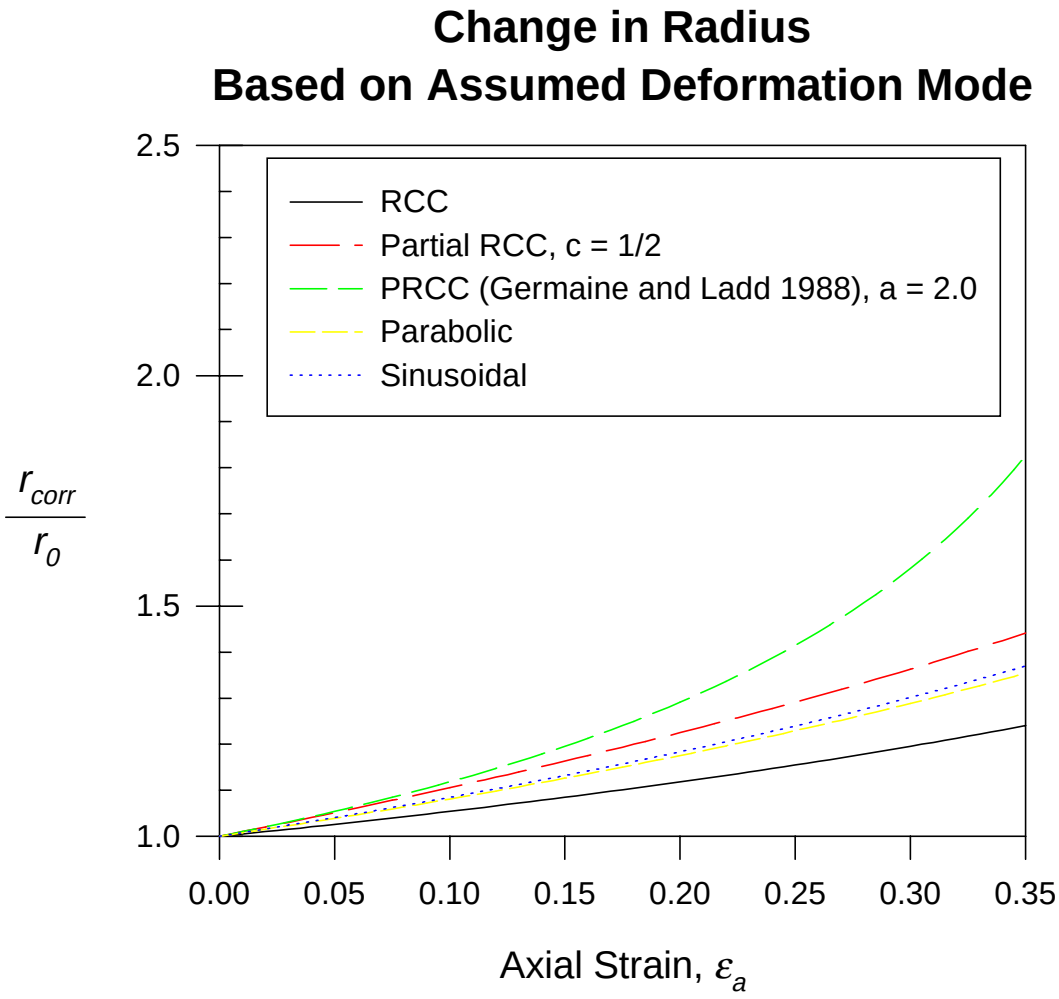

Figure 4.6 - Variation of Radii with Axial Strain for Zero Volume Change

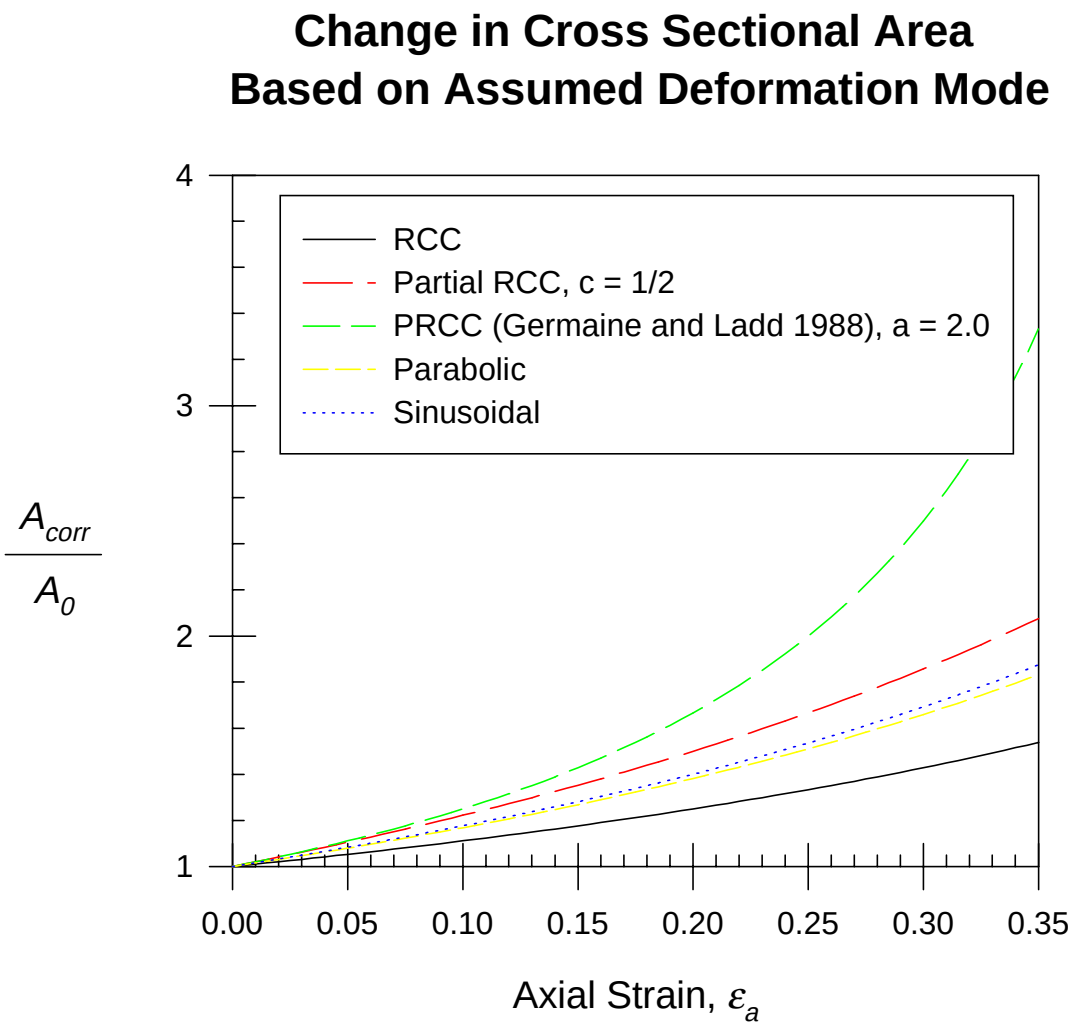

Figure 4.7 - Variation of Area Corrections with Axial Strain

Membrane Stress Corrections

The corrections due to the stresses imposed by the membrane are predominantly dependent on the mode of deformation of the specimen. If RCC deformation is assumed, then the stresses in the membrane in the axial and radial direction are principal stresses since no shear stress develops along the vertical and horizontal planes. In this case, the stresses in the membrane are easily determined based on the deformation of the specimen and the properties of the membrane material.

Henkel and Gilbert

Henkel and Gilbert (1952) published corrections for the effect of the membrane assuming:

1.) The specimen deforms as a right circular cylinder and undergoes no volume change

2.) The membrane is isotropic, linearly elastic, and has equal moduli in compression and tension

3.) Both the soil specimen and membrane are incompressible ($\nu = 0.5$)

4.) The mean diameter of the membrane is constant and is equal to the initial diameter of the specimen

They distinguished between two possible scenarios. In one, the membrane and the specimen deform as a unit, so that the membrane does not buckle, and the membrane acts as a compression shell around the specimen. In this case, they recommended reducing the axial stress in the specimen to account for the axial load carried by the membrane using the following expression:

$$\Delta\sigma_a = \frac{\pi \cdot D \cdot M \cdot \varepsilon \cdot (1-\varepsilon)}{A_{OS}}$$ Equation 4.16

where: $\Delta\sigma_a$ = correction to axial stress (psi)
A_{OS} = initial area of the sample (in^2)
ε = axial strain level
D = initial sample diameter (in)
M = compression modulus of the membrane (lb/in)

In the second case, it is assumed that the membrane buckles and thus carries no axial load. It is further assumed that the total axial length of the membrane remains constant, except for the Poisson effect, as the specimen deforms (Henkel and Gilbert 1952). The correction in this case is based on hoop tension theory, and assumes that the membrane carries no axial load since buckling occurs. Application of this correction increases the confining stress in the specimen. Henkel and Gilbert (1952) suggested correcting the confining stress using the following expression:

$$\Delta\sigma_3 = \frac{2 \cdot M \cdot \left(1-\sqrt{1-\varepsilon}\right)}{D \cdot (1-\varepsilon)}$$ Equation 4.17

where: $\Delta\sigma_3$ = correction to minor principal stress (psi)
M = compression modulus of the membrane (lb/in)
D = initial sample diameter (in)
ε = axial strain level

Henkel and Gilbert (1952) described a procedure for determining an extension modulus that has units of force per length for the membranes. A ring-shaped membrane specimen was prepared by cutting a unit length of the membrane and the specimen was stretched by hanging weights. The measured force-displacement relationship defined the modulus of the membrane. Based on this procedure, membranes having different thicknesses have different moduli. A corresponding modulus of elasticity, with units of force per area, can be determined by accounting for the thickness of the membrane. The

corresponding modulus of elasticity should be independent of thickness, and will depend on the material composition of the membrane, and to a much lesser extent, the strain level. For purposes of comparison, the modulus used by Henkel and Gilbert (1952) can be approximated as the modulus of elasticity of the membrane material multiplied by the thickness of the membrane.

Duncan and Seed

Duncan and Seed (1965, 1967) also published corrections for the membrane stresses based on RCC deformation, but allowed for volume change of the specimen during shear and recognized that the membrane stresses developed due to a combination of the two types of loading described by Henkel and Gilbert. In addition, they used the modulus of elasticity and Poisson's ratio for the properties of the membrane. Their corrections are based on the following assumptions:

1.) The specimen deforms as a right circular cylinder
2.) The membrane is linearly elastic and has equal moduli in compression and tension
3.) The membrane is incompressible ($\nu = 0.5$)
4.) The membrane deforms uniformly with the specimen (no buckling)
5.) The mean radius of the membrane is equal to the radius of the specimen

Duncan and Seed (1965) first derived expressions for the stresses in the membrane assuming that the axial strain in the specimen and the axial strain in the membrane are equal, and that both the specimen and the membrane are incompressible and deform uniformly as a right circular cylinder. They based the strains on linear strain-displacement relationships, but accounted for nonlinear terms to determine volume change. Based on these conditions, the

expressions developed by Duncan and Seed (1965) for the stresses in the membrane are as follows:

$$\sigma_{zm} = \frac{2E_m}{3}\left[1 + 2\varepsilon_{at} - \sqrt{\frac{1-\varepsilon_V}{1-\varepsilon_{at}}}\right] \qquad \text{Equation 4.18}$$

$$\sigma_{cm} = \frac{2E_m}{3}\left[2 + \varepsilon_{at} - 2\sqrt{\frac{1-\varepsilon_V}{1-\varepsilon_{at}}}\right] \qquad \text{Equation 4.19}$$

where: σ_{zm} = vertical stress in the membrane
σ_{cm} = circumferential stress in the membrane
E_m = modulus of elasticity of the membrane
ε_{at} = total axial strain
ε_V = volumetric strain

The expression for the corrections to the axial and lateral stress based on the stresses in the membrane proposed by Duncan and Seed are:

$$\Delta\sigma_{am} = -\sigma_{zm}\frac{A_m}{A_s} \qquad \text{Equation 4.20}$$

$$\Delta\sigma_{lm} = -\sigma_{cm}\frac{t_m}{r_s} \qquad \text{Equation 4.21}$$

where: $\Delta\sigma_{am}$ = correction to axial stress
$\Delta\sigma_{lm}$ = correction to lateral stress
A_m = membrane cross sectional area
A_s = specimen cross sectional area
t_m = membrane thickness
r_s = specimen radius

Assuming that RCC deformation occurs and that the mean radius of the membrane is equal to the radius of the specimen, but allowing for net volume change to occur, Duncan and Seed (1967) presented the following expressions

for the corrections to the axial and lateral stresses based on the stresses in the membrane as determined by Equation 4.18 and Equation 4.19:

$$\Delta\sigma_{am} = -\frac{2E_m}{3}\left[1+2\varepsilon_{at}-\sqrt{\frac{1-\varepsilon_V}{1-\varepsilon_{at}}}\right]\frac{A_{om}}{A_{os}(1-\varepsilon_V)} \qquad \text{Equation 4.22}$$

$$\Delta\sigma_{lm} = -\frac{2E_m}{3}\left[2+\varepsilon_{at}-2\sqrt{\frac{1-\varepsilon_V}{1-\varepsilon_{at}}}\right]\frac{t_{om}}{r_{os}(1-\varepsilon_V)} \qquad \text{Equation 4.23}$$

where:
A_{om} = initial membrane cross sectional area
A_{os} = initial specimen cross sectional area
t_{om} = initial membrane thickness
r_{os} = initial specimen radius

Geometric Approximations in the RCC Solution

Returning to Equation 4.20 and Equation 4.21 for the corrected stresses, the accuracy associated with the assumptions about the radius of the membrane can be investigated. For RCC deformation, the exact expression for the ratio of membrane cross sectional area to specimen cross sectional area, which is used to calculate the axial stress correction, is given by:

$$\frac{A_m}{A_s} = \frac{A_{om}}{A_{os}(1-\varepsilon_V)} = \frac{1}{(1-\varepsilon_V)}\cdot\left[2\cdot\frac{t_{om}}{r_{os}}+\left(\frac{t_{om}}{r_{os}}\right)^2\right] \qquad \text{Equation 4.24}$$

where:
A_m = membrane cross sectional area
A_s = specimen cross sectional area
A_{om} = initial membrane cross sectional area
A_{os} = initial specimen cross sectional area
ε_V = volumetric strain
t_{om} = initial membrane thickness
r_{os} = initial specimen radius

Assuming that the mean radius of the membrane is equal to the radius of the specimen as Duncan and Seed (1967) did results in the following expression for the ratio of the cross sectional areas:

$$\frac{A_m}{A_s} = \frac{A_{om}}{A_{os}(1-\varepsilon_V)} = \frac{1}{(1-\varepsilon_V)} \cdot \left(\frac{2t_{om}}{r_{os}} \right) \qquad \text{Equation 4.25}$$

As can be seen from comparing Equation 4.24 to Equation 4.25, the effect of assuming that the mean radius of the membrane is equal to the radius of the specimen is equivalent to ignoring the higher order term in Equation 4.24. Since the ratio of membrane thickness to specimen radius is typically very small, neglecting the higher order term results in a very small error in the calculated ratio of cross sectional areas that is used to calculate the axial stress correction in Equation 4.20.

For RCC deformation, the exact expression for the ratio of membrane thickness to specimen radius, which is used to calculate the lateral stress correction in Equation 4.21, is given by:

$$\frac{t_m}{r_s} = \sqrt{1 + \frac{1}{(1-\varepsilon_V)} \cdot \left[2 \cdot \frac{t_{om}}{r_{os}} + \left(\frac{t_{om}}{r_{os}} \right)^2 \right]} - 1 \qquad \text{Equation 4.26}$$

where: t_m = membrane thickness
r_s = specimen radius

Assuming that the mean radius of the membrane is equal to the radius of the specimen as Duncan and Seed (1967) did results in the following expression for the ratio of membrane thickness to specimen radius:

$$\frac{t_m}{r_s} = \frac{t_{om}}{r_{os} \cdot (1 - \varepsilon_V)}$$ Equation 4.27

While the effect of assuming that the mean radius of the membrane is equal to the radius of the specimen is not as easily identified from Equation 4.26 and Equation 4.27, it can be readily seen that the two expressions are equivalent if the volumetric strain is equal to zero, as would be the case in an undrained test. If the volumetric strain is not equal to zero, then some error will be introduced by approximating the mean membrane radius with the specimen radius, and the magnitude of the error increases as volumetric strain increases. For a given volumetric strain level, the error increases as the ratio of thickness to radius increases. Since this ratio is typically very small, the error associated with using the approximate membrane radius should be insignificant.

Equilibrium Considerations for RCC Deformation

In general, the radial and circumferential strains in the membrane are not necessarily constant across the thickness of membrane. Average strains can be determined by integration, and in some cases, the strains do not vary. Figure 4.8 shows the components contributing to the vertical force equilibrium of the membrane and specimen. Figure 4.9 shows the components contributing to the horizontal force equilibrium of the membrane and specimen.

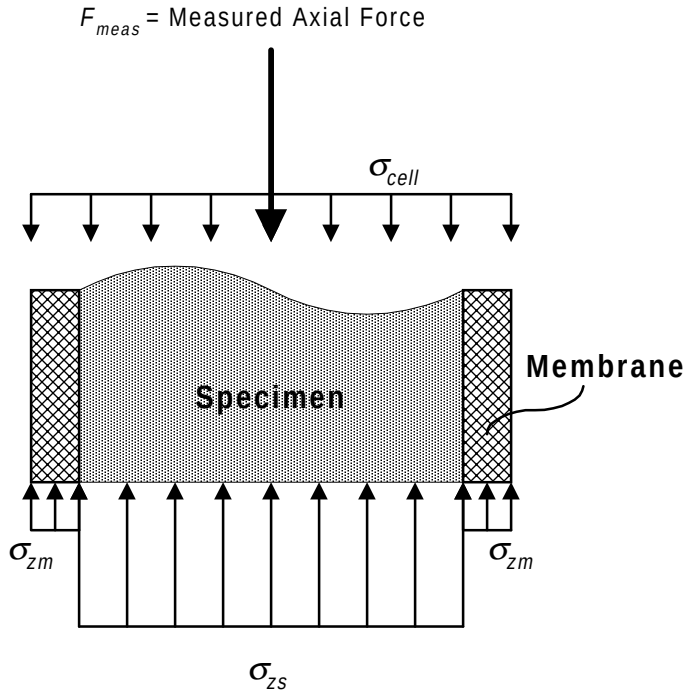

Figure 4.8 - Vertical Force Equilibrium for the Specimen and Membrane

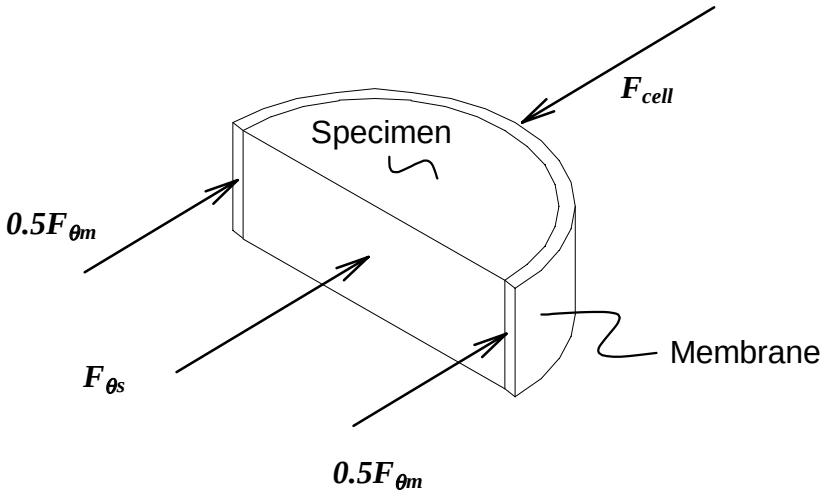

Figure 4.9 - Horizontal Force Equilibrium for the Specimen and Membrane

Based on the average stresses in the soil specimen and membrane, horizontal and vertical force equilibrium requires that:

$$\left(\sigma_{\theta s}\right)_{avg} = \sigma_{cell} + \left[\sigma_{cell} - \left(\sigma_{\theta m}\right)_{avg}\right] \cdot \left(\frac{t_m}{r_s}\right) \qquad \text{Equation 4.28}$$

$$\sigma_{zs} = \frac{F_{meas}}{A_s} - \left(\sigma_{zm} - \sigma_{cell}\right) \cdot \left(\frac{A_m}{A_s}\right) + \sigma_{cell} \qquad \text{Equation 4.29}$$

where:
$\left(\sigma_{\theta s}\right)_{avg}$ = average circumferential stress in the specimen
$\left(\sigma_{\theta m}\right)_{avg}$ = average circumferential stress in the membrane
σ_{zs} = average axial stress in the specimen
σ_{zm} = average axial stress in the membrane
σ_{cell} = cell pressure
F_{meas} = measured axial force
t_m = actual membrane thickness
r_s = actual specimen radius
A_m = actual membrane cross-sectional area
A_s = actual specimen cross-sectional area

The corrections applied to the lateral stress and axial deviator stress, respectively, are:

$$\Delta\sigma_{\theta s} = \left[\sigma_{cell} - \left(\sigma_{\theta m}\right)_{avg}\right] \cdot \left(\frac{t_m}{r_s}\right) \qquad \text{Equation 4.30}$$

$$\Delta\sigma_{zs} = -\left(\sigma_{zm} - \sigma_{cell}\right) \cdot \left[\frac{A_m}{A_s}\right] \qquad \text{Equation 4.31}$$

where:
$\Delta\sigma_{\theta s}$ = correction to lateral stress in the specimen
$\Delta\sigma_{zs}$ = correction to axial deviator stress in the specimen

Application of the appropriate corrections requires that the ratio of membrane area to specimen area and the ratio of membrane thickness to specimen radius are known. These ratios are defined by:

$$\frac{A_m}{A_s} = \frac{1}{(1-\varepsilon_V)} \cdot \left[2 \cdot \frac{t_{om}}{r_{os}} + \left(\frac{t_{om}}{r_{os}} \right)^2 \right] \qquad \text{Equation 4.32}$$

$$\frac{t_m}{r_s} = \sqrt{1 + \frac{1}{(1-\varepsilon_V)} \cdot \left[2 \cdot \frac{t_{om}}{r_{os}} + \left(\frac{t_{om}}{r_{os}} \right)^2 \right]} - 1 \qquad \text{Equation 4.33}$$

RCC Solution for Stresses in the Membrane

A solution for stresses in the membrane resulting from RCC deformation due to an axial load and an applied external pressure can be determined by superposing the solution for a thick-walled cylinder subjected to internal and external pressures with the solution for a thick-walled cylinder subjected to an axial load. Solutions for these individual problems can be found in many classical elasticity and engineering mechanics texts (Den Hartog 1952, Timoshenko and Goodier 1970, Saada 1974, Boresi et al. 1978). Appendix C provides details of the derivation of the solution. The expressions for the stresses in the membrane are:

$$\sigma_r = \frac{P_o \cdot b^2 \cdot \left(1 - \frac{a^2}{r^2}\right) - P_i \cdot a^2 \cdot \left(1 - \frac{b^2}{r^2}\right)}{b^2 - a^2} \qquad \text{Equation 4.34}$$

$$\sigma_z = P_a \qquad \text{Equation 4.35}$$

$$\sigma_\theta = \frac{P_o \cdot b^2 \cdot \left(1 + \frac{a^2}{r^2}\right) - P_i \cdot a^2 \cdot \left(1 + \frac{b^2}{r^2}\right)}{b^2 - a^2} \qquad \text{Equation 4.36}$$

and the corresponding expressions for the strains in the membrane are:

$$\varepsilon_r = \frac{1}{E}\left\{\frac{\left(P_o \cdot b^2 - P_i \cdot a^2\right)\cdot(1-\nu) - \frac{a^2 \cdot b^2}{r^2}\cdot\left(P_o - P_i\right)\cdot(1+\nu)}{b^2 - a^2} - P_a \cdot \nu\right\} \qquad \text{Equation 4.37}$$

$$\varepsilon_z = \frac{1}{E}\left\{P_a - \frac{\left(P_o \cdot b^2 - P_i \cdot a^2\right)}{b^2 - a^2}\cdot 2 \cdot \nu\right\} \qquad \text{Equation 4.38}$$

$$\varepsilon_\theta = \frac{1}{E}\left\{\frac{\left(P_o \cdot b^2 - P_i \cdot a^2\right)\cdot(1-\nu) + \frac{a^2 \cdot b^2}{r^2}\cdot\left(P_o - P_i\right)\cdot(1+\nu)}{b^2 - a^2} - P_a \cdot \nu\right\} \qquad \text{Equation 4.39}$$

where: σ_r = radial stress
σ_z = axial stress
σ_θ = circumferential stress
ε_r = radial strain
ε_z = axial strain
ε_θ = circumferential strain
P_a = axial pressure
P_i = internal pressure
P_o = external pressure
a = radius of inner surface
b = radius of outer surface
r = radial coordinate
E = modulus of elasticity
ν = Poisson's ratio

These equations demonstrate that for the boundary conditions imposed, all stresses and strains are independent of the axial and circumferential coordinates since RCC deformation is assumed. Furthermore, the axial stress and the axial strain are independent of position entirely, and are thus constant at all points in the cylinder. The radial and circumferential stresses and strains depend on the stresses applied to inner and outer surfaces of the cylinder as well as the radial coordinate at the point of interest. In general, neither the radial and circumferential stresses nor the radial and circumferential strains are equal. Comparing Equation 4.34 and Equation 4.36 shows that a necessary and sufficient condition for equal radial and circumferential stresses is that the internal and external pressures are equal. Likewise, comparing Equation 4.37 and Equation 4.39 shows that a necessary and sufficient condition for equal radial and circumferential strains is that the internal and external pressures are equal. Since a radial stress correction due to the effects of the membrane implicitly requires that the internal and external pressures, are not equal, any radial stress correction developed must recognize the difference and variation in radial and circumferential stresses and strains.

Special Cases of the Superposed Solution

The solution can be examined for a homogeneous right circular cylinder subjected to an axial and radial pressure. In this case, which corresponds to a = 0, the stresses and strains are:

$$\sigma_r = \sigma_\theta = P_o \qquad \varepsilon_r = \varepsilon_\theta = \frac{1}{E}\cdot\left[P_o\cdot(1-\nu) - P_a\cdot\nu\right]$$

$$\sigma_z = P_a \qquad \varepsilon_z = \frac{1}{E}\cdot\left[P_a - P_o\cdot(2\cdot\nu)\right]$$

This solution demonstrates that the stresses and strains within a uniform right circular cylinder are homogeneous since they are independent of position. In addition, the radial and circumferential stresses are equal and the radial and circumferential strains are equal. Examples to which these conditions apply are the triaxial loading of a specimen without a membrane, or to the loading of the specimen and the membrane together if the material properties of each are identical.

If the material properties of the specimen and the membrane are identical, the problem is analogous to a uniform right circular cylinder having a radius equal to the radius of the specimen plus the thickness of the membrane. In this case, the internal pressure is equal to the external pressure, so the membrane has no influence on the radial stress in the specimen. The axial stress is constant throughout both the specimen and membrane.

If the two materials do not have identical properties, the uniform cylinder problem (soil specimen) and the hollow cylinder problem (membrane) can be solved simultaneously. The values of pressure applied to each will not necessarily be equal. The boundary conditions imposed are:

1.) The axial strain in each cylinder is equal: $\varepsilon_{zm} = \varepsilon_{zs} = \varepsilon_a$

2.) The radial displacements at the specimen-membrane interface are equal: $u_{rm} = u_{rs}$ at $r = a$, which requires that $\varepsilon_{\theta m} = \varepsilon_{rs}$

3.) The radial stress at the specimen-membrane interface are equal: $\sigma_{rm} = \sigma_{rs}$ at $r = a$

The solution for the stresses under combined loading of the specimen and membrane in this case is:

$$\sigma_{rs} = P_i$$
$$\sigma_{zs} = \varepsilon_a \cdot E_s + 2 \cdot \nu_s \cdot P_i$$
$$\sigma_{\theta s} = P_i$$

$$\sigma_{rm} = \frac{P_o \cdot b^2 \cdot \left(1 - \frac{a^2}{r^2}\right) - P_i \cdot a^2 \cdot \left(1 - \frac{b^2}{r^2}\right)}{b^2 - a^2}$$
$$\sigma_{zm} = \varepsilon_a \cdot E_m + \frac{2 \cdot \nu_m}{b^2 - a^2} \cdot \left(P_o \cdot b^2 - P_i \cdot a^2\right)$$
$$\sigma_{\theta m} = \frac{P_o \cdot b^2 \cdot \left(1 + \frac{a^2}{r^2}\right) - P_i \cdot a^2 \cdot \left(1 + \frac{b^2}{r^2}\right)}{b^2 - a^2}$$

where:

$$P_i = \frac{\varepsilon_a \cdot E_m \cdot \left(b^2 - a^2\right) \cdot \left(\nu_s - \nu_m\right) + 2 \cdot P_o \cdot b^2 \cdot \left(1 + \nu_m\right) \cdot \left(1 - \nu_m\right)}{\left\{\frac{E_m}{E_s} \cdot \left(b^2 - a^2\right) \cdot \left(1 + \nu_s\right) \cdot \left(1 - 2 \cdot \nu_s\right) + \left[a^2 \cdot \left(1 + \nu_m\right) \cdot \left(1 - 2 \cdot \nu_m\right) + b^2 \cdot \left(1 + \nu_m\right)\right]\right\}}$$

Equation 4.40

If the material properties of both materials are identical, then $P_i = P_o$ and the solution is identical to that for the uniform cylinder.

If both materials have a value of Poisson's ratio of one half, then again $P_i = P_o$, and the expressions for the stresses are:

$$\sigma_{rs} = \sigma_{cell}$$
$$\sigma_{zs} = \varepsilon_a \cdot E_s + \sigma_{cell}$$
$$\sigma_{\theta s} = \sigma_{cell}$$

$$\sigma_{rm} = \sigma_{cell}$$
$$\sigma_{zm} = \varepsilon_a \cdot E_m + \sigma_{cell}$$
$$\sigma_{\theta m} = \sigma_{cell}$$

The internal and external pressures are equal, and the stresses and strains in each material are homogeneous. However, the axial stresses in the two materials are not equal because the elastic moduli are different Since the lateral stresses are equal everywhere, the membrane has no effect on the lateral stresses in the specimen, implying that no lateral stress correction is required under these conditions.

This case is analogous to an undrained triaxial test in which the specimen and the membrane are both incompressible and RCC deformation occurs. The solution demonstrates that in the case of RCC deformation and zero volume change conditions no correction to the radial stress in the specimen due to membrane stress effects is warranted. An axial stress correction is applicable to account for the axial load carried by the membrane. The correction to the axial stress is based on Equation 4.31 and can be expressed by:

$$\Delta\sigma_{zs} = -E_m \cdot \varepsilon_a \cdot \left[2 \cdot \left(\frac{t_m}{r_s} \right) + \left(\frac{t_m}{r_s} \right)^2 \right] \qquad \text{Equation 4.41}$$

General Superposed Solution Based on Radial Displacement

Returning to the more general case of a hollow cylinder, at the inner surface of the cylinder, $r = a$, and the lateral stresses and strains are:

$$\sigma_r = P_i$$

$$\sigma_\theta = \frac{2 \cdot P_o \cdot b^2 - P_i \cdot \left(a^2 + b^2 \right)}{b^2 - a^2}$$

$$\varepsilon_r = \frac{1}{E} \left\{ P_i - \left[\frac{P_o \cdot \left(2 \cdot b^2 \right) - P_i \cdot \left(a^2 + b^2 \right)}{b^2 - a^2} + P_a \right] \cdot \nu \right\}$$

$$\varepsilon_\theta = \frac{1}{E} \left[\frac{P_o \cdot \left(2 \cdot b^2 \right) - P_i \cdot \left(a^2 + b^2 \right)}{b^2 - a^2} - \left(P_i + P_a \right) \cdot \nu \right]$$

At the outer surface of the cylinder, $r = b$, and the lateral stresses and strains are:

$$\sigma_r = P_o$$

$$\sigma_\theta = \frac{P_o \cdot \left(b^2 + a^2\right) - 2 \cdot P_i \cdot a^2}{b^2 - a^2}$$

$$\varepsilon_r = \frac{1}{E}\left\{P_o - \left[\frac{P_o \cdot \left(a^2 + b^2\right) - P_i \cdot \left(2 \cdot a^2\right)}{b^2 - a^2} + P_a\right] \cdot \nu\right\}$$

$$\varepsilon_\theta = \frac{1}{E}\left[\frac{P_o \cdot \left(a^2 + b^2\right) - P_i \cdot \left(2 \cdot a^2\right)}{b^2 - a^2} - \left(P_o + P_a\right) \cdot \nu\right]$$

If the geometry and material properties are known, the six equations (Equation 4.34 through Equation 4.39) for the stresses and strains in the membrane contain nine unknowns: the three normal stresses, the three normal strains, and the three pressures. In order to solve the equations, three additional equations must be provided by applying boundary conditions. In the case of a typical triaxial test, the axial pressure applied to the membrane is not known, but the axial displacement is measured. Based on the axial displacement, the average axial strain can be calculated. Equation 4.37

Equation 4.38 shows that the axial strain in the membrane is constant throughout the membrane, and therefore is equal to the average axial strain. This relationship provides one boundary condition:

$$\varepsilon_{zm} = \varepsilon_a = \frac{-\Delta h}{h_0} \qquad \text{Equation 4.42}$$

The external pressure is known, and is equal to the cell pressure, which constitutes a second boundary condition:

$$P_o = \sigma_{cell}$$ Equation 4.43

The internal pressure, which represents the contact stress between the soil specimen and the membrane, is often assumed to be equal to the external, or cell pressure, but is generally unknown. The internal pressure is the actual confining stress (in terms of total stress) acting on the soil specimen. Since the internal pressure is unknown, the third boundary condition is based on displacement compatibility between the soil specimen and the membrane and an assumed lateral deformation in the specimen.

In more general terms, if no material properties of the membrane or specimen are necessarily equal, the radial and circumferential stress and strain fields will be uniform provided that the radial displacement at the specimen-membrane interface is equal to the radial displacement at the inner surface of the membrane due only to the Poisson effect under axial compression. Again, this condition is satisfied if the ratio of lateral strain to axial strain (Poisson's ratio for small strain) is equal for both the specimen and the membrane.

If the membrane is incompressible, but the specimen is compressible and tends to contract during shear, the radial displacement in the specimen will be less than the radial displacement in the membrane at the specimen-membrane interface. In this case, since the membrane is not supported along its inner surface by the specimen, the membrane will likely buckle under the axial load. If the membrane buckles, it will transmit the cell pressure to the specimen, but will have no influence on the radial stress in the specimen. Likewise, the membrane will most likely provide little or no resistance to axial load if it buckles. Qualitatively, at least, an argument could be made that no corrections should be applied due to the stresses in the membrane in triaxial tests in which the soil specimen is contractive and volume change occurs.

If the membrane is incompressible, but the specimen is compressible and tends to dilate during shear, the radial displacement at the surface of the specimen will be greater than the radial displacement that would develop in the membrane at the specimen-membrane interface solely due to the axial load and the Poisson effect. In this case, the displacement at the specimen-membrane interface is continuous and is controlled by the expansion of the soil specimen. The increase in radial displacement results in a decrease in the circumferential strain in the membrane, an increase in the radial strain, and no change in the axial strain compared to the zero volume change case (compressive strain is positive). These changes in strain result in a decrease in the axial and circumferential stresses in the membrane and an increase in the radial stress in the membrane, except at its outer surface. These stress changes result in an increase in the lateral stress in the soil specimen, which can be accounted for by applying a correction to the radial stress. A correction for the axial load resisted by the membrane is applicable, but the magnitude of the correction will be reduced since the axial stress in the membrane is reduced.

The required third boundary condition is based on the radial displacement at the inner surface of the membrane. Using Equation 4.39 for the circumferential strain and the linear strain-displacement relationship, the radial displacement at the inner surface ($r = a$) can be expressed in terms of the pressures as follows:

$$\left(u_{rm}\right)_{r=a} = -a \cdot \left(\varepsilon_{\theta m}\right)_{r=a}$$

$$\left(u_{rm}\right)_{r=a} = -\frac{a}{E}\left\{\frac{P_o \cdot 2 \cdot b^2 - P_i \cdot \left[a^2 \cdot \left(1-\nu\right) + b^2 \cdot \left(1+\nu\right)\right]}{b^2 - a^2} - P_a \cdot \nu\right\} \qquad \text{Equation 4.44}$$

Solving the three equations for the normal strains (Equation 4.37 through Equation 4.39) and the three equations representing the boundary conditions

(Equation 4.42, Equation 4.43, Equation 4.44) results in the following expressions for the axial, internal, and external pressures:

$$P_a = E \cdot \varepsilon_a + \frac{2 \cdot \nu \cdot \left\{ \sigma_{cell} \cdot b^2 + \frac{E \cdot a^2}{1+\nu} \cdot \left[\nu \cdot \varepsilon_a - \frac{1}{a} \left(u_{rm} \right)_{r=a} \right] \right\}}{a^2 \cdot (1-2 \cdot \nu) + b^2}$$

$$P_i = \frac{2 \cdot \sigma_{cell} \cdot b^2 \cdot (1-\nu) - \frac{E}{1+\nu} \cdot \left(b^2 - a^2 \right) \cdot \left[\nu \cdot \varepsilon_a - \frac{1}{a} \left(u_{rm} \right)_{r=a} \right]}{a^2 \cdot (1-2 \cdot \nu) + b^2}$$

$$P_o = \sigma_{cell}$$

The solution for the stresses in the membrane is:

$$\sigma_{rm} = \sigma_{cell} \cdot \frac{1 + \frac{a^2}{r^2} \cdot (1-2 \cdot \nu)}{1 + \frac{a^2}{b^2} \cdot (1-2 \cdot \nu)} + \frac{E}{1+\nu} \cdot \frac{\cdot \left(1 - \frac{b^2}{r^2} \right)}{(1-2 \cdot \nu) + \frac{b^2}{a^2}} \cdot \left[\nu \cdot \varepsilon_a - \frac{1}{a} \cdot \left(u_{rm} \right)_{r=a} \right] \qquad \text{Equation 4.45}$$

$$\sigma_{zm} = E \cdot \varepsilon_a + \frac{2 \cdot \nu}{a^2 \cdot (1-2 \cdot \nu) + b^2} \cdot \left\{ \sigma_{cell} \cdot b^2 + \frac{E}{(1+\nu)} \cdot a^2 \cdot \left[\nu \cdot \varepsilon_a - \frac{1}{a} \cdot \left(u_{rm} \right)_{r=a} \right] \right\} \qquad \text{Equation 4.46}$$

$$\sigma_{\theta m} = \sigma_{cell} \cdot \frac{1 - \frac{a^2}{r^2} \cdot (1-2 \cdot \nu)}{1 + \frac{a^2}{b^2} \cdot (1-2 \cdot \nu)} + \frac{E}{1+\nu} \cdot \frac{\cdot \left(1 + \frac{b^2}{r^2} \right)}{(1-2 \cdot \nu) + \frac{b^2}{a^2}} \cdot \left[\nu \cdot \varepsilon_a - \frac{1}{a} \cdot \left(u_{rm} \right)_{r=a} \right] \qquad \text{Equation 4.47}$$

If Poisson's ratio is equal to one half:

$$\sigma_{rm} = \sigma_{cell} + \frac{2 \cdot E \cdot a^2}{3 \cdot b^2} \cdot \left(1 - \frac{b^2}{r^2}\right) \cdot \left[\frac{1}{2} \cdot \varepsilon_a - \frac{1}{a} \cdot \left(u_{rm}\right)_{r=a}\right]$$

$$\sigma_{zm} = \sigma_{cell} + E \cdot \varepsilon_a + \frac{2 \cdot E \cdot a^2}{3 \cdot b^2} \cdot \left[\frac{1}{2} \cdot \varepsilon_a - \frac{1}{a} \cdot \left(u_{rm}\right)_{r=a}\right]$$

$$\sigma_{\theta m} = \sigma_{cell} + \frac{2 \cdot E \cdot a^2}{3 \cdot b^2} \cdot \left(1 + \frac{b^2}{r^2}\right) \cdot \left[\frac{1}{2} \cdot \varepsilon_a - \frac{1}{a} \cdot \left(u_{rm}\right)_{r=a}\right]$$

The elastic solutions discussed thus far are based on linear, small strain theory, so that Hooke's law is valid. The volumetric strain based on Hooke's law is defined by:

$$\varepsilon_V = \varepsilon_r + \varepsilon_z + \varepsilon_\theta$$

and the radial strain can be calculated using:

$$\varepsilon_r = \varepsilon_\theta = \frac{\varepsilon_V - \varepsilon_z}{2}$$

The area corrections developed for RCC deformation of the specimen, however, are based on linear strain-displacement relationships, but account for nonlinear terms when considering volumetric strain. The true volumetric strain based on linear strain-displacement is defined by:

$$\left(1 - \varepsilon_V\right) = \left(1 - \varepsilon_r\right) \cdot \left(1 - \varepsilon_z\right) \cdot \left(1 - \varepsilon_\theta\right)$$
$$\varepsilon_V = \varepsilon_r + \varepsilon_z + \varepsilon_\theta - \varepsilon_r \varepsilon_z - \varepsilon_z \varepsilon_\theta - \varepsilon_r \varepsilon_\theta + \varepsilon_r \varepsilon_z \varepsilon_\theta$$

and the radial strain is calculated using:

$$\varepsilon_r = \varepsilon_\theta = 1 - \sqrt{\frac{1 - \varepsilon_V}{1 - \varepsilon_z}}$$

In order to calculate the stresses in the membrane based on Hooke's law, displacement continuity at the specimen-membrane interface is considered. The radial displacement at the interface can be calculated based on the area correction for the specimen. However, since this displacement is based on the true volume change, it must be corrected in order to use Hooke's law to calculate the membrane stresses. Otherwise, the nonlinear terms contributing to the true volume change would result in some induced stresses in the membrane that would be artificial. The corrected displacement can be calculated using:

$$\varepsilon_{\theta m} = \left(\varepsilon_{\theta s}\right)_{corr} = \frac{\varepsilon_V - \varepsilon_a}{2}$$

$$\left(u_{rm}\right)_{r=a} = \frac{a}{2} \cdot \left(\varepsilon_a - \varepsilon_V\right) \qquad \text{Equation 4.48}$$

Substituting Equation 4.48 for the radial displacements results in the following expressions for the stresses:

$$\sigma_{rm} = \sigma_{cell} - \frac{E \cdot \varepsilon_V \cdot a^2}{3 \cdot b^2} \cdot \left(\frac{b^2}{r^2} - 1\right) \qquad \text{Equation 4.49}$$

$$\sigma_{zm} = \sigma_{cell} + E \cdot \varepsilon_a + \frac{E \cdot \varepsilon_V \cdot a^2}{3 \cdot b^2} \qquad \text{Equation 4.50}$$

$$\sigma_{\theta m} = \sigma_{cell} + \frac{E \cdot \varepsilon_V \cdot a^2}{3 \cdot b^2} \cdot \left(\frac{b^2}{r^2} + 1\right) \qquad \text{Equation 4.51}$$

In order to calculate the correction to the lateral stress, the average circumferential stress is determined by integrating across the thickness of the membrane as follows:

$$
\begin{aligned}
\left(\sigma_{\theta m}\right)_{avg} &= \frac{1}{b-a}\int_a^b \sigma_{\theta m}\,dr \\
&= \frac{1}{b-a}\int_a^b \left[\sigma_{cell} + \frac{E\cdot\varepsilon_V\cdot a^2}{3\cdot b^2}\cdot\left(\frac{b^2}{r^2}+1\right)\right]dr \\
&= \frac{1}{b-a}\left[\left(\sigma_{cell} + \frac{E\cdot\varepsilon_V\cdot a^2}{3\cdot b^2}\right)\cdot r - \frac{E\cdot\varepsilon_V\cdot a^2}{3\cdot r}\right]_a^b \\
&= \frac{1}{b-a}\left[\left(\sigma_{cell} + \frac{E\cdot\varepsilon_V\cdot a^2}{3\cdot b^2}\right)\cdot(b-a) - \frac{E\cdot\varepsilon_V\cdot a^2}{3}\cdot\left(\frac{1}{b}-\frac{1}{a}\right)\right]
\end{aligned}
$$

$$
\left(\sigma_{\theta m}\right)_{avg} = \sigma_{cell} + \frac{E\cdot\varepsilon_V\cdot a}{3\cdot b}\cdot\left(1+\frac{a}{b}\right) \qquad \text{Equation 4.52}
$$

The general equations for corrections due to stresses that develop in the membrane assuming RCC deformation are:

$$
\Delta\sigma_{rs} = \Delta\sigma_{\theta s} = -E_m\cdot\varepsilon_V\cdot\left[\frac{2+\frac{t_{om}}{r_{os}}}{3\cdot\left(1+\frac{t_{om}}{r_{os}}\right)^2}\right]\cdot\left(\sqrt{1+\frac{1}{(1-\varepsilon_V)}\cdot\left[2\cdot\frac{t_{om}}{r_{os}}+\left(\frac{t_{om}}{r_{os}}\right)^2\right]}-1\right) \qquad \text{Equation 4.53}
$$

$$
\Delta\sigma_{zs} = -\frac{E_m}{(1-\varepsilon_V)}\cdot\left[\varepsilon_a + \frac{\varepsilon_V}{3\cdot\left(1+\frac{t_{om}}{r_{os}}\right)^2}\right]\cdot\left[\left(1+\frac{t_{om}}{r_{os}}\right)^2-1\right] \qquad \text{Equation 4.54}
$$

where:
- $\Delta\sigma_{rs}$ = correction to lateral stress in the specimen
- $\Delta\sigma_{zs}$ = correction to axial stress in the specimen
- E_m = elastic modulus of membrane
- ε_a = average axial strain
- ε_V = average volumetric strain
- t_{om} = initial membrane thickness
- r_{os} = initial specimen radius

Equation 4.53 demonstrates that there is no correction to the lateral stress for a specimen that does not undergo volume change. If expansion occurs, the volumetric strain will be negative, and the stress correction will be positive. Equation 4.54 shows the dependency of the axial stress correction on both the volumetric and axial strains. For a specimen exhibiting no volume change, the axial stress correction is:

$$\Delta\sigma_{zs} = -E_m \cdot \varepsilon_a \left[\left(1 + \frac{t_{om}}{r_{os}} \right)^2 - 1 \right] \qquad \text{Equation 4.55}$$

Table 4.3 summarizes the corrections that should be applied to the stresses in the specimen due to the effects of the membrane stresses.

Table 4.3 - Membrane Stress Corrections for RCC Deformation

Specimen Conditions	$\Delta\sigma_r$	$\Delta\sigma_z$
Contractive	<0 (Equation 4.53)	$\lvert\Delta\sigma_{zs}\rvert > \left\lvert -E_m \cdot \varepsilon_a \left[\left(1 + \frac{t_{om}}{r_{os}} \right)^2 - 1 \right] \right\rvert$ (Equation 4.54)
No volume change (undrained test)	0	$\Delta\sigma_{zs} = -E_m \cdot \varepsilon_a \left[\left(1 + \frac{t_{om}}{r_{os}} \right)^2 - 1 \right]$
Dilative	>0 (Equation 4.53)	$\lvert\Delta\sigma_{zs}\rvert < \left\lvert -E_m \cdot \varepsilon_a \left[\left(1 + \frac{t_{om}}{r_{os}} \right)^2 - 1 \right] \right\rvert$ (Equation 4.54)

Comparison of Membrane Stress Corrections for RCC Deformation

The stresses that develop in the membrane predicted based on the different methods and assumptions are shown in Figure 4.10 for undrained, unconfined loading ($\varepsilon_V = 0$ and $\sigma_{cell} = 0$) of a specimen with an initial diameter of 2.8 inches and a membrane with a value of elastic modulus of 200 psi and a value of Poisson's ratio of 0.5. The corrections to the axial and lateral stresses based on the different methods are shown as a function of axial strain in Figure 4.11. The correction to the axial stress proposed by Henkel and Gilbert (1952) uses approximate geometry for the specimen and membrane. As a result, at large values of axial strain, it becomes less accurate. Furthermore, Henkel and Gilbert considered each type of loading independently, and intended for one or the other correction to be applied, but not both, since the interaction between the two types of loading is not considered. Therefore, the corrections are not expected to agree with those that do account for the combined interaction of axial and lateral loading of the membrane. The corrections proposed by Duncan and Seed (1967) attribute part of the stretching in the circumferential direction in the membrane to the nonlinear portion of the radial strain in the specimen. As a result, they predict stretching and circumferential stresses in the membrane even for the case of zero volume change. Consequently, the magnitude of the axial stress correction is less than that based on linear volumetric relationships and Hooke's law, and the radial stress correction is greater less than that based on linear volumetric relationships and Hooke's law. Since Equation 4.40 demonstrates that the internal and external pressures must be equal when both materials have values of Poisson's ratio of one half, the corrections based on the linear volumetric relationships appear to better represent the true effect of the actual stresses in the membrane on the stresses in the specimen.

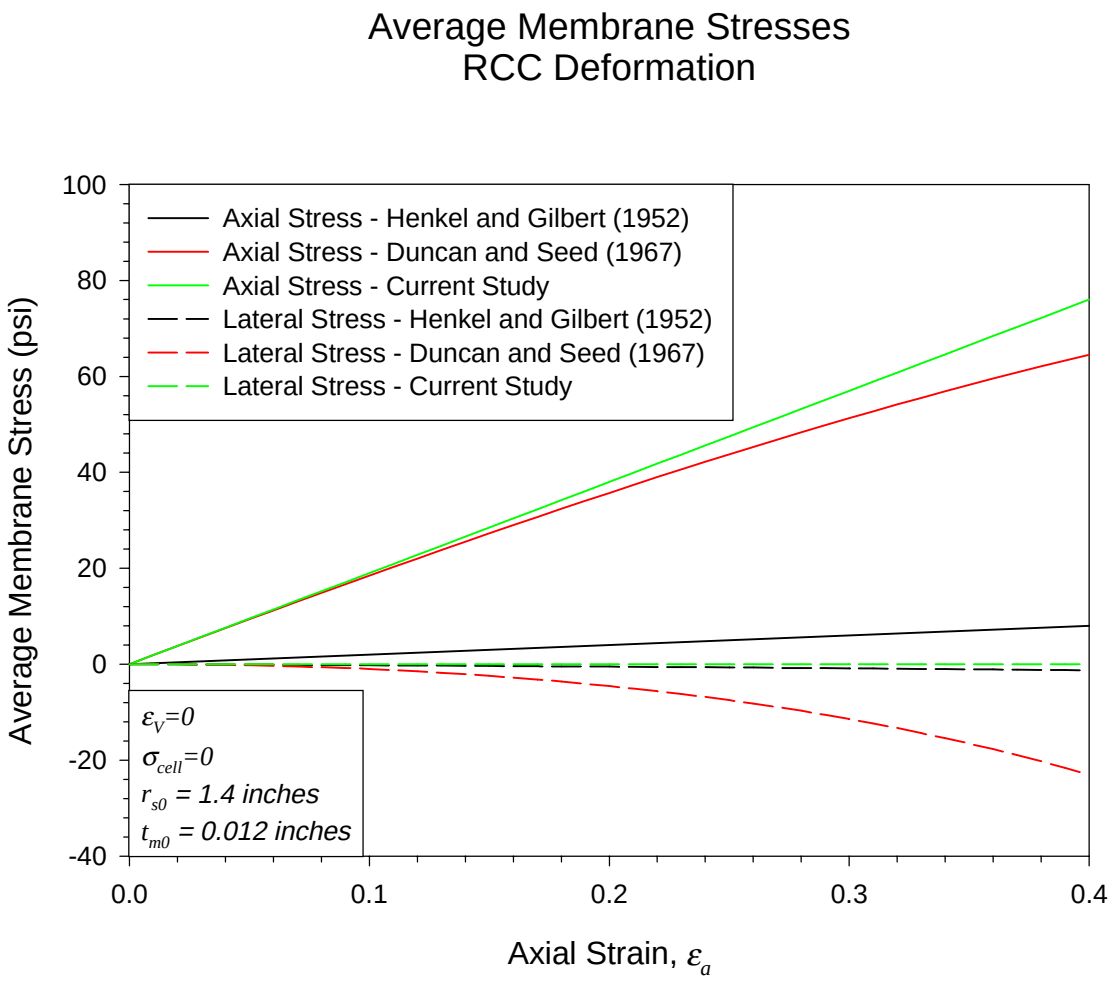

Figure 4.10 - Comparison of Average Membrane Stresses for Undrained Loading Based on RCC Deformation

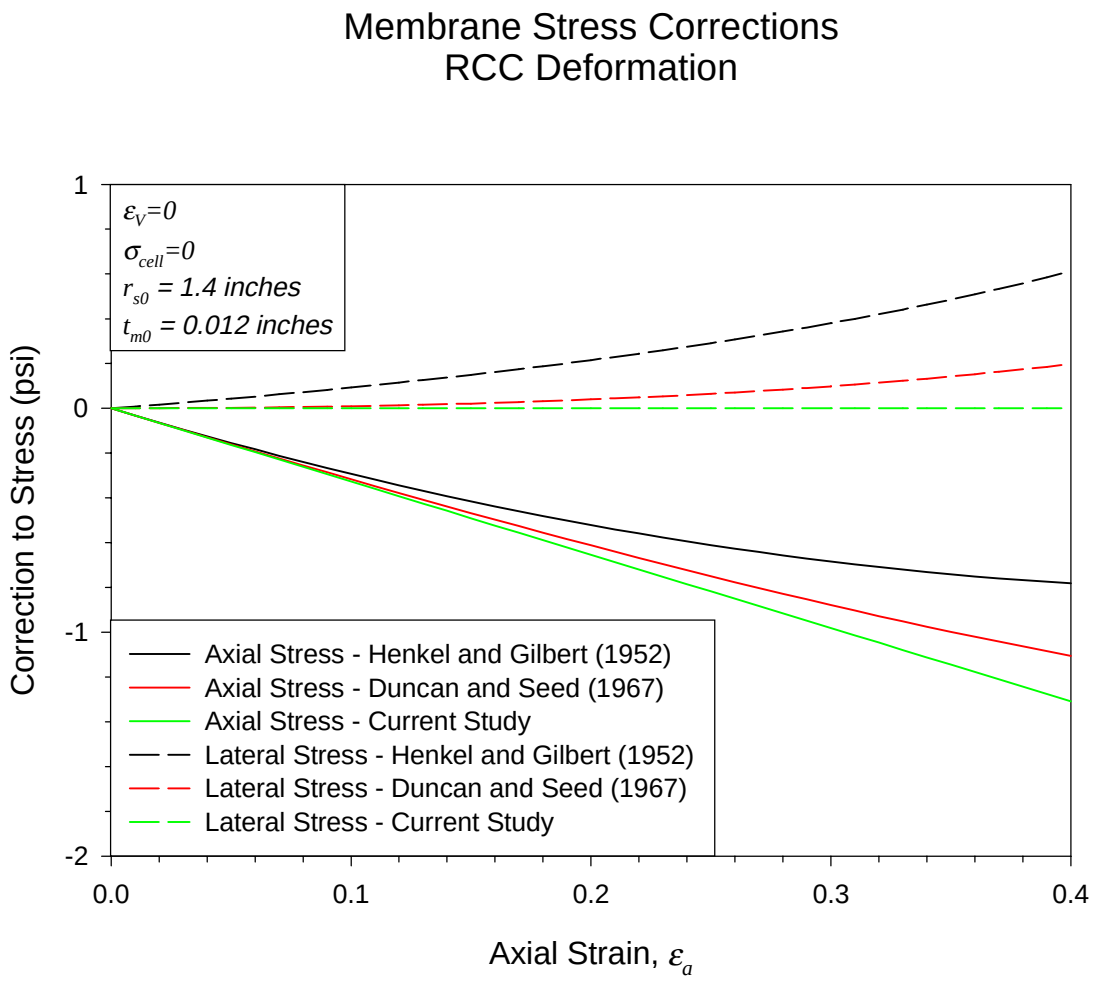

Figure 4.11 - Comparison of Membrane Stress Corrections for Undrained Loading Based on RCC Deformation

Figure 4.12 shows the average stresses in the membrane and Figure 4.13 shows the membrane stress corrections for the same specimen, but with an assumed contractive volume change as shown in both figures. The effect of the decrease in volume of the specimen during shear results in a greater axial stress than for the zero volume change case and a compressive lateral stress.

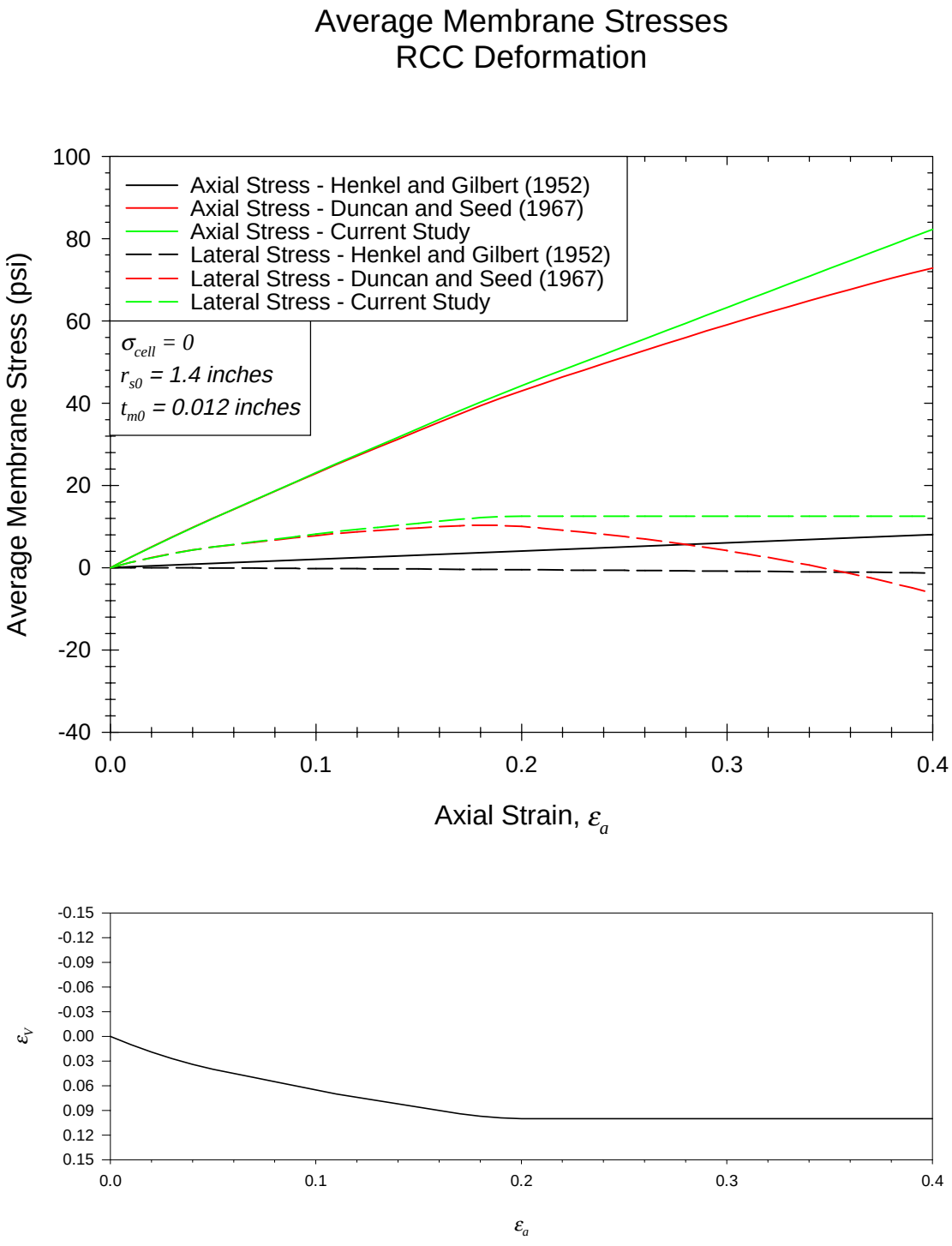

Figure 4.12 - Comparison of Average Membrane Stresses for Contractive Specimen Based on RCC Deformation

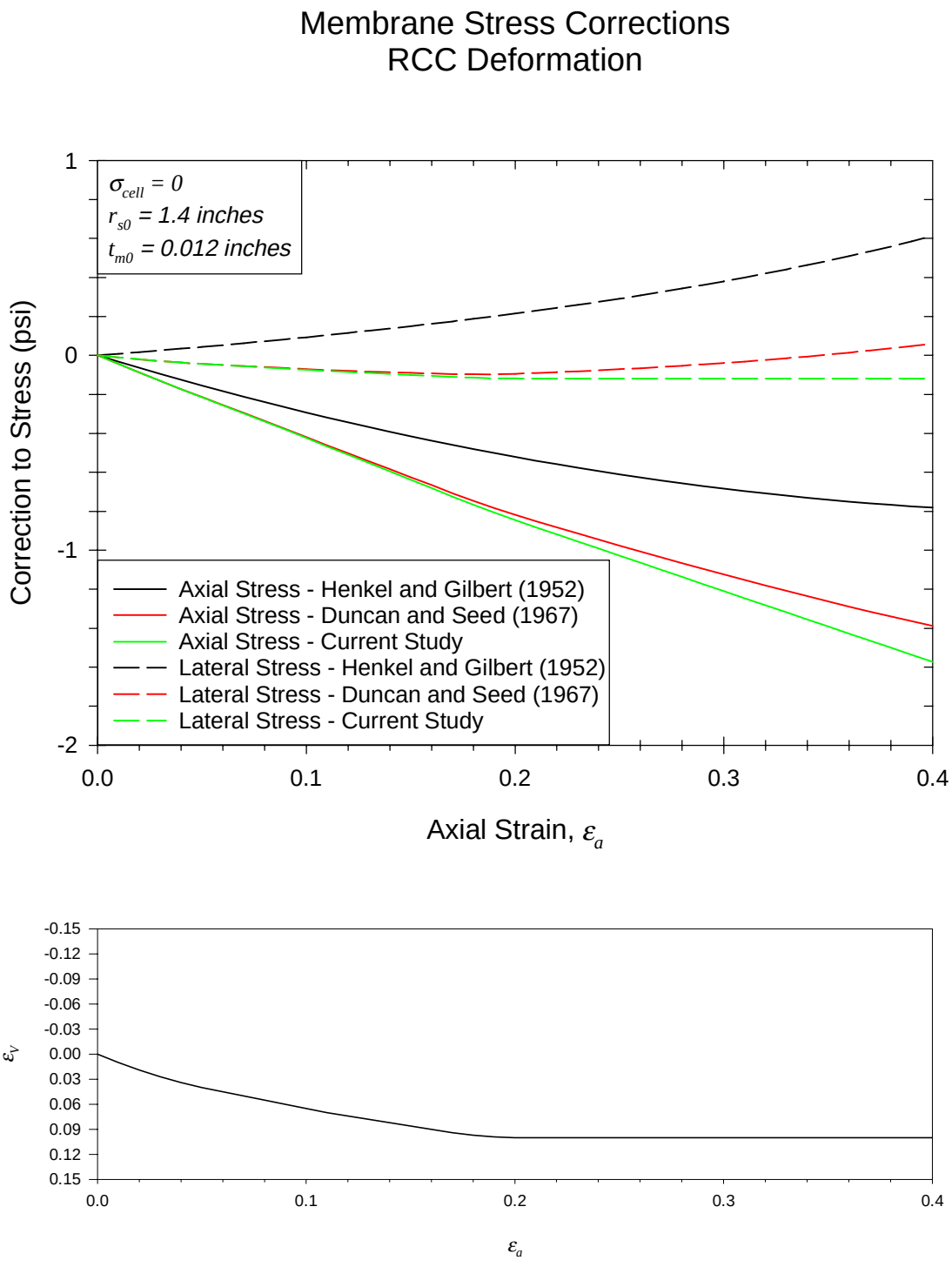

Figure 4.13 - Comparison of Membrane Stress Corrections for Contractive Specimen Based on RCC Deformation

Figure 4.14 shows the average stresses in the membrane and Figure 4.15 shows the membrane stress corrections for the same specimen, but with an assumed dilative volume change as shown in both figures. The effect of the increase in volume of the specimen during shear results in a lower axial stress than for the zero volume change case and a tensile lateral stress. The magnitude of the correction to the axial stress is less than that for the zero volume change case, and the magnitude of the correction to the lateral stress is greater than that for the zero volume change case. Figure 4.15 also demonstrates that the correction to the lateral stress is dependent on the volumetric strain level, but not the axial strain level, since the correction becomes constant when the volumetric strain ceases to change increasing axial strain.

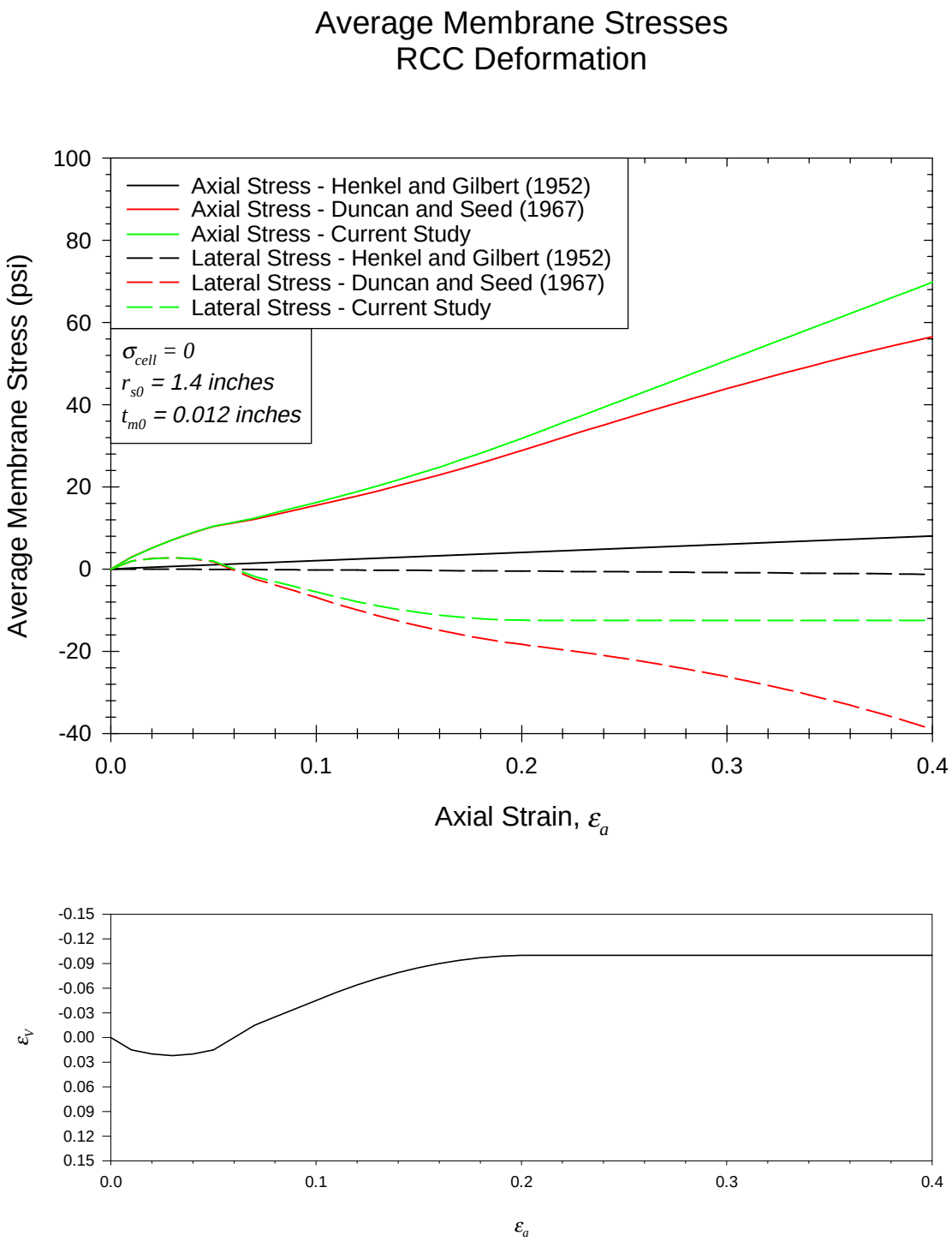

Figure 4.14 - Comparison of Average Membrane Stresses for Dilative Specimen Based on RCC Deformation

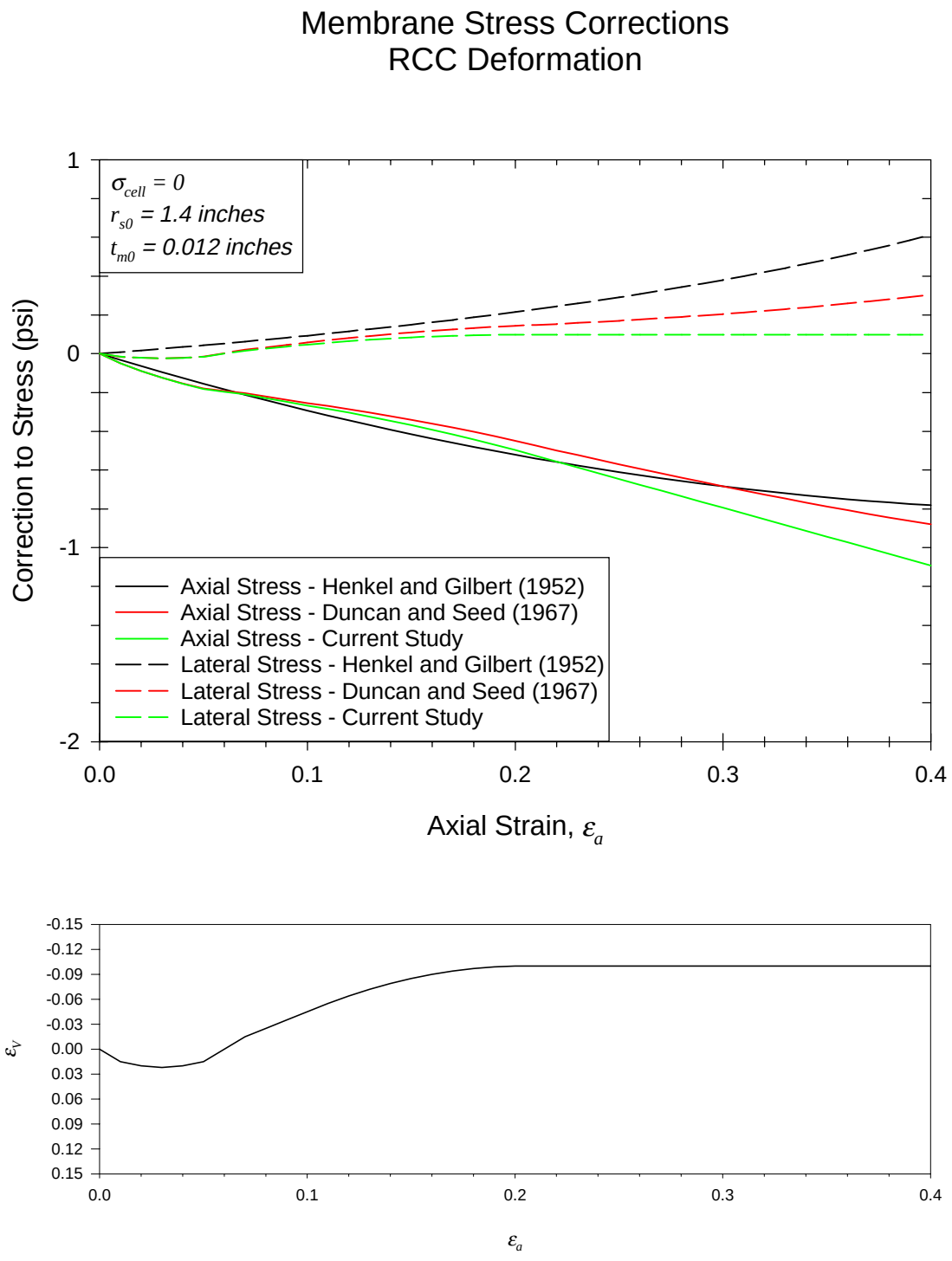

Figure 4.15 - Comparison of Membrane Stress Corrections for Dilative Specimen Based on RCC Deformation

Approximate Solutions for Nonuniform Deformation Modes

If a mode of deformation other than RCC is assumed, the solution for the stresses in the membrane becomes much more complex. The membrane will have nonzero shear stresses on planes perpendicular to the axial and radial directions, and determination of the stresses by simple force equilibrium in these directions is no longer possible.

A good approximation of the stresses in the membrane for nonuniform deformation modes can be derived by assuming that for a small differential height, the mode of deformation is RCC. The radial displacement, and hence the circumferential strain for nonuniform modes of deformation vary in the axial direction. Since the circumferential strain in the membrane varies with height, the axial and circumferential stresses in the membrane will vary with height also. The corrections for the axial and radial stresses in the specimen depend on the assumed distributions of strain in the membrane. The most reasonable assumption is that the strain in each direction varies similarly along the axial direction, so that none of the strains are independent of the axial coordinate. Since the magnitude of the radial strain was shown to be a maximum at the mid-height of the specimen for nonuniform deformation modes, the magnitude of the axial strain and volumetric strain will be a maximum there as well. Using Equation 4.46 and Equation 4.47 for the stresses in the membrane based on radial displacements at the specimen-membrane interface, along with the axial and circumferential strain distributions based on nonuniform deformation, the stresses in the membrane may be estimated.

A reasonable estimate of the axial and radial stresses in this small differential volume of the membrane can be achieved, but it neglects the shear stresses in the membrane as well as the shear stresses on the interface between the surface of the specimen and the membrane. If the strength of the specimen is

determined using the stress state at the mid-height of the specimen as the representative state, the approximation is better since there are no shear stresses on the surface of the specimen. Once an estimate of the stresses in the membrane is obtained, the corrections to the stresses in the specimen can be calculated based on Equation 4.30 and Equation 4.31.

Parabolic Deformation

Assuming that the strains in each direction vary similarly along the axis, the circumferential and axial strains in the membrane are defined by:

$$\varepsilon_{\theta m} = -\left(\frac{z^2}{h^2} - \frac{z}{h}\right)\cdot\left(5 - \sqrt{30\cdot\frac{(1-\varepsilon_V)}{(1-\varepsilon_a)} - 5}\right) \qquad \text{Equation 4.56}$$

$$\varepsilon_{zm} = 1 - \frac{\sqrt{(1-\varepsilon_V)\cdot(1-\varepsilon_a)}}{1+\left(\frac{z^2}{h^2} - \frac{z}{h}\right)\cdot\left(5 - \sqrt{30\cdot\frac{(1-\varepsilon_V)}{(1-\varepsilon_a)} - 5}\right)} \qquad \text{Equation 4.57}$$

Again, the circumferential strain must be corrected to account for the fact that the stresses are determined based on Hooke's law and linear volume change relationships. In the case of nonuniform deformation, this can be accomplished by subtracting the nonlinear portion due to uniaxial loading and adding the linear portion due to uniaxial loading as follows:

$$(\varepsilon_{\theta m})_{corr} = -\left(\frac{z^2}{h^2} - \frac{z}{h}\right)\cdot\left(5 - \sqrt{30\cdot\frac{(1-\varepsilon_V)}{(1-\varepsilon_a)} - 5}\right) - \left(1 - \sqrt{\frac{(1-\varepsilon_V)}{(1-\varepsilon_a)}}\right) + \frac{1}{2}\cdot(\varepsilon_V - \varepsilon_a)$$

Since the strains vary along the axis, so does the ratio of cross sectional areas which is determined by:

$$\frac{A_m}{A_s} = \frac{2 \cdot \frac{t_{om}}{r_{os}} + \left(\frac{t_{om}}{r_{os}}\right)^2}{\sqrt{(1-\varepsilon_V)\cdot(1-\varepsilon_a)}\cdot\left[1+\left(\frac{z^2}{h^2}-\frac{z}{h}\right)\cdot\left(5-\sqrt{30\cdot\frac{(1-\varepsilon_V)}{(1-\varepsilon_a)}-5}\right)\right]} \qquad \text{Equation 4.58}$$

While the expressions for the stress corrections are rather lengthy, the calculation of the stress corrections is straight forward, using the same equations for the corrections based on RCC deformation in conjunction with the expressions for the estimated stresses in the membrane and the estimated area ratio based on nonuniform deformation.

Sinusoidal Deformation

Following the development of the corrections based on parabolic bulging, the corrections based on sinusoidal bulging can be developed. Assuming that the strains in each direction vary similarly along the axis, the circumferential and axial strains in the membrane are defined by:

$$\varepsilon_{\theta m} = \left(\frac{4}{\pi} - \sqrt{\frac{16}{\pi^2} - 2 + 2\cdot\frac{(1-\varepsilon_V)}{(1-\varepsilon_a)}}\right)\cdot\sin\left(\pi\cdot\frac{z}{h}\right) \qquad \text{Equation 4.59}$$

$$\varepsilon_{zm} = 1 - \frac{\sqrt{(1-\varepsilon_V)\cdot(1-\varepsilon_a)}}{1-\left(\frac{4}{\pi} - \sqrt{\frac{16}{\pi^2} - 2 + 2\cdot\frac{(1-\varepsilon_V)}{(1-\varepsilon_a)}}\right)\cdot\sin\left(\pi\cdot\frac{z}{h}\right)} \qquad \text{Equation 4.60}$$

Again, the circumferential strain must be corrected to account for the fact that the stresses are determined based on Hooke's law and linear volume change relationships. This can be accomplished by subtracting the nonlinear portion due to uniaxial loading and adding the linear portion due to uniaxial loading as follows:

$$\left(\varepsilon_{\theta m}\right)_{corr} = \left(\frac{4}{\pi} - \sqrt{\frac{16}{\pi^2} - 2 + 2\cdot\frac{\left(1-\varepsilon_V\right)}{\left(1-\varepsilon_a\right)}}\right)\cdot\sin\left(\pi\cdot\frac{z}{h}\right) - \left(1 - \sqrt{\frac{\left(1-\varepsilon_V\right)}{\left(1-\varepsilon_a\right)}}\right) + \frac{1}{2}\cdot\left(\varepsilon_V - \varepsilon_a\right)$$

Since the strains vary along the axis, so does the ratio of cross sectional areas which is determined by:

$$\frac{A_m}{A_s} = \frac{2\cdot\frac{t_{om}}{r_{os}} + \left(\frac{t_{om}}{r_{os}}\right)^2}{\sqrt{\left(1-\varepsilon_V\right)\cdot\left(1-\varepsilon_a\right)}\cdot\left[1 - \left(\frac{4}{\pi} - \sqrt{\frac{16}{\pi^2} - 2 + 2\cdot\frac{\left(1-\varepsilon_V\right)}{\left(1-\varepsilon_a\right)}}\right)\cdot\sin\left(\pi\cdot\frac{z}{h}\right)\right]} \qquad \text{Equation 4.61}$$

As with the parabolic bulging corrections, the expressions for the stress corrections are rather lengthy, but calculation of the corrections is done using the same equations for the corrections based on RCC deformation in conjunction with the expressions for the estimated stresses in the membrane and the estimated area ratio based on nonuniform deformation.

Comparison of Membrane Stress Corrections for Nonuniform Deformation

Figure 4.16 compares the membrane stress corrections based on nonuniform deformation modes with those based on RCC deformation for undrained loading of a specimen with and initial diameter of 2.8 inches encapsulated in a membrane with an initial thickness of 0.012 inches. The corrections are based on the condition at the mid-height of the specimen, where the area change is the greatest and the magnitude of the strains are the greatest. The corrections based on parabolic bulging and sinusoidal bulging are similar as expected since both deformation modes result in similar displacement profiles. Since the circumferential strains in the membrane are greater than those due only to axial loading, the membrane stretches, which results in the development of the average circumferential stress and the corresponding correction as shown in Figure 4.16. This circumferential stretching also results in a reduction of the

axial stress in the membrane, particularly at large strain levels, and reduces the axial stress correction from that based on RCC deformation.

The effects of the membrane stresses for nonuniform deformation modes with zero volume change are similar to those based on RCC deformation with a dilative specimen. This similarity can be expected since the radial expansion at the mid-height for nonuniform deformation is greater than that based on RCC deformation and zero volume change. At an axial strain level of 40%, the correction to the axial stress is approximately -1.2 psi and the correction to the lateral stress is approximately 0.25 psi. Thus, Figure 4.16 demonstrates that based on the assumed specimen conditions and nonuniform deformation modes, the effects of the stresses in the membrane on the stresses in the specimen are minimal.

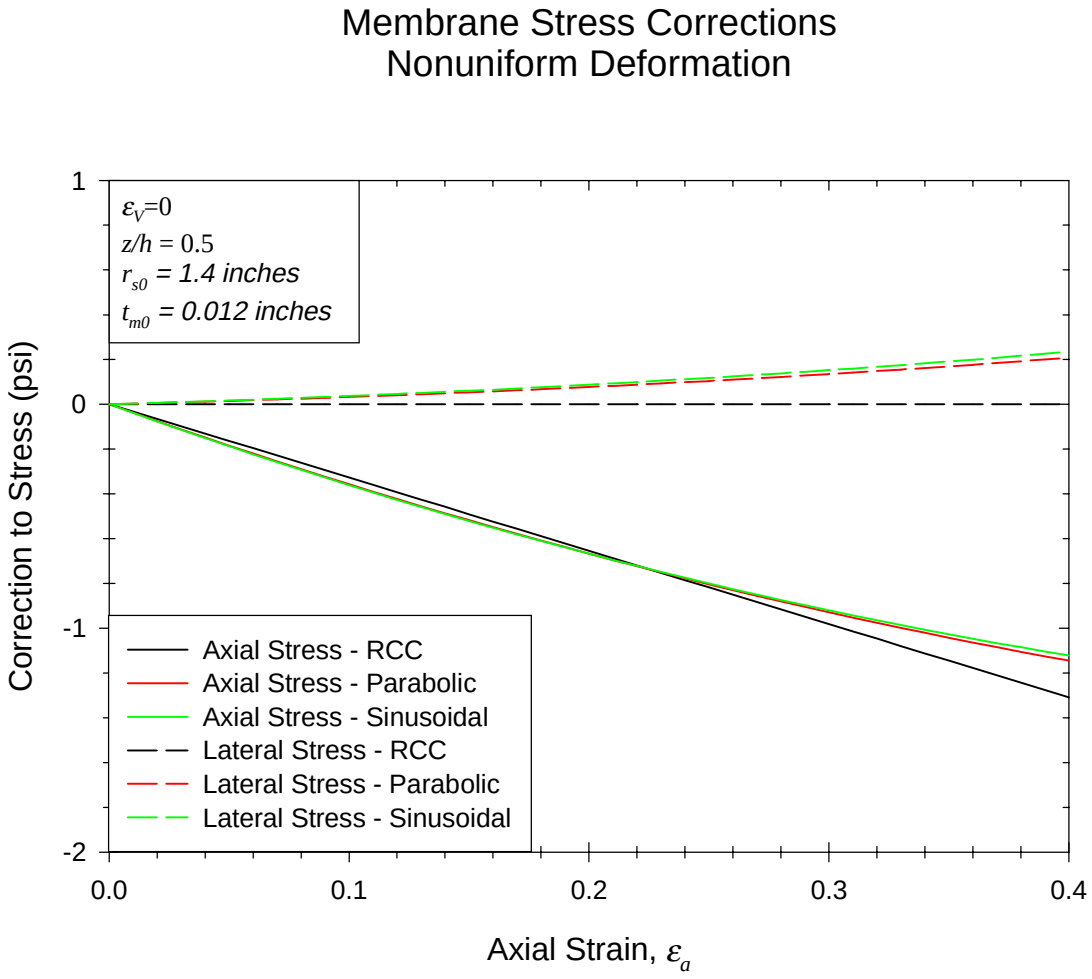

Figure 4.16 - Membrane Stress Corrections for Undrained Loading Based on Nonuniform Deformation

Membrane Penetration

In addition to the influence of the membrane on the axial and radial stresses due to the strains that develop in the membrane, the membrane has an additional effect on triaxial test specimens composed of coarse-grained materials such as gravels and coarse sands. Since the cylindrical surface of the specimen is not smooth, as would be the case if the test specimen were made of polished steel, for example, the membrane conforms somewhat to the irregular shape of the surface. This phenomenon is usually described as *membrane penetration*, since the membrane penetrates into the void spaces along the surface of the specimen. This concept is shown in Figure 4.17.

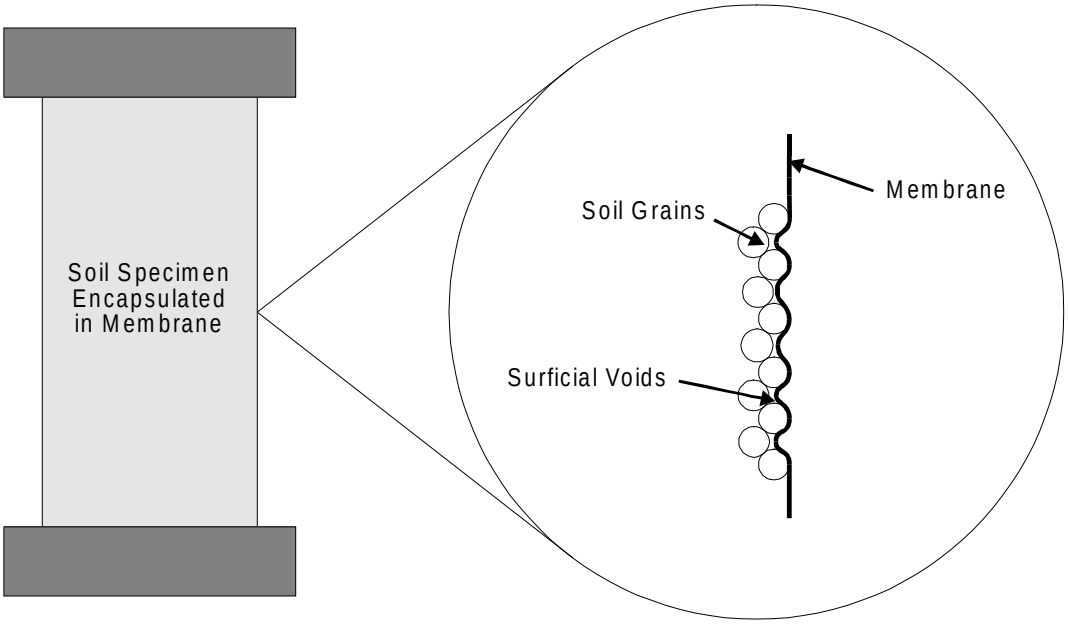

Figure 4.17 - Membrane Penetration into Surficial Voids

If the effective stress in the specimen is zero and the membrane diameter is at least the diameter of the specimen, then membrane penetration will not occur, since there is no tendency for inward movement of the membrane. As the effective stress in the specimen increases, the membrane will tend to penetrate

into the surficial void spaces. Likewise, if some penetration has occurred and the effective stress in the specimen decreases, the membrane will tend to rebound out of the surficial void spaces. During drained loading, the effective stress in the specimen should remain constant during the shear phase of the test, so the membrane penetration should have no great effect during shear. During consolidation of the specimen, however, the effective stress in the specimen increases as consolidation occurs. As the effective stress increases, the tendency for membrane penetration increases. As the membrane penetrates into the surficial void space, the volume change as measured by changes in either the internal pore water volume or the cell fluid volume will increase (Newland and Allely 1957, Raju and Venkataraman 1980, Evans 1992). That is, the measured volume change will not accurately represent the volume change in the void spaces of the specimen, and will indicate a greater volume change than actually occurs.

For undrained tests, this phenomenon for the consolidation phase is identical since the consolidation procedures are the same as for drained tests. During undrained shear, however, the influence of membrane penetration is more significant than for drained shear (Newland and Allely 1959, Kiekbush and Schuppener 1977, Lade and Hernandez 1977, Ramana and Raju 1981). During undrained shear, the tendency for volume change results in an increase or decrease in the pore water pressure since the system is constrained to remain at a constant volume. Although the boundaries of the system comprised of the specimen, membrane, end platens, drainage lines, and pore pressure measuring device prevent any net volume change for the system, the internal movement of the various components, in particular the pore water, is not prevented. Thus, although no net total volume change can occur, on a local basis the soil can undergo volume change as pore water evacuates or migrates within the specimen (Newland and Allely 1959, Evans 1992). This migration of pore water implies that localized volume change, and hence density change

occurs. Since volume change is not prevented on a localized basis during undrained shear, the tendency for membrane penetration or rebound can result in migration of pore water out of or into, respectively, the surficial voids. The migration of pore water toward or away from the surficial voids can have two effects: the density of some regions of the specimen can change, and the tendency for pore pressure development can be altered.

If a specimen exhibits a dilative tendency during undrained shear, the effective stress will increase as the pore pressure decreases, and the tendency for membrane penetration will increase. The increase in membrane penetration requires migration of pore water away from the surficial voids toward the internal regions of the specimen, and those regions of the specimen consequently can experience an increase in void ratio to account for the increase in water content. The tendency for pore pressure reduction can also decrease, resulting in a lower effective stress in the specimen than would occur without membrane penetration.

If a specimen exhibits a contractive tendency during undrained shear, the effective stress will decrease as the pore pressure increases, and the tendency for membrane penetration will decrease. Any penetration that occurred during consolidation will tend to rebound, and the rebound requires migration of pore water into the surficial voids from the internal regions of the specimen. Consequently, the density of the internal regions of the specimen can increase as the water content decreases. The tendency for pore pressure generation can also decrease, resulting in a higher effective stress in the specimen than would occur without membrane penetration.

In soil specimens that permit membrane penetration, the membrane penetration affects the consolidation phase of either CD triaxial tests or CU triaxial tests by increasing the measured volume change during shear.

Furthermore, since the membrane penetration effects are really related to changes in effective stress, the membrane penetration influences the shear phase of both CU tests or *compensated* CD tests wherein the effective stress is varied during the test to maintain constant volume. In CD tests, the effective stress is typically constant, so the membrane penetration change, if any, during shear is negligible. In CU tests, the effects are more important. First, since localized volume change can occur, the density of the specimen in the region that controls failure can change. In addition, since the boundaries that enclose the pore water are flexible, the magnitude of the pore pressures induced during shear is affected.

Measurement of Membrane Penetration

Newland and Allely (1957, 1959) first recognized the importance of the fit (or lack of fit) of the membrane to the specimen and that even if no cavitation occurred, volume change in an undrained test specimen was still possible. They noted that erroneously large volume changes were recorded in both drained tests and simulated undrained tests, where the effective stress was increased or decreased so as to maintain constant volume, on granular materials. They further noted that the effect was negligible for materials finer than coarse sand and decreased as either the specimen size or membrane thickness increased (Newland and Allely 1959). Newland and Allely (1959) first attempted to measure the membrane penetration by subjecting triaxial specimens to hydrostatic changes in stress. Based on the assumption that the soil responds isotropically to hydrostatic changes in stress, they measured the axial deformation and calculated the *true* volumetric strain as three times the axial strain. Using this method, the membrane penetration was calculated as the difference in the measured volumetric strain and the *true* volumetric strain, as shown in Equation 4.62.

$$(\varepsilon_V)_{true} = (\varepsilon_V)_{meas} - 3 \cdot \varepsilon_a \qquad \text{Equation 4.62}$$

where: $(\varepsilon_V)_{true}$ = true volumetric strain
$(\varepsilon_V)_{meas}$ = measured volumetric strain
ε_a = measured axial strain under hydrostatic load

Problems with this method have been identified, the most significant of which is that the assumption of isotropic behavior at small strains is not always satisfied (El-Sohby 1964, Roscoe 1970, Vaid and Negussey 1984). Furthermore, even if the response is isotropic, slight errors in the measurement of axial strain are magnified when calculating the *true* volumetric strain, and since the magnitude of the volume change associated with membrane penetration is often relatively small, these errors in measurement may be significant.

A second method for measuring membrane penetration, which entailed fitting an internal, coaxial core into the soil specimen was first proposed by Roscoe et al. (1963), and later studied by others (El-Sohby 1964, Lee 1966, Raju and Sadasivan 1974, Vaid and Negussey 1984). Roscoe et al. (1963) used brass rods of different diameters as the core material, and suggested that extrapolating the relationship between measured volume change and core diameter to a core diameter equal to the specimen diameter would yield the value of the membrane penetration. Noting, however, that the presence of the rod greatly influenced the density and fabric of the specimen around the rod, Roscoe et al. (1963) suggested that the method proposed by Newland and Allely (1959) based on isotropic response to hydrostatic loading was preferred. El-Sohby (1964) disagreed, and suggested that the anisotropic response of most sands to hydrostatic changes in stress precluded use of the method based on isotropic response.

Reduction of Membrane Penetration

Attempts have been made to reduce the membrane penetration by stiffening the membrane. Lade and Hernandez (1977) placed steel shims between the membrane and the specimen in order to reduce the flexibility of the membrane. Kiekbush and Schuppener (1977) lined the membrane with liquid rubber in order to reduce its flexibility. Raju and Venkataraman (1980) used polyethylene strips between the membrane and the specimen, and coated the membrane with polyethylene as well. Another means of offsetting the effects of membrane penetration that has been investigated is to adjust the pore water volume during shear based on the measured effective stress changes and the assumed relationship between membrane penetration and change in effective stress (Raju and Venkataraman 1980, Ramana and Raju 1981). Evans (1992) examined the reduction of membrane penetration in tests on gravel specimens by sluicing sand into the pores of the gravel, so that the effective pore size on the surface of the specimen was reduced. Most attempts at reducing membrane penetration during the test were fairly successful on the basis that the membrane penetration was reduced to 15% to 20% of that occurring in tests that used standard procedures. In addition, in almost all of the cases mentioned, a 100% increase in pore pressure development during shear was reported for tests in which the membrane penetration was reduced. However, each of the methods for reducing the membrane penetration introduces new effects and sources of error in the measured results of the tests. The influence of these new sources of error on all aspects of the measured properties has not been determined. In addition, the complexity of the testing procedures, especially specimen preparation, is greatly increased by the methods for reducing the membrane penetration. As a result, the reduction of membrane penetration during shear at present does not appear to be viable for routine testing.

Corrections for Membrane Penetration

The other alternative for accounting for the effects of membrane penetration is to apply corrections to the test results. In order to correct the test data to account for the membrane penetration effects, the membrane penetration that is expected to occur must be estimated. The membrane penetration is dependent upon the following:

1.) Effective stress on the specimen

2.) Properties of the membrane (elastic modulus and thickness)

3.) Size of the voids at the interface between the membrane and the specimen surface.

The size of the surficial voids is a function of the grain size and shape, gradation, and density. Previous research has shown that the most significant of these factors is the grain size (Frydman et al. 1973, Baldi and Nova 1984). Since the total volume change due to membrane penetration is dependent upon the area of the contact surface, it is useful to normalize the volume change by the contact area to remove specimen size effects from the relationship. This normalized volume change is referred to as the *unit membrane penetration,* and is defined by:

$$\varepsilon_{mp} = \frac{\Delta V_{mp}}{A_{surf}} \qquad \text{Equation 4.63}$$

where: ε_{mp} = unit membrane penetration
ΔV_{mp} = total volume change due to membrane penetration
A_{surf} = contact surface area between membrane and specimen

The volumetric strain due to membrane penetration can be described by:

$$\left(\varepsilon_V\right)_{mp} = \frac{\Delta V_{mp}}{V_0} = \varepsilon_{mp} \cdot \frac{2}{r_0}$$ Equation 4.64

where: $\left(\varepsilon_V\right)_{mp}$ = volumetric strain due to membrane penetration
V_0 = initial specimen volume
r_0 = initial specimen radius

The relationship between unit membrane penetration and effective stress can be adequately represented by a linear relationship between the membrane penetration and the logarithm of effective stress (Frydman et al. 1973, Ramana and Raju 1981, Vaid and Negussey 1984). An example of this type of relationship is shown in Figure 4.18 and is described by:

$$\varepsilon_{mp} = S \cdot \log\left(\frac{\sigma'_f}{\sigma'_i}\right)$$ Equation 4.65

where: S = slope
σ'_f = final effective stress
σ'_i = initial effective stress

Since the mean grain size was considered to be the primary factor controlling membrane penetration for a given effective stress change, Frydman et al. (1973) presented slope data from tests on materials with grain sizes ranging from 0.15 mm to 2.0 mm. A relationship between the slope in Equation 4.65 and mean grain size that approximates the data presented can be expressed as follows:

$$S = 0.0135 \cdot \log\left(d_{50}\right) + .0125$$ Equation 4.66

where: S = slope of unit membrane penetration relationship (cm)
d_{50} = mean grain size (mm)

Due to an error in interpreting the intercept on the log scale, the equation presented by Frydman et al. (1973): $S = 0.014 \cdot \log(d_{50}) - 0.001$ is incorrect.

Figure 4.18 - Relationship Between Membrane Penetration and Effective Stress

Ramana and Raju (1982) defined the slope for samples with densities ranging from dense to loose using the following relationship:

$$S = 10^{\log(d_{50})+.0125} \qquad \text{Equation 4.67}$$

Figure 4.19 shows the relationships for volumetric strain due to membrane penetration predicted by the expressions of Frydman et al. (1973), Ramana and Raju (1982), and Vaid and Negussey (1984) for a 2.8-inch diameter by 6-inch long specimen for which the volume was determined at an effective stress of 10 psi.

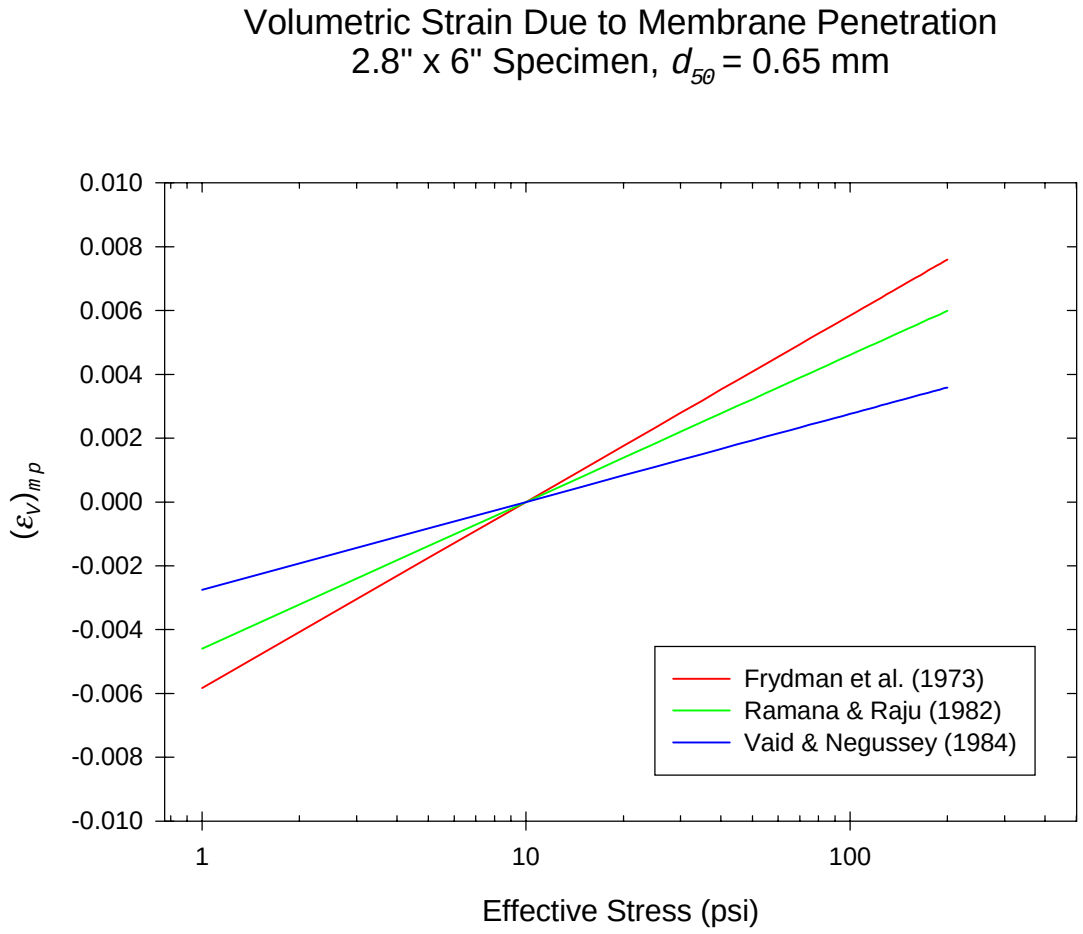

Figure 4.19 - Volumetric Strain Due to Membrane Penetration for Typical Sand Specimens

Based on a relationship between effective stress and membrane penetration, the volume change data for the consolidation phase can be corrected to better represent the actual change in void ratio of the specimen. In specimens that are susceptible to membrane penetration, the actual volume change of the specimen will be less than the measured volume change during consolidation, since some of the measured volume change will actually be due to the membrane penetration that occurs as the effective stress increases during consolidation. In order to correct the volume change during consolidation, the volume change due to membrane penetration is estimated based on the

specimen geometry, the mean grain size, and the change in effective stress during consolidation. The estimated volume change due to membrane penetration is subtracted from the measured volume change to determine the actual volume change of the specimen during consolidation.

Figure 4.19 demonstrates that the membrane penetration effect on typical sand specimens with mean grain sizes less than or equal to 0.65 mm will result in a volumetric strain of less than 0.8% for an order of magnitude change in effective stress, regardless of which relationship is used. Although the effect increases as mean grain size increases, the volumetric strain error can be considered negligible provided that extremely large effective stress changes do not occur for typical tests on sands with smaller mean grain sizes.

Volume and Pore Pressure Considerations as a Result of Changes in Effective Stress During Shear

During undrained shear, the membrane penetration can have two effects as noted previously. Volume change can occur in the interior of the specimen as a result of the change in membrane penetration on the specimen surface, which is in turn a result of the change in effective stress. This volume change can be estimated using the same procedure as that described for correcting the volume after the consolidation phase. If the specimen is contractive, the effective stress will decrease, the membrane penetration will decrease, and pore water will migrate toward the surface of the specimen, so the density of the interior region of the specimen will increase. Likewise, if the specimen is dilative, the effective stress will increase, the membrane penetration will increase, and pore water will migrate away from the surface of the specimen, so the density of the interior region of the specimen will decrease.

The tendency for pore pressure development during shear is reduced due to the flexibility of the membrane. If the specimen is dilative, the compliance

reduces the tendency for decrease in pore pressure, and the resulting effective stress is lower than if the membrane compliance were zero (Lade and Hernandez 1977, Raju and Venkataraman 1980, Evans et al. 1992). If the specimen is contractive, the compliance reduces the tendency for increase in pore pressure, and the resulting effective stress is greater than if the membrane compliance were zero (Kiekbush and Schuppener 1977, Lade and Hernandez 1977, Raju and Venkataraman 1980, Evans et al. 1992). Lade and Hernandez (1977) modified the expressions for Skempton's pore pressure parameters to account for the effects of the flexibility of the membrane, and verified qualitatively the effects of membrane compliance on pore pressure development. However, due to the complex nature of the relationship between membrane penetration, tendency for volume change, and tendency for pore pressure development during the various stress states encountered during undrained triaxial shear, no viable method for correcting the measured pore pressures to reflect those that would occur in a zero compliance system has been developed.

Summary of Net Effect of Area and Membrane Corrections

Uniform Deformation

Applying the correction for the specimen area increase reduces the calculated deviator stress based on raw data. Applying the correction for the axial stress in the membrane further reduces the calculated deviator stress. The correction to the radial stress due to the membrane stresses can result in a confining pressure greater than the cell pressure for dilative specimens and a confining pressure less than the cell pressure for contractive specimens. For zero volume change conditions, the lateral stresses in the both the specimen and the membrane are equal to the cell pressure, so no lateral stress correction applies. The net effect of applying these corrections at failure is a reduction of

the measured shear strength. If the axial strain measurements are assumed to be accurate, the reduction of the deviator stress also implies a reduction of the axial stiffness or modulus of the specimen.

Nonuniform Deformation

To describe the effects of the corrections for nonuniform deformation, the state of the specimen at different sections along the height of the specimen can be examined. At the ends of the specimen, it is assumed that no radial strain occurs. As a result, there is no change in specimen area or the circumference of the membrane. The corrections for the stresses in the membrane result in a decrease in both the axial stress and the lateral stress. Since the correction to the axial stress is more significant, the net effect of applying the corrections is to reduce the calculated deviator stress as well as the calculated confining stress at the ends of the specimen.

At the mid-height section of the specimen, the values of the radial strain in the specimen, and hence the area correction are at a maximum. As mentioned previously, the correction for the axial stress in the membrane is applied by calculating a correction to the measured axial force, and can be assumed to be constant along the height of the specimen. The lateral stress will increase due to the stresses in the membrane. At the mid-height section, the calculated deviator stress will be reduced by applying the correction due to the membrane stresses, and will be further reduced due to the increase in area. The lateral stress will increase due to the membrane stress correction. As a result, the shear strength based on the corrections will be at its minimum value at the mid-height of the specimen and will increase with distance toward the ends of the specimen.

At intermediate points between the mid-height and the ends, the corrected shear strength will be greater than that at the mid-height, but less than that at

the ends. The most typical approach has been to use the shear strength properties based on corrections at the mid-height since this results in the lowest corrected measured shear strength.

While this approach makes sense when examining only the corrections mentioned above, it still ignores the influence of the friction at the end platens. In fact, in order to constrain slip at the end platens as is assumed for nonuniform deformation, a significant shear stress acting inward toward the axis of the specimen along the end is required. This shear stress applied at the ends will increase both the actual deviator stress and the actual minor principal stress over some region in the vicinity of the ends. Since this shear stress is unaccounted for, the actual Mohr circle at failure for the region affected by the end friction is larger in diameter and located farther from the origin (higher minor principal stress) than the Mohr circle at failure calculated based on the corrections for area change and membrane effects. Although stress level will vary within the specimen itself when nonuniform deformation occurs, the overall shear strength parameters will be overestimated as a result of the friction on the ends of the specimen.

Effect of Membrane Penetration on Steady State

The effect of applying a volume correction for the membrane penetration is illustrated in Figure 4.20. Since the steady state line and the correction for membrane penetration are both approximately linearly related to the logarithm of effective stress, the membrane penetration correction implies that during undrained shear the state of the specimen actually follows a path along a line with the slope of the membrane penetration curve as opposed to a horizontal line. While this effect has been exaggerated in Figure 4.20, the influence on the steady state line that is determined based on undrained test data is

evident. The slope of the steady state line decreases when the membrane penetration effect is taken into account.

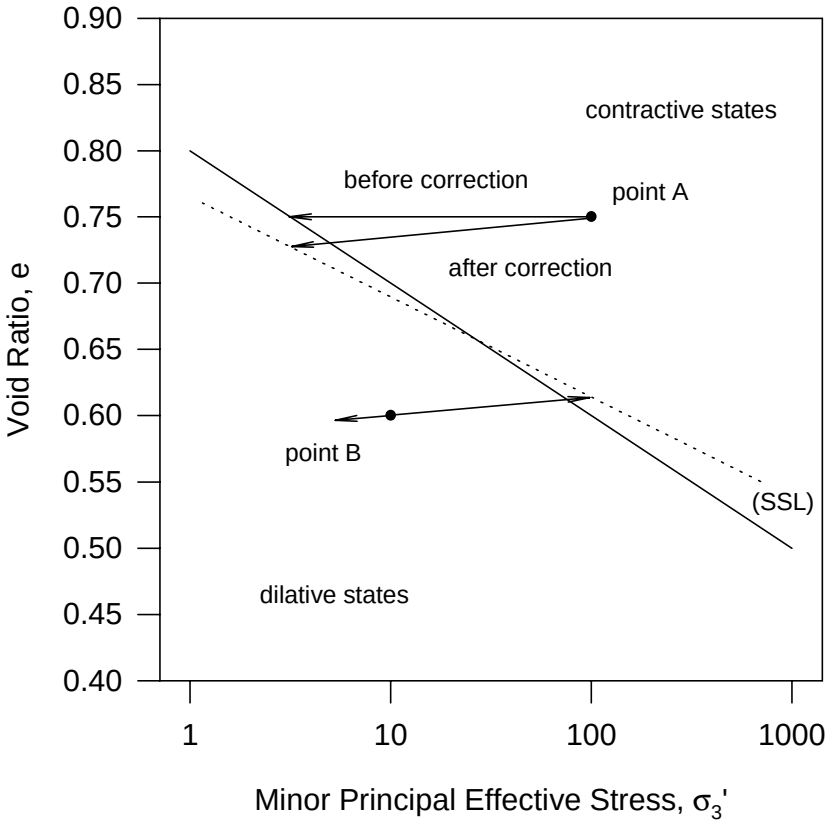

Figure 4.20 - Influence of Membrane Penetration on the Steady State Line

Unfortunately, the influence of membrane compliance on pore pressure development during undrained shear cannot be characterized as readily. Lade and Hernandez (1977) showed that although the membrane penetration had a significant effect on pore pressure development, the effective stress strength envelope was not affected. Their conclusions are based in part on the assumption that the envelope is independent of stress path, which is influenced by membrane compliance effects. If the steady state strength envelope is presumed to be unaffected as well, then the steady state

relationship should be unaffected by the membrane penetration effects on pore pressure development. Due to the complexity of the relationship between the effective stress changes, the membrane penetration, and the tendency for volume change and pore pressure development, the consequences of membrane penetration and compliance on the measured steady state relationship cannot be described completely. Until these consequences have been more explicitly described and verified with laboratory test data, the implications of membrane compliance with regards to measured steady state relationships should be treated with caution and should be considered a possible source of error contributing to the significant scatter commonly observed in measured steady state test data.

CHAPTER 5 EFFECTS OF END RESTRAINT

The fact that friction between the end platens affects the results of the triaxial test has been recognized and accepted for quite some time (Taylor 1940). The exact nature of the effect has never been fully explained, however. Many studies have been performed in an attempt to quantify this effect (Rowe and Barden 1964, Barden and McDermott 1965, Bishop and Green 1965, Duncan and Dunlop 1968, Perloff and Pombo 1969, Raju et al. 1972, Lee 1978). In order to minimize end effects, the most routine practice is to use conventional end platens and specimens with a length to diameter ratio (L/D) of two or greater, which minimizes any end effects during tests to determine peak shear strength parameters (Head 1986). Since the specimen undergoes large deformations during tests to determine steady state shear strength parameters, it is expected that the significance of the friction on the specimen ends will be greater. The practice of using slender specimens ($L/D \geq 2$) to minimize the influence of the end effects on measured parameters may not be valid for steady state triaxial tests. As the specimen is sheared beyond the peak stress level, the actual stress-strain characteristics of the end platen-soil interface will have more effect on the measured response of the specimen. While the development of lubricated end platens for triaxial testing has been investigated, their use has typically been for testing of cohesive materials. It seems plausible that an end platen lubrication scheme that is effective for granular materials and at large displacements might be necessary to minimize end restraint effects for steady state conditions.

Effects of Friction on the Specimen Ends

Volume Change Effects

For drained loading, end restraint causes nonuniform volumetric strains to develop within the specimen (Shockley and Ahlvin 1960, Duncan and Dunlop 1968). Consequently, the average or measured volumetric strain may not accurately depict the volumetric strain. Shockley and Ahlvin (1960) noted that the variation in density within sand specimens during drained loading could be as much as 8 to 10 pounds per cubic foot at an axial strain level of only 10 percent. They also found that regardless of density, the sand tended to dilate in the failure zones and contract at the specimen ends. Bishop and Green (1965) concluded that for drained tests on sand, end restraint did not appear to affect the volumetric strain at failure.

For undrained loading of a saturated specimen, end restraint results in localized volume change within the specimen as water migrates within the specimen as induced pore pressures equalize. Duncan and Dunlop (1968) concluded that for tests on saturated clays, these effects are unimportant unless they result in changes in measured strength, pore pressure, or stress-strain behavior. Whitman et al. (1960) presented data that showed that the water content of saturated normally consolidated clay specimens was an average of 0.6 percent greater at the ends than at the middle after undrained loading, indicating that the ends of the specimen are less dense than the failure region. For over-consolidated clays the variation was the opposite, with the ends becoming denser (Whitman et al. 1960).

Pore Pressure Effects

The shear stresses induced by the end platens during undrained loading cause the development of nonuniform pore pressures within the specimen (Barden

and McDermott 1965, Blight 1965). As noted previously, the subsequent equalization of the nonuniform pore pressures requires migration of water within the specimen, resulting in local density variations. The extent of the pore pressure variation within the specimen is dependent upon the strain rate (Duncan and Dunlop 1968), since the pore pressures tend to equalize with time. Consequently, the variation of pore pressure increases when the strain rate is increased (Bishop et al. 1960). Although reducing the rate of strain allows more time for equalization of pore pressures, it also results in more water migration, and hence void ratio variation, which affects the measured shear strength (Barden and McDermott 1965).

Stress and Strain Distribution Effects

The restraint on the specimen ends results in nonuniform distributions of total stresses and strains within the specimen. Shockley and Ahlvin (1960) found that for drained loading of sand specimens, the variations in stress and strain were similar and that the axial strain at the specimen ends was nearly zero, with the maximum axial strain occurring just below the mid-height of the specimen. Kirkpatrick and Belshaw (1968) noted that end restraint results in nonuniform strains in sand specimens, but that the deformation pattern approaches homogeneous conditions as the restraint is reduced to zero. Barden and McDermott (1965) concluded that the use of ends with reduced friction characteristics could improve the uniformity of both the stress and deformation patterns within the specimen.

Rowe and Barden (1964) demonstrated that either local density or pore pressure variations (depending on drainage conditions and loading rate) will develop regardless of whether conventional or lubricated end platens are used, but that the stress and deformation patterns would approach the homogeneous case if the friction was eliminated. Olson and Campbell (1964)

found that the use of lubricated ends for undrained tests on clays did not reduce the observed bulging (nonuniform deformation) of the specimen. Bishop and Green (1965) found that for drained tests on sands, the specimen ends did not expand regardless of whether or not lubricated end platens were used.

Januskevicious and Vey (1965) internally instrumented triaxial test specimens of dry sand and found that the strains vary along the length of the specimen when conventional ends are used, but that the local strains are consistent with average values (based on external measurements) when reduced-friction ends are used. When conventional ends were used, the axial strain at the mid-height of the specimen was approximately 120 to 150 percent of the average value, while the strain near the ends was approximately 25 to 50 percent of the average value (Januskevicious and Vey 1965). They also concluded that the variation increased from the axis of the specimen toward the perimeter. For tests on dry sand, Kirkpatrick et al. (1974) found that at the mid-height of the specimen the measured axial strain was 150 percent of the average axial strain at the axis and 175 percent of the average axial strain at the perimeter, supporting the findings of Januskevicious and Vey.

However, Kirkpatrick and Belshaw (1968) found that the axial strains were uniform at the perimeter, but at the axis the axial strain concentrates at the mid-height of the specimen and is essentially zero at the ends. They attributed this phenomenon to the existence of conical quasi-rigid zones at each end platen that results in essentially uniform conditions at the perimeter, but localized strain at the axis (Kirkpatrick and Belshaw 1968). Kirkpatrick and Younger (1970) found that the axial strain at the middle of the specimen was 2 to 3 times greater than the average axial strain, and the axial strain at the ends was approximately 10 to 20 percent of the average axial strain. The variation, which developed at axial strain levels as low as 4 percent, increased as strain

level increased, and was greater at the axis than at the perimeter (Kirkpatrick and Younger 1970).

Effects on Measured Parameters and Shear Strength

As a consequence of the stress and strain distributions within the specimen, the measured stress-strain response will be affected by the friction on the specimen ends (Barden and McDermott 1965, Bishop and Green 1965). Duncan and Dunlop (1968) noted that end restraint results in a slight increase in the slope of the stress-strain curve, a slight decrease in the strain level at failure, and a slight increase in the undrained strength of clay specimens. Whitman et al. (1960) concluded that the undrained strength should not be affected by the inherent local volume changes that will occur during undrained loading of clay specimens. Olson and Campbell (1964) found that the use of lubricated ends for undrained tests on clays did not affect the total stress envelope, but reduced the effective friction angle by 3 degrees. Comparatively, they found that increasing the length to diameter ratio from 1.5 to 3.5 only reduced the effective friction angle by 1.5 degrees. Blight (1965) found no significant difference in the measured undrained strength of clays regardless of whether conventional or reduced-friction end platens were used.

The drained strengths measured when end friction is reduced are slightly lower than those measured in tests with conventional end platens (Bishop et al. 1960, Rowe and Barden 1964). Bishop and Green (1965) noted that end restraint increased the apparent strength, but the increase depended on the L/D ratio, and was minimal for L/D=2. Lee (1978) concluded that the end conditions only slightly influence the drained friction angle, but significantly influence the critical confining pressure. Since the volume change characteristics are affected by end restraint, the measured drained strength is also affected (Lee 1978).

Treatments in Literature to Minimize End Friction

In order to try to minimize the effects of end friction on the measured behavior of triaxial test specimens, various attempts have been made at reducing the frictional resistance of the specimen-end platen interface. Characteristics of various interfaces have been studied, and the effects of end friction reduction on triaxial test results have been investigated.

Interface Direct Shear Tests

In order to investigate the shear behavior of alternative soil-end platen interfaces, researchers have conducted direct shear tests on various interfaces. Rowe and Barden (1964) performed direct shear tests to examine the influences of varying the platen, lubrication, normal stress, and rate of shear on the friction characteristics of the interface. They found that friction angles of 1 degree or less were possible using the grease and latex membrane scheme. Tatsuoka et al. (1984) performed direct shear tests on various lubrication layers and sand specimens using a displacement rate of 0.2 millimeters per second. They measured apparent friction angles less than 1 degree for fine sands and concluded that one layer of grease between two layers of latex provided the best lubrication. Goto et al. (1993) conducted cyclic direct shear tests on grease and latex lubrication schemes and granular soils and measured apparent friction angles less than 1 degree. Lee and Seed (1964) performed direct shear tests on sand specimens using various lubrication schemes and recommended the scheme used by Rowe and Barden. For the grease and latex scheme, they measured apparent friction angles of 1 degree for silt and 8 degrees for Ottawa sand. Lee (1978) conducted direct shear tests on sand interfaces using a grease and latex lubrication scheme using a displacement rate of 0.001 inches per second and concluded that apparent friction angles of 1 degree or less are unachievable using thin latex membranes. Stress

concentrations can develop at the granular contacts of the sand since the sand grains can penetrate the latex, reducing the efficiency of the lubricated ends and resulting in a higher apparent friction angle for granular materials than for fine-grained soils (Lee and Seed 1964, Lee 1978, Goto et al. 1993). As a result of the stress concentrations that can develop at the granular contacts, the maximum shear stress increases as grain size increases (Lee 1978, Goto et al. 1993). Goto et al. (1993) also determined that the friction characteristics of sand interfaces are independent of void ratio.

Rowe and Barden (1964) concluded that the shear behavior of the lubrication scheme is independent of normal stress. However, Tatsuoka et al. (1984) observed that the apparent friction angle increased as normal stress increased and Goto et al. (1993) concluded that the apparent friction angle decreases as normal stress increases.

Rowe and Barden (1964) concluded that the shear behavior of the lubrication scheme is rate dependent due to the viscosity of the grease. Contrary to the findings of Rowe and Barden, Lee and Seed (1964) and Lee (1978) concluded that for sand specimen interfaces, shear behavior is independent of rate of shear.

Lubricated End Platens

Rowe and Barden (1964) investigated the use of radially segmented end platens on rollers and both lead shot and a water bag at the specimen-platen interface to try to minimize lateral restraint effects, but concluded that none of these options was satisfactory. Instead, they recommended a layer of grease and a latex membrane between the platen and the specimen, and concluded that the use of enlarged lubricated end platens could reduce the concentration of excessive dilation in the failure zones, delay the formation of a slip surface, and reduce piston friction (Rowe and Barden 1964). Because shorter specimens

can be used, the test time can be reduced since pore pressure gradients will be lower and the density variations can be minimized (Rowe and Barden 1964, Head 1986). Olson and Campbell (1964) found that the use of lubricated ends for undrained tests on clays reduces the induced pore pressure variation within the specimen. Duncan and Dunlop (1968) studied the effectiveness of the lubrication layer to help explain the variation in results of previous studies. They noted that the coefficient of friction for the lubrication is a function of the thickness of the layer, and that the thickness can decrease with time as the grease extrudes under pressure. The decrease in the value of the coefficient of friction over time was predicted using a theoretical relationship to describe the decrease in thickness of the grease layer based on viscosity, geometry, load, and elapsed time and test results relating the theoretical thickness to measured coefficient of friction (Duncan and Dunlop 1968). Based on Unconsolidated unconfined (UU) triaxial test results, they concluded that the apparent limiting value of friction angle for effective lubrication was 2 degrees. Duncan and Dunlop (1968) concluded that the advantages of using lubricated end platens are insignificant for undrained testing of clays, and that the use of lubricated ends is only warranted for drained tests on sands when unusually accurate volumetric strain measurements at large values of axial strain are required.

Kirkpatrick and Younger (1970) found that axial strains in specimens with L/D=1 using lubricated ends were essentially uniform up to an axial strain level of 10 percent. They concluded that when lubricated ends are used, the strains in the specimen remain essentially uniform until nonuniform deformation is observable. Kirkpatrick et al. (1974) found that lubricated end platens reduced the variation of measured axial strains within the specimen to plus or minus 25 percent of the average axial strain. Raju et al. (1972) determined that the use of lubricated ends resulted in uniform stress and deformation patterns until the peak behavior is observed. They noted that uniform deformation continued

to axial strain levels of 18 percent when lubricated ends were used, compared with 7 to 10 percent when conventional ends were used. Raju et al. (1972) concluded that when lubricated ends were used: less dilation occurred, no failure surface developed, no peak stress occurred for dense sands, the axial strain at the peak deviator stress increased, and the drained friction angle was reduced by 1 to 3 degrees. They proposed that the development of a shear surface and the peak behavior observed in tests on dense sands are not a true material characteristic, but are a function of the test conditions (Raju et al. 1972).

Lee (1978) studied the effects of end restraint on saturated sand specimens. He found that the use of reduced-friction ends in drained tests resulted in a flatter initial slope of the stress-strain curve, a slightly lower strength, and greater tendency for dilation or less tendency for contraction depending on initial conditions. He found that for drained tests, the critical confining pressure and the tendency for dilation increased when reduced-friction ends were used.

In undrained tests, Lee (1978) found that the use of reduced-friction ends resulted in a slightly lower (approximately 5 percent) undrained strength, but had little effect on pore pressures and effective stress parameters. He also found that dense specimens have a greater tendency for negative pore pressure development and loose specimens have less tendency for positive pore pressure development when lubricated ends are used. In undrained tests, Lee (1978) found that the critical confining pressure was increased and the effective stress friction angle was approximately 1 degree lower when reduced-friction ends were used.

Head (1986) recommended the use of lubricated end platens for tests in which strain levels will be greater than 10 percent. To minimize stress concentrations

at granular contacts, Head (1986) recommends using a membrane thickness of 1.5 times the mean grain size for the grease and latex lubrication scheme.

Analytical Solutions for Stress Distributions in an Elastic Cylinder with Restrained Ends

In order to quantify the effects of end restraint on stress, strain, and deformation distributions within the specimen can be examined analytically. The solution for the stresses in a cylinder that is laterally restrained at its ends has been sought for many years. The basic problem is that of a circular cylinder that is loaded axially and subjected to the following boundary conditions:

1.) vertical displacement at the ends is uniform

u_z = constant @ $z = 0, h$

2.) horizontal displacement at the ends is zero

$u_r = 0$ @ $z = 0, h$

3.) radial stress at the cylindrical surface is zero

$\sigma_r = 0$ @ $r = R$

4.) shear stress at the cylindrical surface is zero

$\tau_{rz} = 0$ @ $r = R$

The first published attempt at a solution was developed by Filon (1902), who proposed a solution that was not exact and exhibited convergence problems. Filon (1902) noted that the determination of a complete solution would be very complex, but suggested that the inclusion of higher order terms in his solution would improve convergence. Filon's solution did not completely satisfy the condition of zero horizontal displacement on the ends (boundary condition 2 above), but only required that the horizontal displacement was zero at the intersection of the ends and the cylindrical surface (at $r=R$ and $z=0, h$). This

difference in horizontal displacement boundary conditions resulted in an incorrect distribution of shear stress on the ends of the cylinder (Pickett 1944). The results of Filon's solution indicate that yielding would first occur at the intersection of the ends and the cylindrical surface (at $r=R$ and $z=0, h$) at an average vertical stress approximately one half of that required to initiate yielding in a cylinder that is free to deform laterally at the ends. Filon (1902) noted that the numerical results, which predicted yielding at lower average stresses in the restrained cylinder, contradicted typical test results, which indicated that yielding occurred at higher average stresses in the restrained cylinder.

Pickett (1944) proposed a solution to the problem using the Fourier method, which entails expressing the boundary conditions using Fourier series. His solution satisfied all of the boundary conditions of the basic problem (boundary conditions 1 through 4 above). Pickett's solution did not agree with Filon's solution, due primarily to the difference in displacement boundary conditions and the resulting shear stress distributions.

D'Apolonia and Newmark (1951) used a lattice, or framework, analogy to solve the restrained cylinder problem. The stress distributions resulting from their solution are similar to those resulting from Pickett's solution, but the magnitudes of the stresses calculated using the solution of D'Apolonia and Newmark are slightly smaller in most cases.

Balla (1957, 1960) proposed a solution based on a stress function in cylindrical coordinates. The stress function included products of polynomial functions, trigonometric functions, and Bessel functions, and the results agreed reasonably well with those of Filon (Balla 1957). Balla also included a roughness coefficient to model friction on the ends of the cylinder, and relaxed the corresponding boundary condition (zero horizontal displacement at the

ends) modeling end friction (Balla 1957, 1960). Balla's solution exhibited convergence problems, especially in the expression for vertical stress near any of the boundaries of the cylinder.

Perloff and Pombo (1969) were the first to employ finite element techniques to the solution of the restrained cylinder problem. Their solution also employed an elastic-plastic constitutive law that could model strain hardening and strain softening (Perloff and Pombo 1969). Their results indicate that the errors introduced into the stress-strain relationship by using external measurements only are most significant after yielding occurs in materials that exhibit strain softening, with the calculated stiffness being much less than the true stiffness. They further indicate that the error in the calculated stiffness decreases as the ratio of length to diameter (L/D) increases, and that L/D ratios of 3 or greater are required in order to prevent these errors (Perloff and Pombo 1969). For perfectly plastic and strain-hardening materials, the errors are minimal even after yielding, with the calculated stiffness being only slightly greater than the actual stiffness. It should be noted that the magnitude of the error associated with the calculated stiffness is a function of the constitutive law used in the analysis, so the results of Perloff and Pombo regarding L/D ratios may not apply to other constitutive relationships, although the general trend of decreasing error with increasing L/D ratio should still be valid. Because the end restraint causes both an increase in confinement and a stress concentration, the yield stress for the restrained cylinder can be either greater than or less than that for the unrestrained cylinder, depending on which effect is more pronounced (Perloff and Pombo 1969). For the cases analyzed by Perloff and Pombo (1969), yielding first occurred approximately halfway between the ends and the mid-height of the specimen (at the quarter points), progressed toward the mid-height, and finally progressed toward the ends.

Girijavallabhan (1970) analyzed the problem using a linearly elastic finite element model and compared his results to those of the earlier attempts at analytical solutions for the linearly elastic restrained cylinder, and concluded that the solution of Pickett (1944) appeared to agree fairly well with the finite element solution. Girijavallabhan (1970) also noted the dependency of the difference between the solutions for the restrained and unrestrained cylinder on Poisson's ratio, with the difference becoming much more pronounced as Poisson's ratio increases.

Figure 5.1 shows plots of the axial stress distribution on the end of a specimen with a value of L/D of 1 and a value of Poisson's ratio of 0.25 based on the various solutions. A solution by the finite element method (FEM) is shown as well, and is considered to be the correct solution. The axial stress has been normalized by the average axial stress, computed by dividing the applied force by the cross-sectional area. On most of the end surface, the axial stress is about 10 percent less than the average value, and near the edges of the end surface, the axial stress increases significantly. In a true uniaxial stress state that occurs in the absence of end restraint, the axial stress is equal to average axial stress everywhere. The plots demonstrate that all of the solutions correctly predict the variational trend, and all except Filon (1902) are accurate to within 10 percent.

Figure 5.2 shows plots of the normalized radial stress distribution at the end of the same cylinder. The plots of radial stress demonstrate that some of the solutions were in error. The radial stress in the specimen at the end of the cylinder is approximately 28 to 30 percent of the average axial stress. In a true uniaxial stress state that occurs in the absence of end restraint, the radial stress is equal to zero. The only solution that reasonably predicts the radial stress at the end is Pickett (1944), which diverges from the correct solution

near the perimeter. All other solutions exhibited significant errors in the radial stress computation.

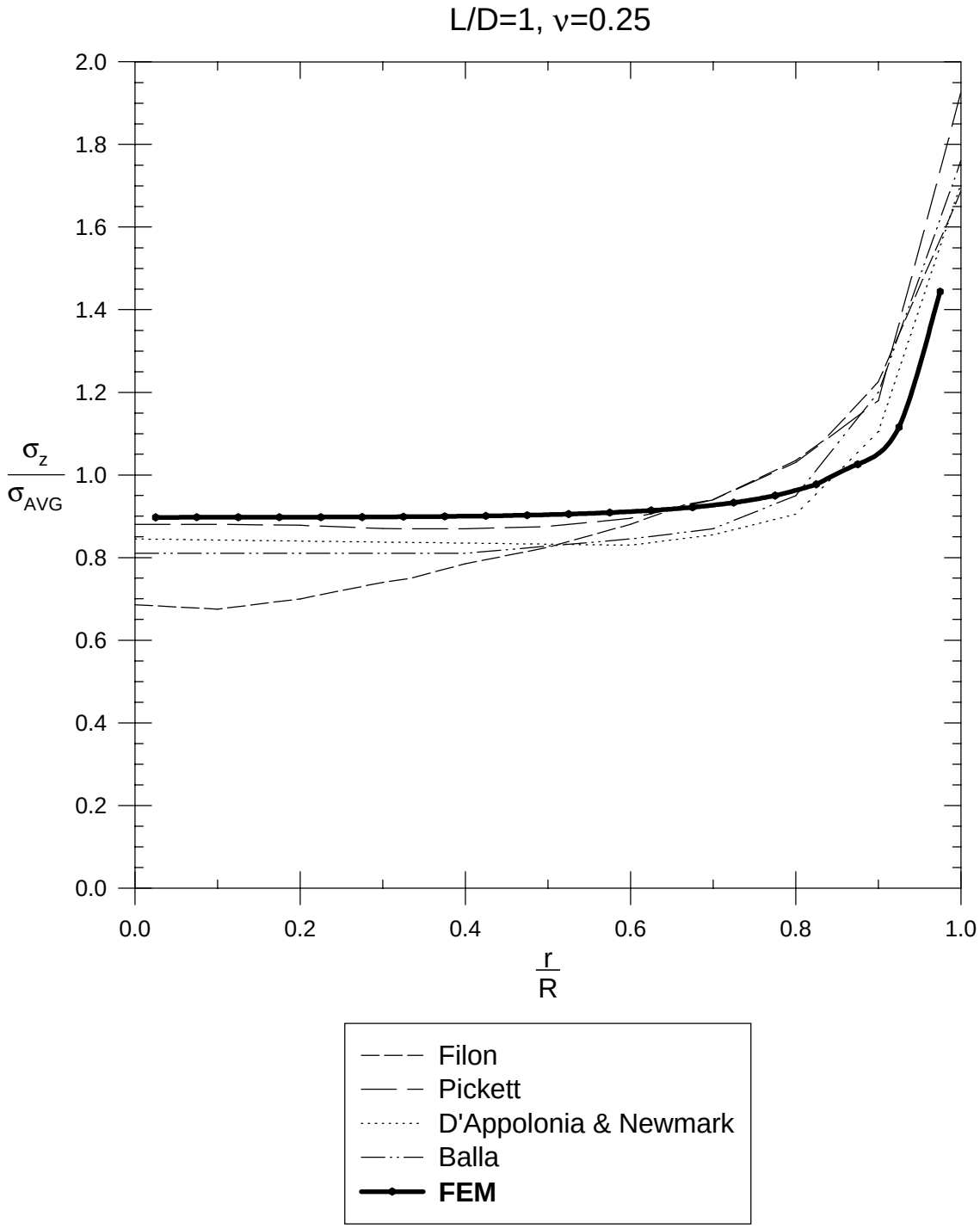

Figure 5.1 - Axial Stress Distributions on the End of an Elastic Cylinder

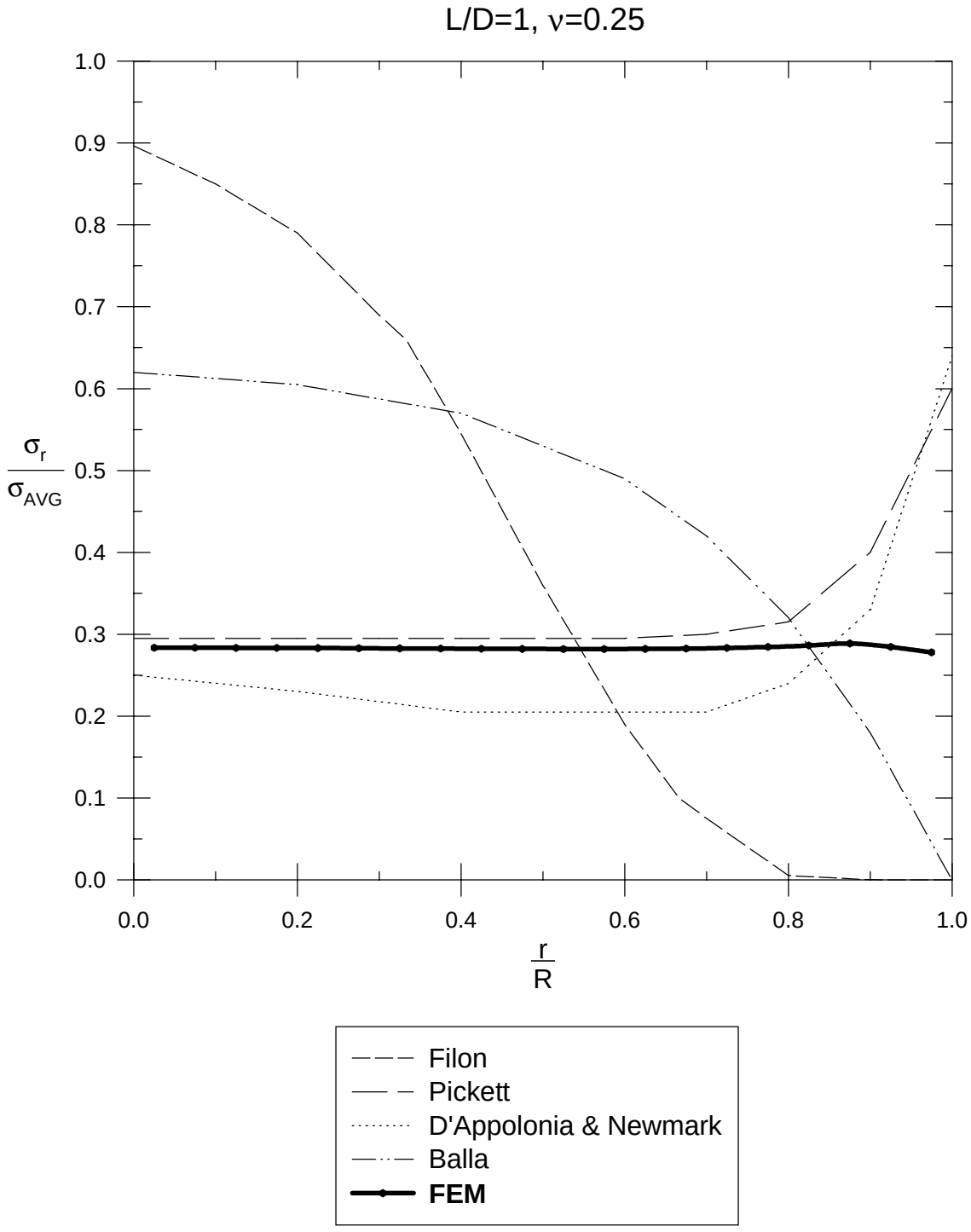

Figure 5.2 - Radial Stress Distributions on the End of an Elastic Cylinder

Figure 5.3 shows plots of the normalized circumferential stress distribution at the end of the same cylinder. Except near the perimeter, the circumferential stress is approximately equal to the radial stress. In a true uniaxial stress state that occurs in the absence of end restraint, the circumferential stress is equal to zero. The results of both Pickett (1944) and D'Apolonia and Newmark (1951) are fairly accurate except at the perimeter, while the other solutions again exhibit significant errors.

Figure 5.4 shows plots of the normalized shear stress distribution on the end of the cylinder. The shear stress is equal to zero at the axis, and increases to an apparent value of 30 percent of the average axial stress at the perimeter. In a true uniaxial stress state that occurs in the absence of end restraint, the shear stress on the end is equal to zero. While all but the solution of Filon (1902) predict the general trend correctly, all solutions over-predict the shear stress distribution. The solution of D'Apolonia and Newmark (1951) was the most accurate in terms of the shear stress on the end of the cylinder.

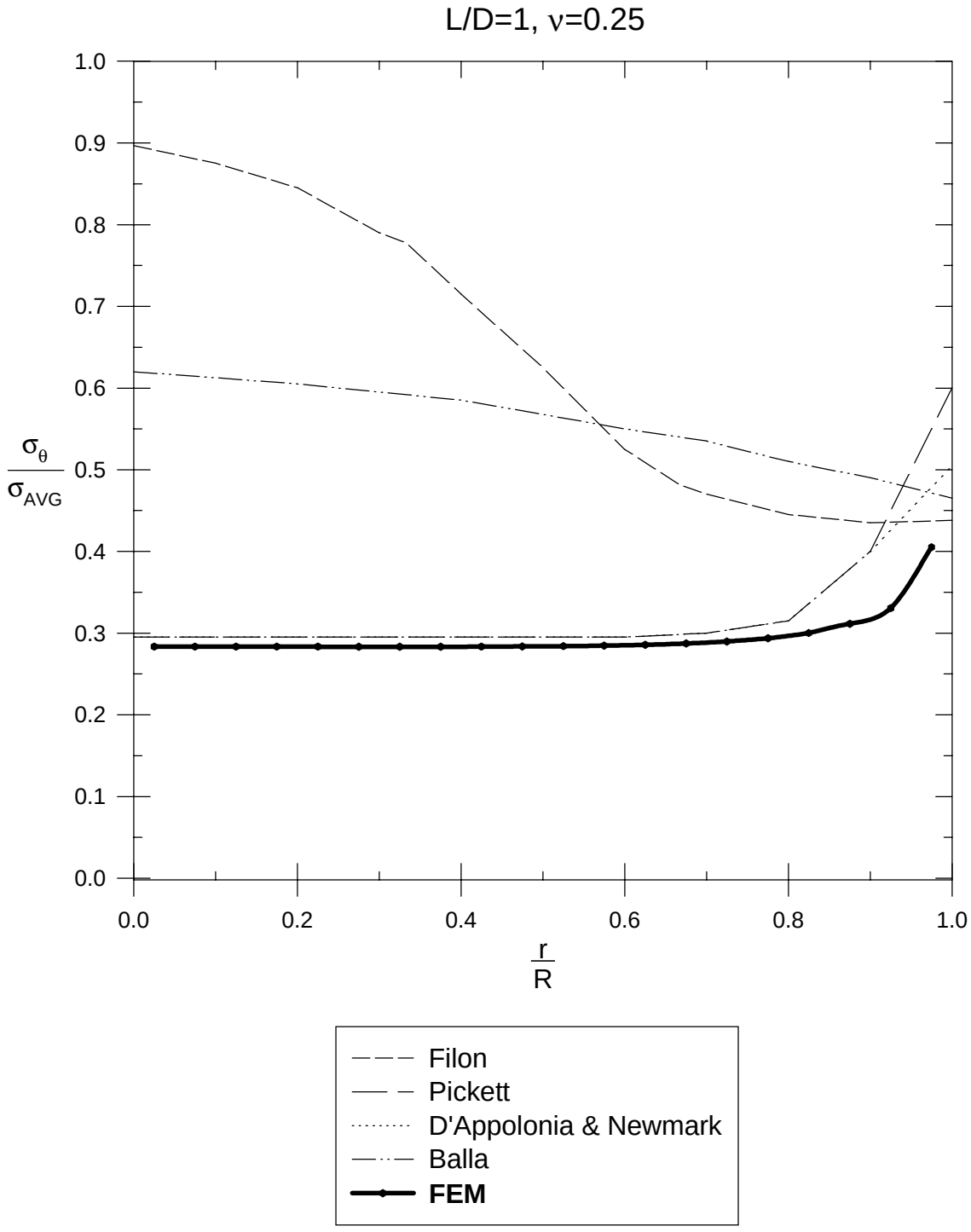

Figure 5.3 - Circumferential Stress Distributions on the End of an Elastic Cylinder

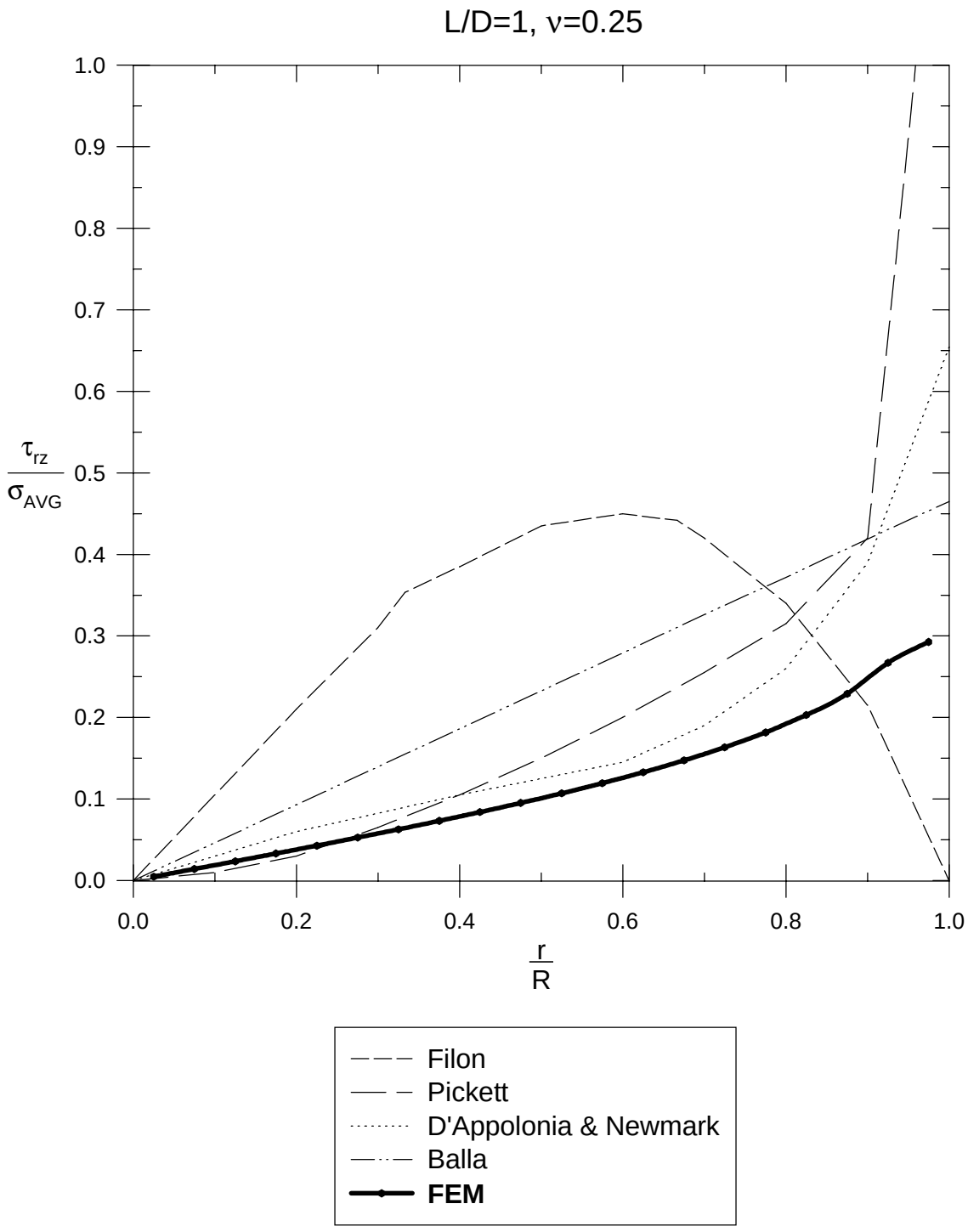

Figure 5.4 - Shear Stress Distributions on the End of an Elastic Cylinder

The stress distributions in the cylinder at the quarter-height (z/h=0.25, 0.75) based on Filon (1902) and the finite element solution are shown in Figure 5.5. In this region of the specimen, the stresses more closely compare with those in an unrestrained cylinder. The effects of the end restraint on the axial stress at this point are minimal. The radial and circumferential stresses are approximately 10 percent of the average axial stress at the axis due to end restraint, but are unaffected at the perimeter. The shear stress is unaffected at the axis and at the perimeter, but is approximately 5 percent of the average axial stress halfway between the axis and the perimeter.

The stress distributions in the cylinder at the mid-height (z/h=0.5) based on Filon (1902), Pickett (1944), and the finite element solution are shown in Figure 5.6. In this region of the specimen, the stresses are nearly unaffected by end restraint, although a slight increase in axial stress due to end restraint is still noticeable.

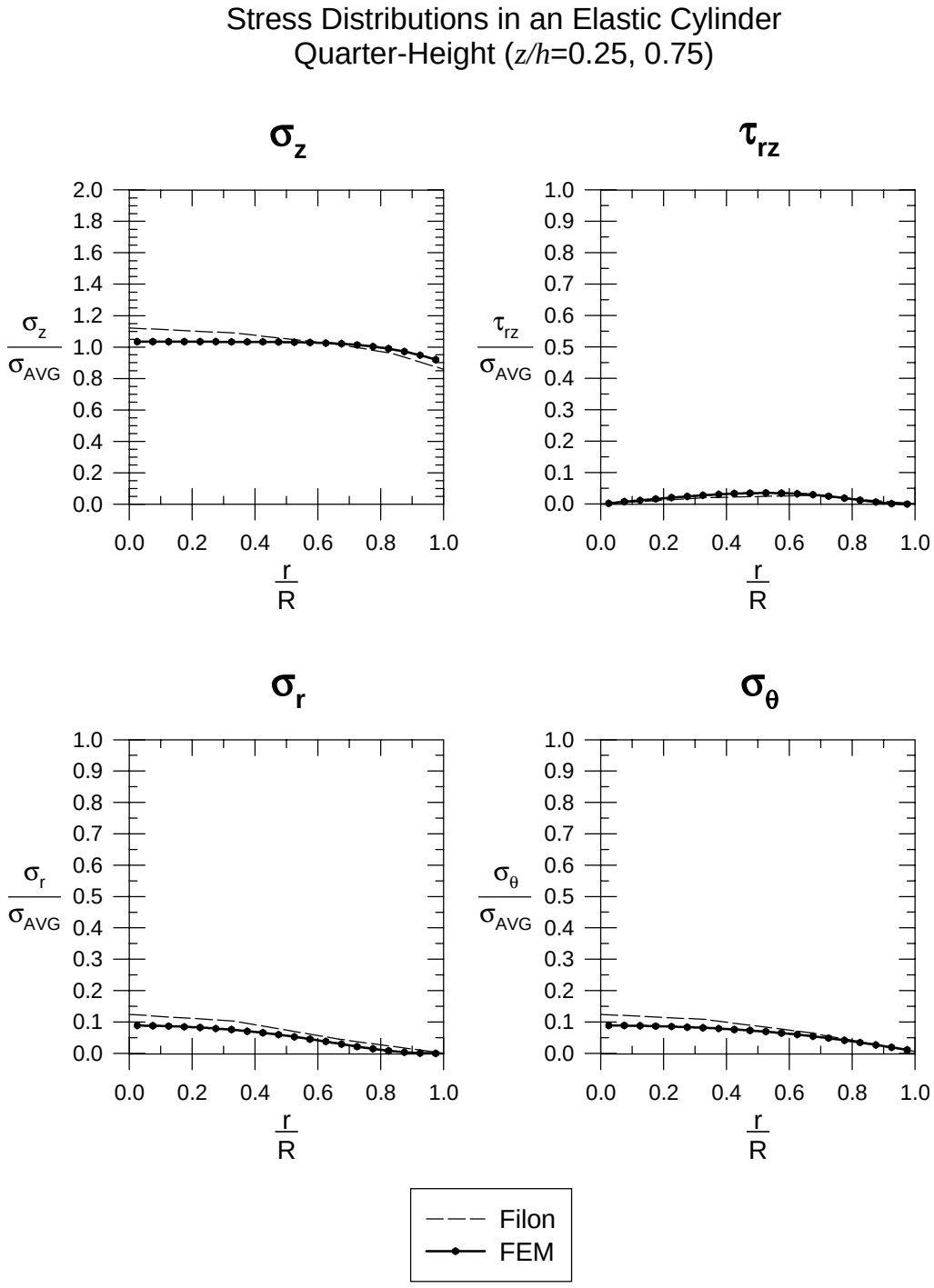

Figure 5.5 - Stress Distributions at the Quarter-Height of an Elastic Cylinder

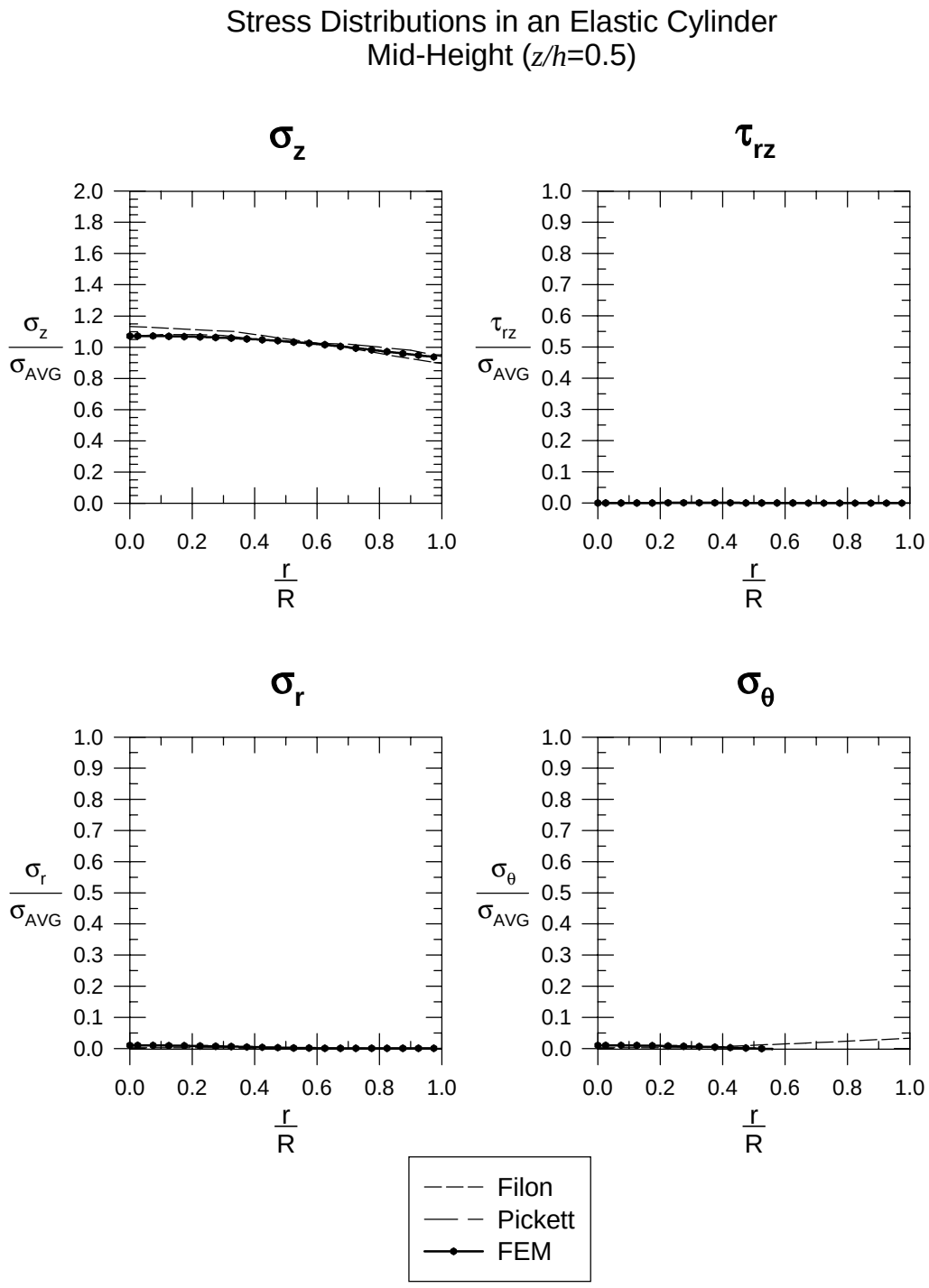

Figure 5.6 - Stress Distributions at the Mid-Height of an Elastic Cylinder

The previous attempts at analytical solutions to the restrained cylinder problem, though not entirely accurate, demonstrated the usefulness of examining the distributions of stresses that result from complete end restraint to better understand the influence of end restraint on measured parameters. Based on the results presented in Figure 5.5 and Figure 5.6, however, it could be concluded that the end restraint is negligible even for and L/D ratio of one. However, it must be remembered that the distributions of stress are a function of Poisson's ratio for an elastic material. Girijavallabhan (1970) demonstrated that the variation in stresses increases significantly as Poisson's ratio increases. More generally, the distributions of stress are a function of the assumed constitutive relationship (Perloff and Pombo 1969). Furthermore, the solutions presented provided only for complete lateral restraint at the specimen ends, which does not accurately represent the true frictional characteristics of the specimen-end platen interface in a triaxial test. Due to the limited applicability of the results of previous analytical solution attempt, finite element analyses were undertaken to examine the effects of specimen end friction based on different material models and by allowing for variation in both stiffness and shear strength in characterizing the interface friction.

CHAPTER 6 INTERFACE DIRECT SHEAR TESTS

Introduction

Series of interface direct shear tests were performed in order to characterize the behavior of the end platen-soil specimen interface. The desired parameters include the shear strength of the interface, in terms of a Mohr-Coulomb shear strength envelope, and the shear stiffness of the interface, relating the shear displacement to shear stress. During a triaxial test, this interface is loaded by an increasing normal stress increment, which is a direct result of the applied deviator stress. In addition, the interface is loaded in shear as a result of the tendency for relative displacement between the end platen and the specimen, which in turn is a consequence of the tendency for greater lateral deformation in the soil than in the end platen.

In a conventional direct shear test, the soil specimen is first loaded one-dimensionally in the direction normal to the slip surface and allowed to consolidate, then loaded in shear along a predetermined slip plane while keeping the normal force on the specimen constant. Such a test is easily adapted to the testing of interface behavior for the following reasons:

1.) The slip plane is predetermined, so the behavior of the interface is easily isolated from the behavior of the two independent materials

2.) The response to applied normal stress increments and the response to applied shear stress increments are measured separately, affording easy calibration of uncoupled stress-displacement constitutive models.

During a triaxial test, the normal and shear stresses on the end platen-specimen interface are changing simultaneously, while during the interface

direct shear test they are not. The behavior under combined stress changes, however, can be modeled easily based on the independently measured response. As a result, even though the direct shear test does not exactly model the loading conditions on the end platen-specimen interface during a triaxial test, it does provide a convenient and reliable way to evaluate both shear strength and shear stress-displacement parameters for modeling the interface behavior.

Description of Test

The testing procedures and equipment were based on the conventional direct shear test for soils, as outlined in *ASTM D3080-90* (ASTM 1995). A standard square direct shear box measuring 4 inches on each side and 2 inches deep, as shown in Figure 6.1, was used. The bottom half of the box was filled with an aluminum blank that measured 0.875 inches in height, allowing 4-inch square plates that were 0.125 inches thick of the various structural (end platen) materials to be placed in the bottom half of the shear box so that they aligned with the slip plane as shown in Figure 6.1. The soil specimen was compacted in a moist condition into the top half of the shear box, then saturated and consolidated according to standard procedures.

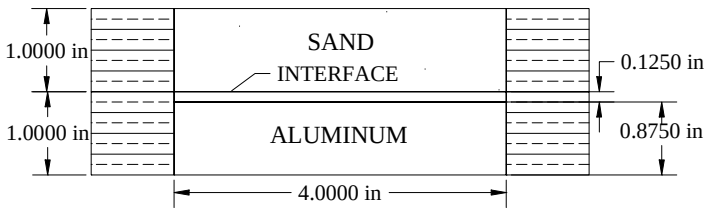

Figure 6.1 - Interface Direct Shear Box

Rate of Displacement

The displacement rate was selected based on expected relative displacement rates along the end platen-specimen interface during the shear phase of a triaxial test. During the test, the specimen, which is less stiff than the end platen, has a greater tendency for lateral deformation than the end platen does for a given increment of deviator stress. As a result, the specimen has a tendency to displace radially relative to the end platen. If the interface were completely rigid (infinite shear stiffness), shear stresses would develop in the radial and circumferential directions as a result of the tendency for radial relative displacement. In the other limiting case, the interface is completely frictionless, so no shear stresses develop and the relative displacement is governed only by the respective tendencies for lateral displacement in the two adjacent materials (the end platen and the soil specimen). In reality, what actually occurs is somewhere in between fully rigid and fully frictionless cases. As the applied deviator stress imparts a tendency for relative displacement between the end platen and the specimen, some displacement occurs, but due

to the frictional nature of the end platen-specimen interface, shear stresses develop and the actual relative displacement is less than would occur if the interface were frictionless. Based on the preceding discussion, it can be seen that the amount of relative displacement that occurs along the end platen-specimen interface for a given increment of applied deviator stress is a function of the shear stiffness and shear strength of the interface.

Furthermore, since the relative displacement is in the radial direction only, continuity requires that there be zero radial displacement, and likewise relative displacement, at the axis of the specimen ($r = 0$). In fact, the amount of relative displacement that occurs along the end platen-specimen interface for a given increment of applied deviator stress is also a function of the distance from the axis to the point of interest, varying from zero at the axis of the specimen to a maximum value at the radius of the specimen.

In view of the variations of the relative displacement with both the shear stiffness and the radius, it is useful to determine the limits for the range of possible rates of relative displacement. Obviously, at the axis of the specimen the rate of relative displacement will be zero regardless of the interface stiffness, which relates shear stress to relative displacement for the interface, or the rate of axial strain resulting from the application of the deviator stress. The maximum rate of relative displacement between the end platen and the soil specimen occurs if the interface is completely frictionless; it occurs at the intersection of the end cross section and the cylindrical surface of the specimen. Based on the following assumptions:

1.) Constant volume (undrained test, completely saturated)

2.) Constant rate of axial strain

3.) Frictionless interface and rigid end platen

4.) r_0 = initial radius of specimen

the following equations can be used to determine the rate of relative displacement along the specimen-platen interface:

$$r = r_0 \frac{1}{\sqrt{1-\varepsilon_a}} \qquad \text{Equation 6.1}$$

$$\Delta r = r - r_0 = r_0\left(\frac{1}{\sqrt{1-\varepsilon_a}} - 1\right) \qquad \text{Equation 6.2}$$

$$\frac{d}{dt}\Delta r = \frac{d}{dt}\left[r_0\left(\frac{1}{\sqrt{1-\frac{\partial \varepsilon_a}{\partial t}(t)}} - 1\right)\right]$$

$$= \frac{r_0 \frac{\partial \varepsilon_a}{\partial t}}{2\sqrt{1-\frac{\partial \varepsilon_a}{\partial t}(t)}^3}$$

$$\frac{d}{dt}\Delta r = \frac{r_0}{2\cdot(1-\varepsilon_a)} \cdot \frac{\partial \varepsilon_a}{\partial t} \qquad \text{Equation 6.3}$$

where: $\frac{d}{dt}\Delta r$ = rate of relative displacement

r_0 = radius of the specimen

$\frac{\partial \varepsilon_a}{\partial t}$ = rate of axial strain

ε_a = axial strain

Equation 6.3 shows that the relative displacement rate at the cylindrical surface increases as each of the following increase: the radius of the specimen, the axial strain rate, and the cumulative axial strain level. For the sands tested for this study, maximum rates of axial strain in the triaxial test were 0.1%/min. Table 6.1 shows rates of relative displacement computed based on Equation 6.3 for typical values of specimen radius and axial strain and an axial strain rate of 0.1%/min.

Table 6.1 - Rates of Relative Displacement

Axial Strain (%)	Rate of Relative Displacement (in/min)	
	r_0 = 0.7 in	r_0 = 1.4 in
0	0.000350	0.000700
10	0.000410	0.000820
20	0.000489	0.000978
30	0.000598	0.001195
40	0.000753	0.001506
50	0.000990	0.001980

Based on the rates computed in Table 6.1, a rate of displacement of 0.0015 in/min was selected for the interface direct shear tests. This value represents the maximum possible rate of relative displacement on the end platen-specimen interface during a triaxial test on a 2.8-inch diameter specimen if the test is continued to an axial strain level of 40%.

Description of Interfaces

For each interface, three tests were performed at different normal stresses in order to determine the Mohr-Coulomb shear strength envelope and examine the variation of shear stress-displacement behavior with normal stress. Seven different interfaces were tested. Three of these interfaces, as shown in Figure 6.2, consisted of materials conventionally used for triaxial test end platens: polished aluminum (interface 1), fine sintered bronze (interface 2), and coarse sintered bronze (interface 3). For a typical 2.8-inch diameter end platen for testing sand specimens, the platen would likely be made of polished aluminum

or stainless steel with a sintered bronze inset to facilitate drainage. In the nomenclature used to describe the interface direct shear tests, "/" indicates a probable slip surface, while "-" indicates a probable non-slip surface.

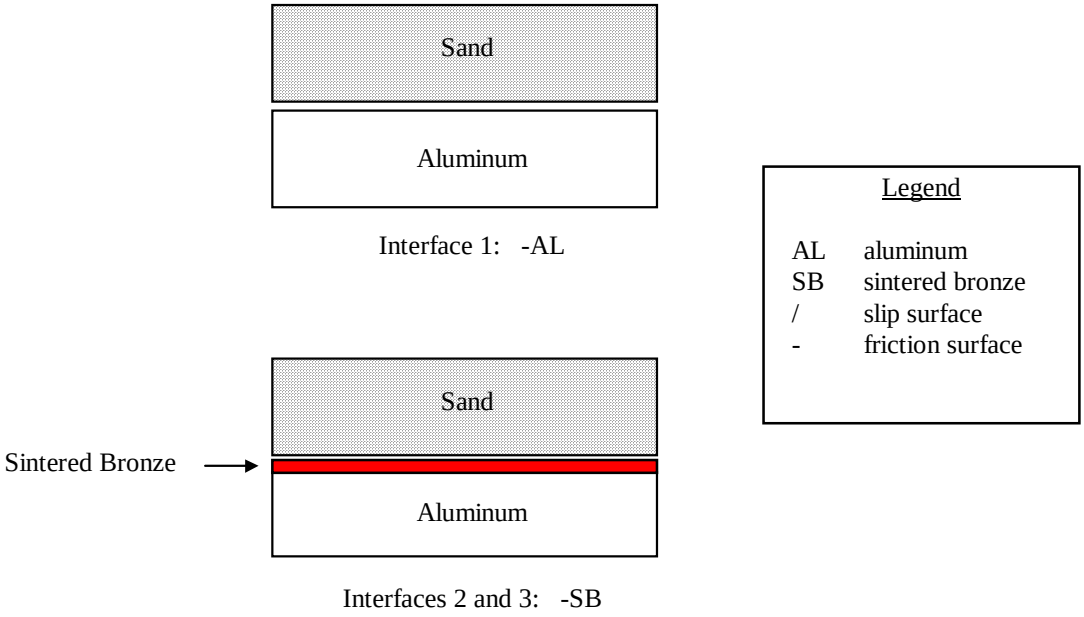

Figure 6.2 - Conventional Interface Configurations

Four interface schemes consisted of different materials to reduce the friction between the end platen and the specimen. The four reduced friction interfaces are shown in Figure 6.3. One configuration consisted of two layers of 0.008-inch thick latex dental dam, with a thin layer of Dow Corning high vacuum grease between the two layers of dental dam and between the bottom layer of dental dam and the aluminum (interface 4). This is the configuration most widely adopted to reduce end platen friction for tests on weak cohesive soils (Whitman et al. 1960, Olson and Campbell 1964, Duncan and Dunlop 1968). The remaining three configurations employed 0.005-inch thick Teflon™ tape. In the first configuration (interface 5), the tape adhered to the aluminum, and the sand was sheared across the Teflon surface. In the second Teflon scheme (interface 6), the Teflon tape adhered to both sides of a 0.003-inch thick steel

shim, which was cut to the dimensions of the shear box. A third layer of Teflon tape adhered to the aluminum, so that the most likely slip surface was between the two layers of Teflon, although slip between the sand and the Teflon was also possible. The third configuration (interface 7) was the same as interface 6, except that the Teflon/Teflon interface was lubricated with a thin layer of vacuum grease. A photograph interface 7 after approximately 0.5 inches of relative displacement is shown in Figure 6.4. Light Castle sand was used as the specimen material for all of the interface direct shear tests.

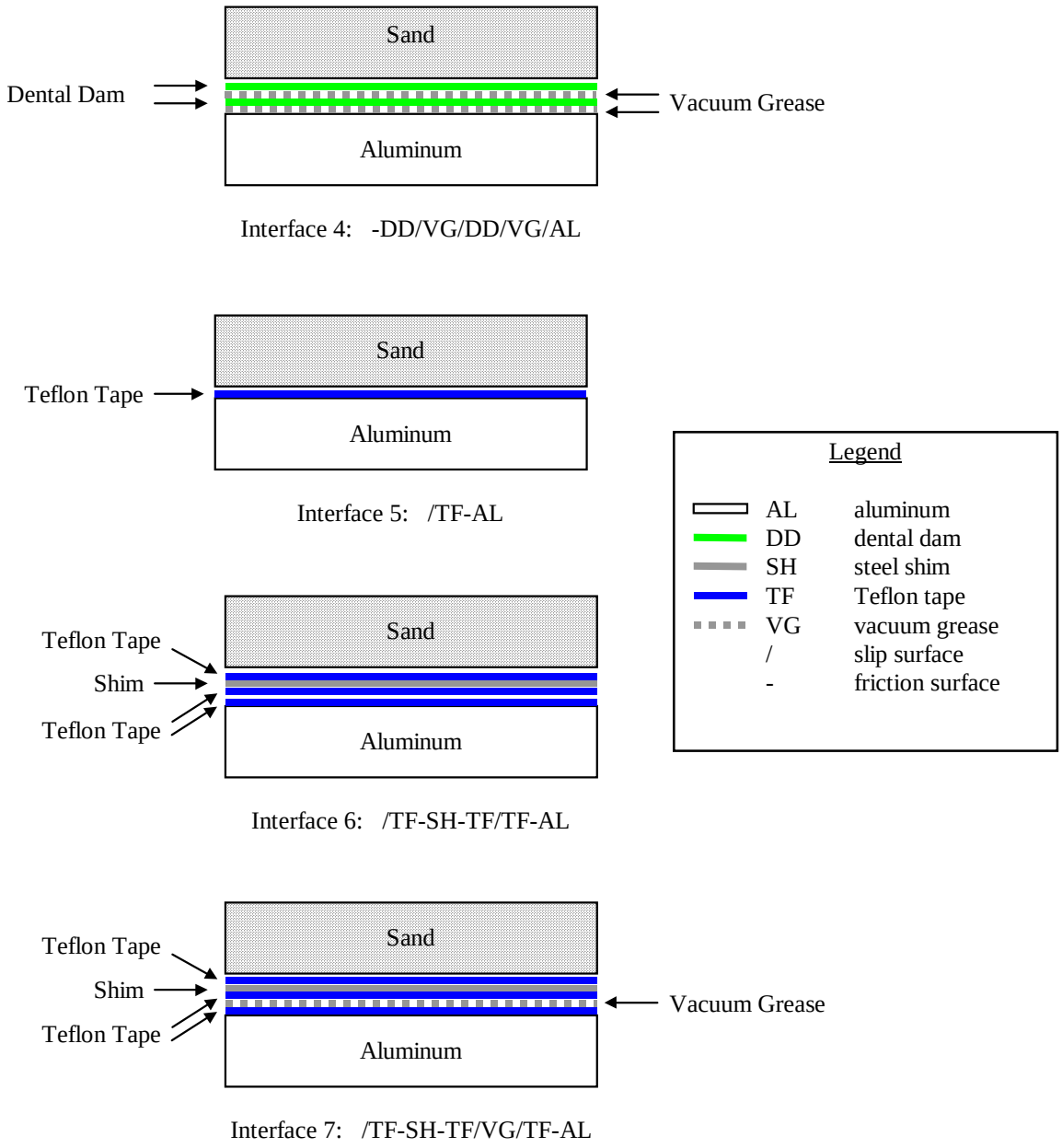

Figure 6.3 - Reduced Friction Interface Configurations

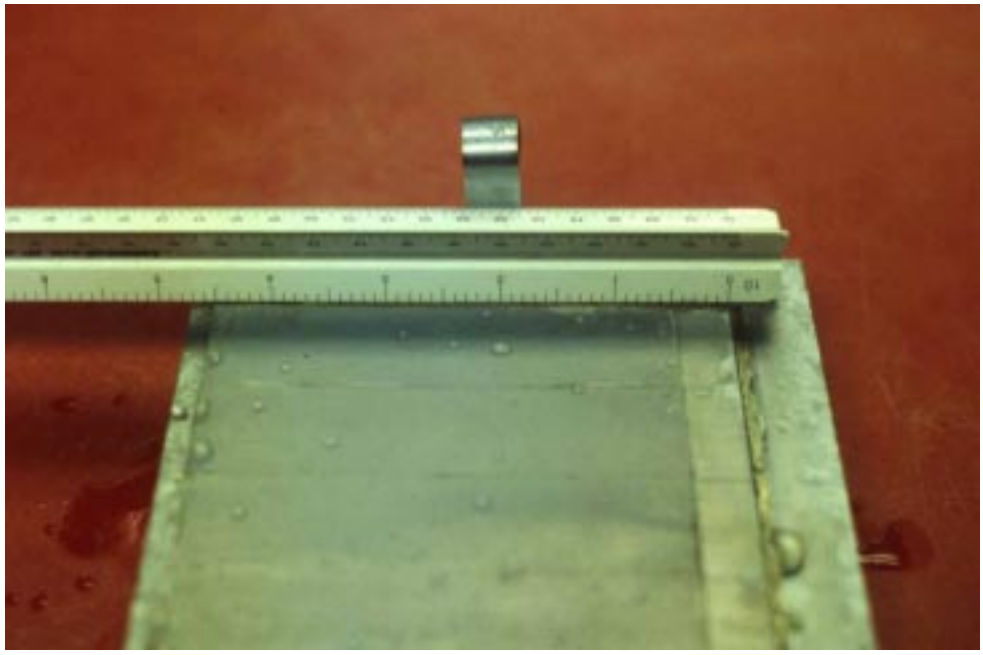

Figure 6.4 - Photograph of Lubricated Interface After Test

Results

Interface Shear Strength

Plots of the reduced data for all of the interface direct shear tests may be found in Appendix F. The Mohr-Coulomb shear strength parameters for each of the interfaces are summarized in Table 6.2. The interface friction angles shown in Table 6.2 are based on the assumption that the interface is cohesionless. The data showed this to be the case for all but interface 4, the single Teflon layer. The friction angle for interface 4 shown in Table 6.2 is based on $c = 0$, but and envelope with a positive cohesion intercept and lower friction angle than that shown in Table 6.2 would better match the test results. Interface 4 was neither the strongest nor the weakest of the seven interfaces tested, so the reason for this discrepancy as compared to the other interfaces was not investigated.

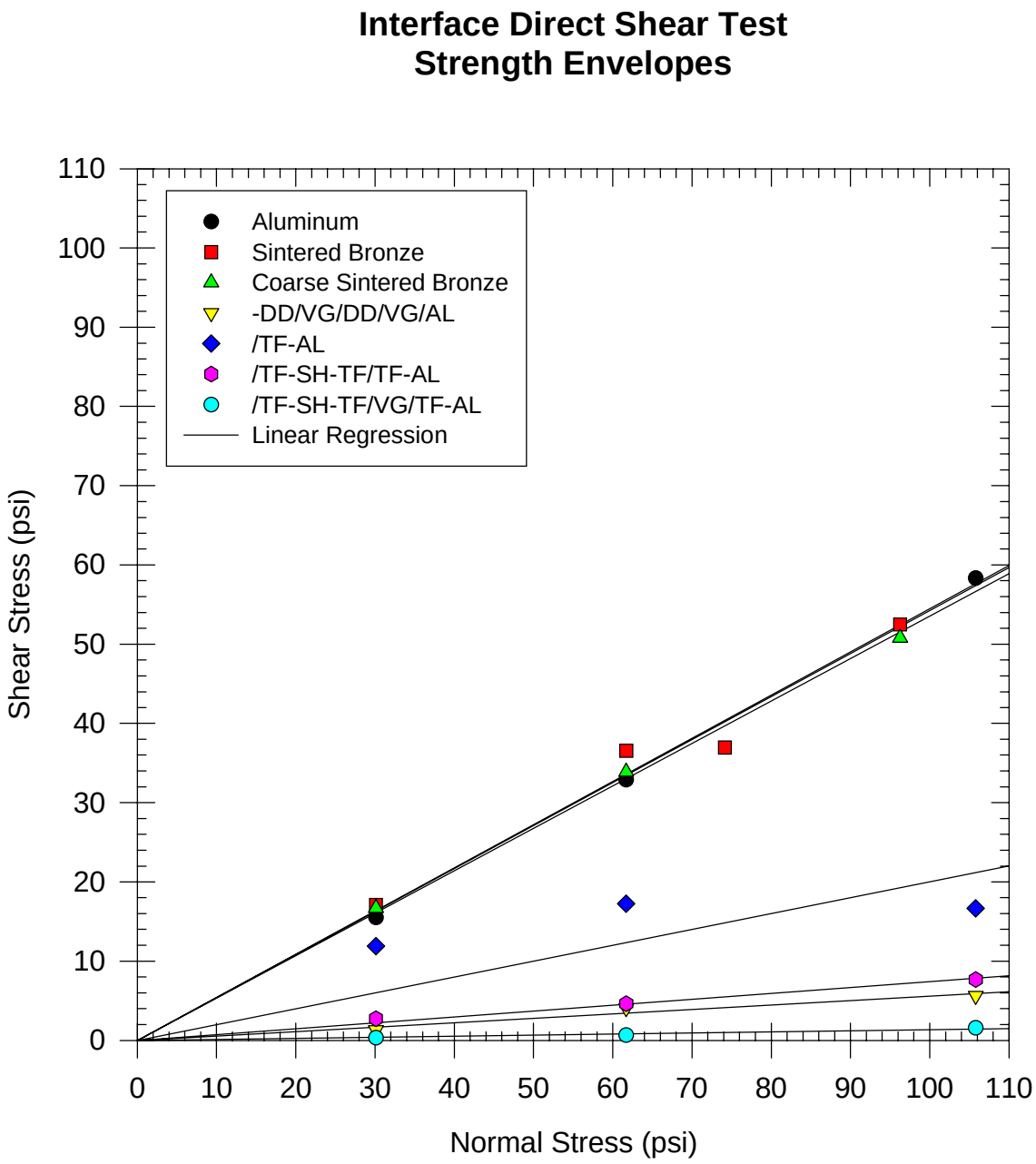

Figure 6.5 - Interface Shear Strength Envelopes

Table 6.2 - Shear Strength Parameters Determined from Interface Direct Shear Tests

Interface Configuration		ϕ **(deg) if** c **= 0**
Aluminum	-AL	28.5
Sintered Bronze	-SB	28.5
Coarse Sintered Bronze	-SB	28
Dental Dam/Vacuum Grease	-DD/VG/DD/VG/AL	3.2
Teflon (1 layer)	/TF-AL	11.3
Teflon (3 layers)	/TF-SH-TF/TF-AL	4.2
Teflon/Vacuum Grease	/TF-SH-TF/VG/TF-AL	0.8

Table 6.3 shows a summary of the results for each test. In Table 6.3, the maximum shear stress is the absolute maximum shear stress measured during the test, and the displacement at τ_{max} is the corresponding displacement. In many cases, the maximum shear stress occurred at very large displacements, and based on the shear stress-displacement plots it was apparent that the interfaces had actually failed at much smaller displacements. The values for displacement at failure in Table 6.3 indicate the tests where this was the case and these values represent a more reasonable estimate of the displacement at failure based upon the shape of the shear stress-displacement plots.

Table 6.3 - Summary of Interface Direct Shear Test Results

Interface	σ_n (psi)	τ_{max} (psi)	Displacement @ τ_{max} (in)	Displacement @ failure (in)
Aluminum	30 62 106	15.5 33 58.5	0.244 0.085 0.110	0.075
Sintered Bronze	30 62 74 96	17 36.5 37 52.5	0.141 0.134 0.194 0.129	0.100 0.150
Coarse Sintered Bronze	30 62 96	16.5 34 51	0.167 0.223 0.154	0.080 0.130
-DD/VG/DD/VG/AL	30 62 106	1.3 4.1 5.6	0.319 0.399 0.335	
/TF-AL	30 62 106	11.9 17.2 16.7	0.300 0.074 0.056	0.090 0.055 0.040
/TF-SH-TF/TF-AL	30 62 106	2.8 4.6 7.7	0.019 0.037 0.033	 0.025
/TF-SH-TF/VG/TF-AL	30 62 106	0.3 0.6 1.6	0.341 0.037 0.266	

Shear Stress-Displacement Relationship

In order to model the interface behavior, the shear stress-relative displacement relationship was assumed to be bilinear, with an initial straight-line portion

representing linear elastic displacement, and a zero-stiffness, or horizontal portion representing the post-failure behavior. The interface behaves in a linearly elastic fashion if the shear stress level is below the shear strength as determined by the Mohr-Coulomb envelope for the interface (pre-failure), and displaces under a constant shear stress if the shear stress level is equal to the Mohr-Coulomb strength (post-failure). A comparison of bilinear relationships with actual interface direct shear test data is shown in Figure 6.6. While the measured shear stress-relative displacement curves exhibit some nonlinearity, the simplification of the bilinear response seems to be reasonable for the purposes of the present investigation.

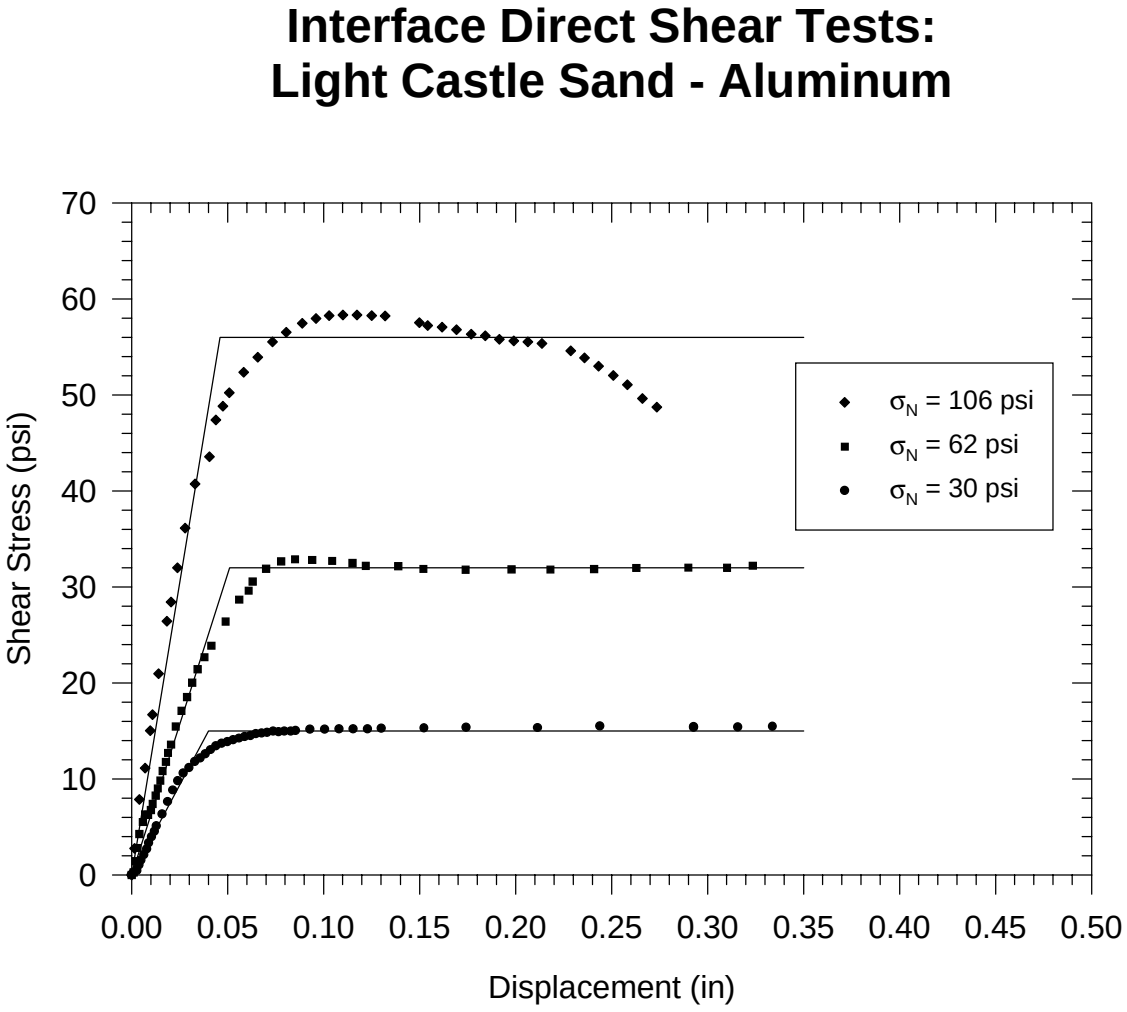

Figure 6.6 - Stress Displacement Relationship for Interface Direct Shear Tests

The initial shear stiffness is dependent upon the normal stress level in most cases. The relationship between the initial shear stiffness and the normal stress was modeled using the expression proposed by Clough and Duncan (1969):

$$k_{si} = k_j \cdot \gamma_w \cdot \left(\frac{\sigma_n}{\sigma_{atm}} \right)^n \qquad \text{Equation 6.4}$$

where: k_{si} = initial shear stiffness
k_j = coefficient for power curve
γ_w = unit weight of water
σ_n = normal stress on the interface
σ_{atm} = atmospheric pressure
n = exponent for power curve

Table 6.4 shows the values of the coefficient k_j and the exponent n for the seven interfaces tested in this study. If the value of n is equal to zero, then the value of the initial shear stiffness is independent of the normal stress and is equal to $k_j \cdot \gamma_w$. If the value of n is equal to one, then the relationship between normal stress and initial shear stiffness is linear, and the linear coefficient is equal to $\frac{k \cdot \gamma_w}{\sigma_{atm}}$

Table 6.4 - Values of Parameters for Initial Shear Stiffness Expression for Interface Behavior

Interface	k **(coefficient)**	n **(exponent)**
AL	4680	1.00
SB	6940	0.65
CSB	5140	0.73
-DD/VG/DD/VG/AL	1370	0.07
/TF-AL	5380	0.45
/TF-AL-TF/TF-AL	2910	0.38
/TF-AL-TF/VG/TF-AL	121	1.00

Equation 6.4, along with the parameters in Table 6.4, was used to model the end platen-specimen interface behavior in the finite element analysis of the stress conditions in triaxial test specimens.

Summary

Seven series of interface direct shear tests were performed in order to characterize the Mohr-Coulomb shear strength envelope and the shear stress-relative displacement relationship for seven different interface configurations. The tests were performed in a conventional direct shear box, but with half of the box occupied by either aluminum or sintered bronze and half of the box occupied by sand. Most of the tests exhibited a nonlinear shear stress-relative displacement relationship prior to failure, and continued displacement under a constant shear stress after failure. For the purposes of the current investigation, the overall shear stress-relative displacement relationship for the interfaces tested can be adequately modeled by a bilinear relationship. The test results showed that the initial shear stiffness was dependent upon the normal stress on the interface, and this relationship was modeled using a power curve in the form of Equation 6.4.

The interfaces typically found in triaxial tests using conventional end platens exhibited significant shear resistance, with shear strengths approximately equal to 80% of the shear resistance of the soil alone. The lubrication schemes tested exhibited significantly reduced shear resistance. The interface offering the least shear resistance of all that were tested was the Teflon scheme with vacuum grease as a lubricant, which had a friction angle that was less than one degree. Since minimizing friction on the ends is the primary goal of using lubricated end platens in the triaxial test, this scheme was the one adopted for the lubricated end triaxial tests performed as part of this study.